ESCOLA DE CIÊNCIAS
PROGRAMA DE PÓS-GRADUAÇÃO EM BIOLOGIA CELULAR E MOLECULAR
DOUTORADO EM BIOLOGIA CELULAR E MOLECULAR

KELLY GOULART LIMA

AVALIAÇÃO DO EFEITO DO GALATO DE OCTILA SOBRE A PROLIFERAÇÃO CELULAR E METABOLISMO LIPÍDICO NA LINHAGEM DE CARCINOMA HEPATOCELULAR HEPG2

Porto Alegre
2018

PONTIFÍCIA UNIVERSIDADE CATÓLICA DO RIO GRANDE DO SUL
ESCOLA DE CIÊNCIAS
PROGRAMA DE PÓS-GRADUAÇÃO EM BIOLOGIA CELULAR E MOLECULAR

AVALIAÇÃO DO EFEITO DO GALATO DE OCTILA SOBRE A PROLIFERAÇÃO CELULAR E METABOLISMO LIPÍDICO NA LINHAGEM DE CARCINOMA HEPATOCELULAR HEPG2

Tese apresentada ao Programa de Pós-Graduação em Biologia Celular e Molecular da Pontifícia Universidade Católica do Rio Grande do Sul como requisito parcial para a obtenção do grau de Doutora em Biologia Celular e Molecular.

KELLY GOULART LIMA

ORIENTADOR: Prof. Dr. Jarbas Rodrigues de Oliveira

Porto Alegre
2018

Ficha Catalográfica

L732a Lima, Kelly Goulart

Avaliação do efeito do galato de octila sobre a proliferação celular e metabolismo lipídico na linhagem de carcinoma hepatocelular HepG2 / Kelly Goulart Lima . – 2018.

104 f.

Tese (Doutorado) – Programa de Pós-Graduação em Biologia Celular e Molecular, PUCRS.

Orientador: Prof. Dr. Jarbas Rodrigues de Oliveira.

1. galato de octila. 2. carcinoma hepatocelular. 3. células HepG2. 4. antiproliferação. 5. metabolismo lipídico. I. Oliveira, Jarbas Rodrigues de. II. Título.

Elaborada pelo Sistema de Geração Automática de Ficha Catalográfica da PUCRS
com os dados fornecidos pelo(a) autor(a).
Bibliotecário responsável: Marcelo Votto Texeira CRB-10/1974

KELLY GOULART LIMA

AVALIAÇÃO DO EFEITO DO GALATO DE OCTILA SOBRE A PROLIFERAÇÃO CELULAR E METABOLISMO LIPÍDICO NA LINHAGEM DE CARCINOMA HEPATOCELULAR HEPG2

Tese apresentada ao Programa de Pós-Graduação em Biologia Celular e Molecular da Pontifícia Universidade Católica do Rio Grande do Sul como requisito parcial para a obtenção do grau de Doutora em Biologia Celular e Molecular.

Aprovada em: ____ de _____ de _____.

BANCA EXAMINADORA

_____
Prof.ª Dr.ª Marilene Porawski

_____
Prof.ª Dr.ª Maria Martha Campos

_____
Prof.ª Dr.ª Denise Cantarelli Machado

Porto Alegre
2018

Aos meus familiares e amigos que
sempre me apoiaram, incentivaram e
torceram pelo meu sucesso.

AGRADECIMENTOS

Aos meus amados pais, irmãos, à vozinha Joana, à dinda Rosani, aos meus primos, meus tios e demais familiares que sempre acreditaram no meu potencial e me incentivaram e apoiaram desde criança.

Ao meu noivo Jonas, meu amor, sempre ao meu lado me apoiando em todos os momentos.

Aos meus sobrinhos João Gabriel, Davi Lucca e Eduardo pelos momentos de descontração e carinho.

Ao meu querido orientador pela oportunidade, confiança e incentivo constante. Tenho grande orgulho em fazer parte desse grupo de pesquisa e agradeço todo o aprendizado. Considero-te um modelo a ser seguido, pois consegue ensinar de forma leve, com riqueza de exemplos e experiências que cativa a todos os alunos.

A todos os colegas do Laboratório de Biofísica Celular e Inflamação, por todo auxílio desde o início das minhas atividades no laboratório, em especial à Gabriela Haute, à Maria Claudia Garcia e ao Eduardo Caberlon, que sempre estiveram disponíveis passar seus conhecimentos a ajudar no que fosse preciso.

Aos amigos que fiz durante o Doutorado, em especial à Gisele Funchal, Elisa Silva e Camille Reghelin.

Aos meus amigos Gabriele Krause, Eduardo Filippi-Chiela e Leo Anderson Martins, os quais ajudaram no planejamento, execução de experimentos e análise de dados. A ajuda de vocês enriqueceu grandemente esse trabalho!

Aos meus queridos alunos de iniciação científica: Luiza Luz, Laura Alice e Vitor Levorse. A ajuda de vocês foi muito importante para a realização deste trabalho, meus sinceros agradecimentos.

Ao prof. Léder Xavier pelo auxílio nas análises de imagens e revisão dos artigos. Não tenho como mensurar quão importante foi sua ajuda para aprimorar nossos artigos.

Aos professores Fernanda Bordignon, Márcio Vinicius Donadio e Denizar Melo pelas importantes sugestões e ideias em nossas reuniões periódicas.

À prof.ª Drª Ana Lígia Bender e ao Eduardo Pedrazza do Laboratório de Imunodiagnóstico pelo apoio através do compartilhamento de equipamentos e instrumentos de laboratório.

À Moema Vieira e Marina do LabCEMM que ajudaram enormemente na obtenção das imagens de microscopia eletrônica de transmissão e microscopia de varredura à laser.

À funcionária Zíngara Leal T. Lubaszewski pelo apoio administrativo e pronto atendimento sempre que precisamos.

Aos meus colegas do Hospital Materno-Infantil Presidente Vargas, em especial à Carolina Pederzolli e Letícia Ganassini, as quais sempre se disponibilizaram a trocas de turno e de plantões para que eu pudesse realizar meus experimentos na PUCRS.

“Feliz aquele que transfere o que
sabe e aprende o que ensina”

Cora Coralina

RESUMO

O galato de octila (GO) é um antioxidante utilizado na indústria de alimentos, cosméticos e de medicamentos que tem mostrado efeito antitumoral em linhagem celular de leucemia, melanoma e linfoma de células B, assim como em modelo animal de metástase pulmonar. O Carcinoma hepatocelular (CH) é o principal câncer primário hepático que afeta a população mundial. Embora a ressecção cirúrgica, a ablação e o transplante hepático sejam considerados terapias curativas, poucos pacientes são elegíveis. A aplicação dessas opções terapêuticas é indicada somente para estágios iniciais da doença e infelizmente a maioria dos pacientes é diagnosticado em estágio avançado. Além disso, existem relatos na literatura de resistência à única droga aprovada para tratamento sistêmico, o sorafenibe. Nesse estudo, nós investigamos o efeito do GO sobre a proliferação celular e metabolismo lipídico nas células de carcinoma hepatocelular HepG2. Além disso, desenvolvemos um protocolo para avaliação quantitativa de gotas lipídicas. Nós reportamos, pela primeira vez, que o tratamento com GO por 24 horas inibiu a proliferação das células HepG2 por reduzir a atividade e massa mitocondrial, que levou à redução dos níveis de ATP. Essa redução no fornecimento de energia desencadeou a diminuição na expressão da proteína Ki67, levando à parada do ciclo celular em fase S. Além disso, o uso de dois tratamentos com GO com intervalo de 24 horas induziu perda da funcionalidade mitocondrial e apoptose, sem induzir resistência. Esses resultados mostraram que o GO tem como alvo a mitocôndria, sendo um candidato para novas pesquisas sobre terapias para o CH. Reportamos também, pela primeira vez, o efeito do GO sobre o metabolismo lipídico, visto que nossos resultados mostraram que o composto foi capaz de aumentar a quantidade de lipídeos, os níveis de triglicerídeos e a área de gotas lipídicas, sem envolver a via de sinalização mTOR/SREBP-1c ou a modificação da expressão dos genes PPAR-α e PPAR-γ. Uma vez que a capacidade do GO em inibir a atividade mitocondrial e induzir a apoptose é conhecida, é fortemente sugerido que a redução da β-oxidação mitocondrial de ácidos graxos esteja envolvida no mecanismo do GO no acúmulo de lipídeos. Descrevemos também, pela primeira vez, um protocolo para avaliação quantitativa de gotas lipídicas usando microscopia confocal de varredura a laser que comparado à microscopia de

fluorescência convencional, proporcionou grande ganho na qualidade das imagens.

Palavras-chave: galato de octila, carcinoma hepatocelular, células HepG2, antiproliferação, metabolismo lipídico.

ABSTRACT

Octyl gallate (OG) is an antioxidant used in the food, cosmetic and medications industries that has shown antitumor effect on cell lineage of leukemia, melanoma and B cell lymphoma, as well as on animal model of pulmonary metastasis. Hepatocellular carcinoma (HC) is the main primary liver cancer affecting the world's population. Although surgical resection, ablation and liver transplantation are curative options, few patients are eligible for these therapies. The application of these therapeutic options is indicated only in the early stages of the disease and unfortunately most patients are diagnosed at advanced stage. In addition, there are reports in the literature of resistance to the only drug approved for systemic treatment, sorafenibe. In this study, we investigated the effect of OG on cell proliferation and lipidic metabolism in hepatocellular carcinoma HepG2 cells. Moreover, we developed a protocol for the quantitative evaluation of lipid droplets. We report, for the first time, that treatment with OG for 24 h inhibited HepG2 cell growth by decreasing mitochondrial activity and mass, which led to the reduction of ATP levels. This reduction in the energy supply triggered a decrease in Ki67 protein expression, leading to cycle arrest in S phase. In addition, the use of two treatments with OG with interval 24 hours induced loss of mitochondrial functionality and apoptosis without inducing resistance. These results showed that OG targets the mitochondria and is a candidate for new research on therapies for CH. We also report, for the first time, the effect of OG on lipidic metabolism, since our results showed that OG was able to increase the amount of lipids, triglyceride levels and the area of lipid droplets without involving the mTOR/SREBP-1c signaling pathway or modification of PPAR-α and PPAR-γ gene expression. As the ability of OG to inhibit mitochondrial activity and induce apoptosis is known, it is strongly suggested that reduction of mitochondrial fatty acid b-oxidation is involved in the OG mechanism in the accumulation of lipids. We also describe, for the first time, a protocol for the quantitative evaluation of lipid droplets using confocal laser scanning microscopy that compared to conventional fluorescence microscopy, provided great gain in the quality of the images.

Key words: octyl gallate, hepatocellular carcinoma, HepG2 cells, antiproliferation, lipidic metabolism.

LISTA DE ILUSTRAÇÕES

LISTA DE SIGLAS

AG - ácido gálico

AISF - Associação Italiana para o estudo do fígado

AVOs - organelas vesiculares ácidas

BCLC - Barcelona Clinic Liver Cancer

CH - carcinoma hepatocelular

CI50 - concentração inibitória de 50% das células

CPH - células progenitoras hepáticas

CTTH - células tronco tumorais hepáticas

DCFH-DA – dichloro-dihydro-fluorescein diacetate

DMSO – dimetilsulfóxido

ECOG - Eastern cooperative oncology group

FDA - Food and Drug Administration

GO - galato de octila

GSH – glutationa reduzida

HPLC - High performance liquid chromatography

IDA - ingesta diária aceitável

LD_{50} – dose letal mediana

LDH - lactato desidrogenase

MET - Microscopia Eletrônica de Transmissão

OMS - Organização Mundial da Saúde

OR – Oil red

TBARS – thiobarbituric acid reactive substances

VEGR - receptor de crescimento endotelial vascular

VHB - vírus da hepatite B

VHC - vírus da hepatite C

SUMÁRIO

CAPÍTULO I

1. INTRODUÇÃO
2. JUSTIFICATIVA
3. OBJETIVOS

1. INTRODUÇÃO

1.1. CARCINOMA HEPATOCELULAR

O carcinoma hepatocelular (CH) representa de 70% a 90% dos cânceres hepáticos primários e seu desenvolvimento está relacionado, na maioria dos casos, à lesão hepática crônica, como a cirrose. Outros tipos de tumores que atingem o fígado incluem o colangiocarcinoma (acomete os ductos biliares), o angiossarcoma (câncer raro que se origina dos vasos sanguíneos) e o hepatoblastoma (câncer raro que atinge recém nascidos e crianças nos primeiros anos de vida) (INCA, 2017).

Os principais fatores de risco para o desenvolvimento do CH são: infecção crônica causada pelo vírus da Hepatite B (VHB) ou da Hepatite C (VHC), consumo de alimentos contaminados com aflatoxina (toxina produzida pelo fungo *Aspergillus flavus* geralmente contaminante de grãos e cereais armazenados inadequadamente), obesidade, Diabetes mellitus tipo 2, cirrose por abuso de álcool, esteatose hepática e tabagismo (TORRE et al., 2016). Esses fatores de risco estão intimamente ligados à formação e desenvolvimento da cirrose, caracterizada pela fibrose progressiva e reorganização da microarquitetura vascular, a qual está presente em 80 a 90% dos pacientes com CH (FITZMORRIS et al., 2014).

O CH é considerado muito agressivo e altamente letal, pois somente 7% dos pacientes tem sobrevida superior a cinco anos (BOSCH et al., 2004). As principais características clínicas incluem hepatomegalia, dor no quadrante superior direito, perda de peso, perda de apetite, mal-estar, icterícia e ascite (INCA, 2017). A sua morfologia pode variar de nódulos multifocais, massas solitárias até um câncer difusamente infiltrativo. De acordo com a histologia das lesões hepáticas, o tumor pode ser considerado bem diferenciado ou até mesmo indiferenciado e altamente anaplásico (MITCHELL et al., 2006).

As principais técnicas utilizadas no Brasil para o diagnóstico do CH são a Tomografia Computadorizada, Ressonância Magnética Nuclear e a Laparoscopia (INCA, 2017). Nos Estados Unidos, O Instituto Nacional do Câncer utiliza a análise do marcador tumoral alfa-fetoproteína e a ultrassonografia para “screnning” da doença e os casos com alteração nos exames iniciais são reavaliados através de biópsia. A Tomografia Computadorizada é utilizada para populações de alto risco, por apresentar

maior sensibilidade e especificidade que os métodos utilizados inicialmente (NATIONAL CANCER INSTITUTE, 2017).

1.1.1. Epidemiologia

O câncer hepático primário é o sexto mais comum tipo de câncer no mundo, sendo o carcinoma hepatocelular o principal tipo histológico (aproximadamente 80%) e em segundo lugar o colangiocarcinoma (aproximadamente 15%). A Ásia e a África apresentam as maiores taxas de incidência de câncer hepático. Em torno de 75% dos casos ocorrem na Ásia, sendo a China o país que representa mais de 50% desses casos (MCGLYNN; PETRICK; LONDON, 2015). Segundo os últimos dados publicados pela Organização Mundial da Saúde (OMS), referente ao ano de 2012, o câncer de fígado é a segunda causa de morte por câncer em homens e a sexta em mulheres no mundo, sendo responsável por 746.000 mortes (9,1% do total) (TORRE et al., 2016).

A incidência do câncer hepático é de duas a três vezes maior em homens do que em mulheres em quase todos os países. Essa diferença não tem sido completamente elucidada, porém sabe-se que os principais fatores de risco são mais prevalentes em homens; além disso, existem hipóteses de que diferenças nos hormônios esteróides, na resposta imunológica e na epigenética possam estar relacionadas às maiores taxas entre homens (MCGLYNN; PETRICK; LONDON, 2015).

A infecção crônica pelo VHB, um dos principais fatores de risco para o desenvolvimento de CH, foi responsável por 887.000 mortes em 2015 no mundo, principalmente pela indução de cirrose e CH. Estima-se que 257 milhões de pessoas estejam vivendo com a infecção por VHB, por isso ela é considerada um dos principais problemas de saúde pública. A prevalência da infecção é maior na região do Pacífico Ocidental e África, onde aproximadamente 6% da população adulta é infectada. Felizmente, a vacina está disponível desde 1982 e apresenta 95% de eficácia. A Organização Mundial da Saúde recomenda a vacinação dentro de 24 horas após o nascimento e duas a três doses posteriores, conforme protocolo de vacinação. A prevalência de Hepatite B nas crianças abaixo de 5 anos reduziu de 4,7% para 1,3%

após a implementação da vacina, mostrando a importância do investimento na prevenção dessas infecções (WORLD HEALTH ORGANIZATION, 2017a).

Outro vírus considerado hepatocarcinogênico é o vírus da Hepatite C (VHC), o qual apresenta múltiplos genótipos e apresenta distribuição variável de acordo com a região territorial estudada. A cada ano, 399.000 pessoas morrem de hepatite C no mundo, principalmente pelas complicações da cirrose e do CH. Estima-se que 71 milhões de pessoas tenham a infecção crônica causada pelo VHC e um número significante delas desenvolverá cirrose e CH. As regiões mais afetadas são Mediterrâneo Oriental e Europa, com prevalência de 2,3% e 1,5% respectivamente. Infelizmente não existe no momento vacina para Hepatite C, entretanto pesquisas nessa área estão em andamento (WORLD HEALTH ORGANIZATION, 2017b).

1.1.2. Hepatocarcinogênese

A hepatocarcinogênese envolve alterações genéticas e o desenvolvimento de células tumorais hepáticas a partir de hepatócitos adultos ou células tronco hepáticas. As principais alterações genéticas somáticas encontradas no CH são mutações, alterações no número de cópias de genes, rearranjos intra-cromossomais e inter-cromossomais (CASTELLI; PELOSI; TESTA, 2017). Os genes mais frequentemente alterados, os quais tem papel importante no desenvolvimento do CH incluem TP53 (supressor tumoral), MYC (proto-oncogene), WNT (proto-oncogene), CTNNB1 (beta-catenin, proto-oncogene); genes relacionados ao ciclo celular, como CCND1 (ciclina D1) e CDKN2A (inibidor de ciclina 2A dependente de quinase); genes envolvidos na estabilidade do telômero (TERT); em mecanismos epigenéticos (IDH1 e IDH2) e remodelamento de cromatina (ARID1, ARID2, MLL, BAP1 and EZH2) (MARQUARDT; ANDERSEN; THORGEIRSSON, 2015; SHIBATA; ABURATANI, 2014).

Estudo recente identificou novos genes mutados considerados indutores de CH incluindo LZTR1, EEF1A1, SF3B1 e SMARCA4. Além disso, encontraram alterações significativas (mutação ou silenciamento por hipermetilação) dos genes ALB, APOB e CPS1, que provavelmente resultaram em reprogramação metabólica do CH (CANCER GENOME ATLAS RESEARCH NETWORK. ELECTRONIC ADDRESS: WHEELER@BCM.EDU et al., 2017).

As vias de sinalização mais frequentemente alteradas no CH são: ativação da expressão da telomerase a partir de mutações no promotor TERT (mais de 60%), inibindo a senescência e assim mantendo a capacidade proliferativa das células (LIU; YUAN; XU, 2016); ativação da via WNT/beta-catenin (54%), a qual induz renovação e proliferação excessiva de células tronco predispondo as células à tumorigênese (MACDONALD; TAMAI; HE, 2009); ativação da via PI3K-AKT-mTOR (51%), que tem papel na sobrevida e crescimento celular (PORTA; PAGLINO; MOSCA, 2014); mutação ou redução da expressão do TP53 (49%), impedindo o controle do ciclo celular e a indução de apoptose (CHEN et al., 2003); ativação da via MAPK (43%), promovendo crescimento celular descontrolado (HUYNH et al., 2003), ativação de vias de diferenciação hepática (34%); regulação epigenética (32%); remodelamento de cromatina (28%); estresse oxidativo (12%); IL-6/JAK-STAT (9%), induzindo transformação oncogênica dos hepatócitos (SCHMIDT-ARRAS; ROSE-JOHN, 2016) e TGF-beta (SCHULZE et al., 2015).

Os hepatócitos correspondem a mais de 80% das células parenquimais hepáticas ativas e são considerados o principal tipo celular de origem para o CH. Outro tipo celular importante são as células epiteliais dos ductos biliares, também conhecidas como células progenitoras hepáticas (CPH), as quais tem como função principal a reposição de hepatócitos e colangiócitos danificados. Um modelo que mimetizou a hepatocarcinogênese humana mostrou que as CPH também podem dar origem ao CH agressivo, assim como lesões benignas (TUMMALA et al., 2017). Interessantemente, o mesmo estudo citado mostrou que os hepatócitos transformados têm a capacidade de ativar a proliferação e transformação das CPH em CH através de efeitos parácrinos induzidos por α-cetoglutarato (mantém as CPH em estado indiferenciado) e pela gelectina-3 (mantém a capacidade de auto-renovação e diferenciação das CPH).

Acredita-se que as células progenitoras hepáticas podem adquirir mutações oncogênicas e se transformarem em células tronco tumorais hepáticas (CTTH). Essas mutações geralmente estão relacionadas à infecção crônica pelo vírus da Hepatite B, vírus da Hepatite C ou a algum tipo de inflamação crônica. As CTTH apresentam vias de sinalização para autoproliferação desregulada e capacidade de gerar células tumorais maduras, com isso apresentam um papel importante na progressão de tumores hepáticos (PANG; POON, 2012). Além disso, as CTTH têm sido relacionadas à falha terapêutica, uma vez que apresentam resistência à quimioterapia convencional

e à radioterapia, visto que essas células apresentam altos níveis de proteínas transportadoras que têm a capacidade de expulsar drogas da célula, como transportadores ABC (BORGHT et al., 2006; ROS et al., 2003).

Alguns marcadores usados para identificar as células tronco tumorais hepáticas têm sido descobertos, como CD13, CD44, CD24, CD90, CD133, EpCAM, DLK1 e ALDH1 (CASTELLI; PELOSI; TESTA, 2017). Esses marcadores estão sendo usados para desenvolver novas estratégias terapêuticas baseadas em nanotecnologia (WANG et al., 2014) ou em alvos imunológicos (PAN et al., 2015) com o objetivo de eliminar as CTTH.

1.1.3. Estadiamento do Tumor e Estratégias de Tratamento

A escolha do tipo de tratamento para o CH e o prognóstico do paciente depende da avaliação do estadiamento do tumor, a qual é uma etapa inicial de grande importância. O principal algoritmo utilizado mundialmente para o diagnóstico e estadiamento do CH é o “Barcelona Clinic Liver Cancer” (BCLC) (BRUIX; LLOVET, 2002).

O estágio tumoral é classificado, segundo o algoritmo BCLC, em muito inicial, inicial, intermediário, avançado e terminal (FORNER; LLOVET; BRUIX, 2012). A função hepática é avaliada conforme a classificação Child-Pugh modificada, na qual se utiliza um sistema de pontuação que leva em consideração a bilirrubina sérica, a albumina sérica, presença de ascite, presença de distúrbio neurológico e o tempo de protrombina. A pontuação descrita na tabela 1 é somada, obtendo-se um escore de 5 a 15. Escores de 5 a 6 são a classe A de Child-Pugh, escores de 7 a 9 classe B e escores de 10 a 15 classe C (PUGH et al., 1973).

Tabela 1 – Classificação de Child-Pugh

Fator	1 ponto	2 pontos	3 pontos
Bilirrubina sérica (mg/dL)	< 2,0	2,0 - 3,0	> 3,0
Albumina sérica (g/dL)	> 3,5	3,0 - 3,5	< 3,0
Ascite	Nenhuma	Facilmente controlada	Mal controlada
Distúrbio neurológico	Nenhum	Mínimo	Coma avançado

Tempo de protrombina (INR)	< 1,7	1,7 - 2,3	> 2,3

Fonte: Pugh et al (1973).

O estado geral do paciente é classificado conforme os critérios descritos pelo Eastern cooperative oncology group (ECOG), o qual avalia as capacidades do paciente com relação ao trabalho, o autocuidado e o tempo de confinamento na cadeira ou cama (OKEN et al., 1982). A tabela 2 apresenta a classificação ECOG.

Tabela 2 – Classificação ECOG

Status	Descrição
0	Totalmente ativo, capaz de realizar todas as funções pré-doença sem restrições.
1	Restrito para atividade fisicamente extenuante, capacidade de caminhar e realizar trabalhos de natureza leve ou sedendária (trabalho leve em casa, trabalho em escritório)
2	Capacidade de caminhar e realizar autocuidado, mas incapaz de realizar atividades do trabalho, ativo < 50% das horas de vigília.
3	Capacidade restrita ao autocuidado com limitação. Confinado à cama ou cadeira > 50% das horas de vigília.
4	Completamente incapaz. Não consegue realizar nenhuma atividade de autocuidado. Completamente confinado à cama ou cadeira.
5	Morto.

Fonte: Oken et al (1982).

As terapias disponíveis para o CH são apresentadas na figura 1, com base na classificação BCLC.

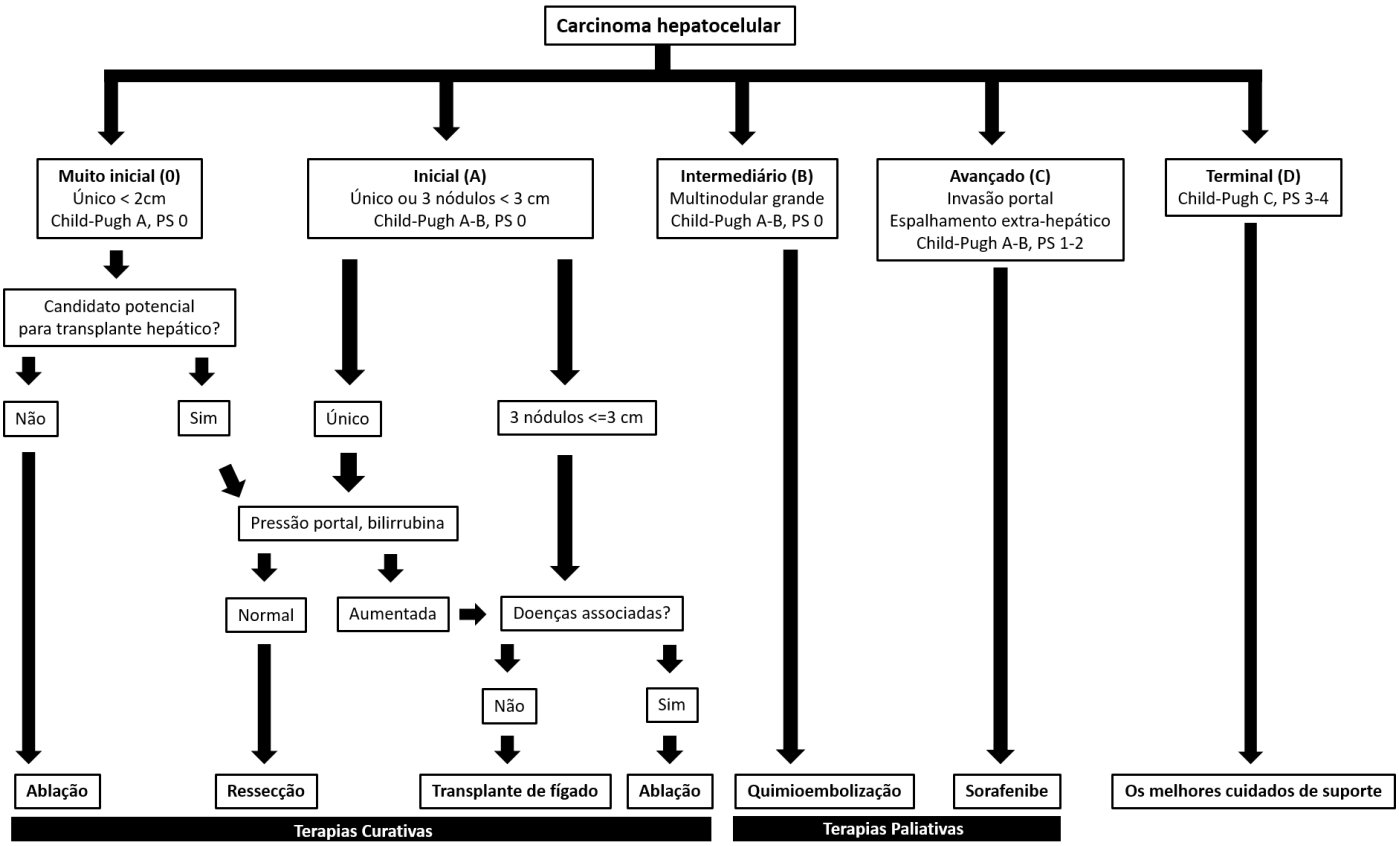

Figura 1 – Estadiamento BCLC e Estratégias de Tratamento
Fonte: Forner et al (2012).

Legenda: PS: status “performance” ECOG.

Consideram-se terapias curativas a ressecção cirúrgica, a ablação e o transplante de fígado. A ressecção cirúrgica e o transplante hepático são as terapias mais conhecidas e tradicionais. A elegibilidade para transplante hepático é avaliada mundialmente com base nos critérios de Milão, os quais são amplamente aceitos para reduzir a recorrência do CH após transplante e equilibrar a alocação de órgãos entre pacientes com e sem CH (ZHU, 2016). Os critérios de Milão foram definidos após estudo de Mazzaferro et al, os quais reportaram que o transplante hepático foi um tratamento efetivo para o CH não ressecável em pacientes com cirrose. Os critérios definidos nesse estudo para realização do transplante hepático e até hoje aplicados são a existência de um único tumor com diâmetro igual ou inferior a 5 cm ou até 3 tumores com diâmetro igual ou inferior a 3 cm (MAZZAFERRO et al., 1996).

A ablação consiste em uma técnica que causa a necrose das células tumorais através de substâncias químicas (ex: etanol, ácido acético) ou com a aplicação de crioterapia, radiofrequência, laser ou microondas. Essa técnica é aplicada localmente, guiando-se por imagens de ultrassom (FITZMORRIS et al., 2014). Entretanto, essas

opções curativas são indicadas somente para pacientes em estágio inicial da doença e infelizmente a maioria dos pacientes tem o diagnóstico em estágio avançado (FORNER; LLOVET; BRUIX, 2012).

Entre as opções paliativas, a quimioembolização transarterial é uma técnica que combina a administração local de quimioterápicos, sendo os principais utilizados a cisplatina e a adriamicina e, a embolização da artéria que supre o tumor com nutrientes. Outro tratamento paliativo se aplica a pacientes com tumor avançado e utiliza a quimioterapia sistêmica por via oral com sorafenibe. Essa droga é a única aprovada pelo “Food and Drug Administration” (FDA) para tratamento do CH avançado. Esse medicamento é um inibidor multiquinase que age no receptor de crescimento endotelial vascular (VEGR) (FITZMORRIS et al., 2014).

Há evidências de que o sorafenibe aumenta a sobrevida dos pacientes, porém o benefício é considerado limitado. Um estudo com 602 pacientes com CH avançado mostrou que essa droga aumentou pouco a sobrevida dos pacientes quando comparada ao placebo (10,7 meses vs. 7,9 meses). Além disso, há relatos de efeitos adversos importantes (LLOVET et al., 2008a, 2008b) e resistência adquirida à droga (ZHAI; SUN, 2013), mostrando a necessidade de realização de mais pesquisas para o desenvolvimento de novas drogas mais efetivas.

A Associação Italiana para o estudo do fígado (AISF) recomenda o sistema BCLC para estadiamento do CH, porém faz algumas ressalvas. A primeira é de que os pacientes não devem ser classificados como estágio avançado (C) somente devido a apresentar PS 1, visto que a relação entre os sintomas e o tumor é incerta. Além disso, inclui a avaliação do nível sérico de alfa-fetoproteína antes de iniciar o tratamento, pois considera esse marcador importante para determinar a resposta ao tratamento e o risco de exclusão da lista de espera para transplante hepático.

Outra recomendação é o uso de ressonância magnética ao invés de tomografia computadorizada para estadiamento do CH quando o paciente for candidato potencial para tratamento cirúrgico ou por ablação. Isso se deve à maior precisão da ressonância magnética, apesar de ser mais onerosa. Também é indicada tomografia computadorizada de tórax quando o paciente é candidato à cirurgia ou quando o CH está além dos critérios de Milão. A última ressalva é a necessidade de incluir a avaliação do risco de sangramento relacionado à hipertensão-portal no estadiamento dos pacientes (BOLONDI et al., 2013).

Com relação ao tratamento, a AISF descreveu um algoritmo com algumas modificações comparado ao BCLC. Nesse algoritmo a AISF inclui o acompanhamento da resposta com base na análise de imagens de ressonância magnética ou tomografia computadorizada e opções alternativas para tratamento dos tumores não tratáveis por terapias curativas (BOLONDI et al., 2013).

1.2. LINHAGEM HEPG2

Numerosas linhagens celulares tumorais são utilizadas na pesquisa para o entendimento da progressão de doenças, desenvolvimento de diagnóstico e triagem para novas drogas antitumorais (CHEN et al., 2015). A linhagem celular HepG2 imortalizada foi isolada em 1979 a partir da biópsia hepática de um paciente caucasiano de quinze anos que possuía um hepatoblastoma, e desde então foi introduzida em estudos científicos (ADEN et al., 1979). Essa linhagem apresenta morfologia epitelial, crescimento aderente e não é tumorigênica em camundongos imunossuprimidos.

Vários estudos utilizam a HepG2 como modelo *in vitro* de células hepáticas, principalmente para pesquisar o metabolismo de novas drogas, visto que a mesma mantém funções metabólicas semelhantes aos hepatócitos (JAVITT, 1990). Além disso, outras vantagens no uso das células HepG2 são sua disponibilidade ilimitada e estabilidade fenotípica (GERETS et al., 2012). Estudos experimentais *in vitro* que buscam novas opções terapêuticas para o CH frequentemente utilizam essa linhagem como modelo, por ser uma célula tumoral hepática (GUO et al., 2017; LIMA et al., 2016; QIU et al., 2015).

Entre as principais linhagens celulares de CH (HepG2, HuH 7, Hep3B e PLC/PRF/5), a HepG2 é a mais usada e a que apresenta maior semelhança com relação à expressão gênica, quando comparada a amostras de carcinoma hepatocelular. Essa maior correlação da expressão gênica é muito importante para a pesquisa translacional, permitindo adequado teste de hipóteses (CHEN et al., 2015).

1.3. GALATO DE OCTILA

A atividade antitumoral de componentes extraídos de plantas e seus derivados semi-sintéticos tem sido avaliada por diversos estudos. O ácido gálico (AG), um ácido fenólico de origem natural, tem mostrado efeitos antitumorais em diversas linhagens (INOUE et al., 1995; LU et al., 2010; YOSHIOKA et al., 2000), inclusive no CH (LIMA et al., 2016). O galato de octila (GO) é um éster de ácido gálico, o qual pode ser produzido semi-sinteticamente a partir do ácido gálico ou isolado dos frutos da *Terminalia bellerica* (LATHA; DAISY, 2013). O galato de octila difere do ácido gálico

somente por ter oito átomos de carbono na cadeia lateral alifática. Essa diferença estrutural aumenta sua lipofilicidade, afinidade e permeabilidade através da membrana plasmática, permitindo efeito mais potente quando comparado ao precursor ácido gálico. A figura 2 apresenta a estrutura química do galato de octila e ácido gálico (ELER et al., 2013).

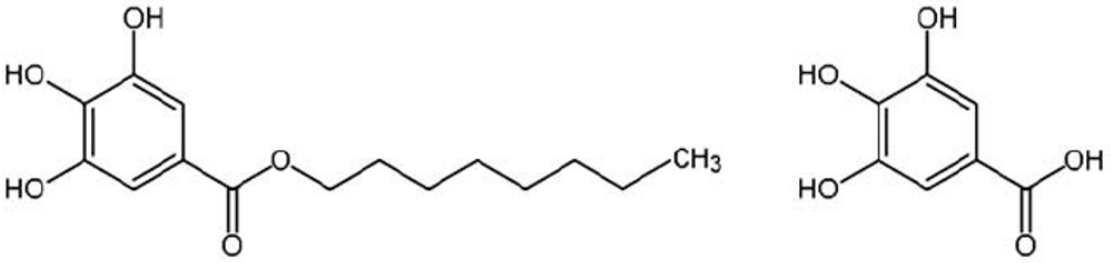

galato de octila ácido gálico

Figura 2 – Estrutura química do galato de octila e ácido gálico.
Fonte: Eler et al. (2013, p. 36)

O GO é um antioxidante utilizado em certos alimentos em alguns países, mas atualmente não há definição da quantidade aceitável para ingesta diária, devido à falta de estudos sobre a sua farmacocinética e metabolismo (WORLD HEALTH ORGANIZATION, 1997). Além disso, é usado como um aditivo antioxidante na indústria farmacêutica e de cosméticos (LOCATELLI; FILIPPIN-MONTEIRO; CRECZYNSKI-PASA, 2013).

No Brasil, o galato de octila não é usado como aditivo em alimentos, uma vez que não faz parte da lista de aditivos do programa Codex Alimentarius, o qual é usado como referência em nosso país. Esse programa é coordenado pela Organização das Nações Unidas para Agricultura e Alimentação e pela Organização Mundial da Saúde (OMS) e foi criado em 1963, com o objetivo de estabelecer normas internacionais na área de alimentos (FOOD AND AGRICULTURE ORGANIZATION OF UNITED NATIONS; WORLD HEALTH ORGANIZATION, 1995).

Alguns trabalhos evidenciam que esse antioxidante apresenta efeito antimicrobiano (GONÇALVES WOLF et al., 2017), anti-hiperglicêmico (ELER et al., 2015; LATHA; DAISY, 2013), antiviral (UOZAKI et al., 2007) e antifúngico (HSU; CHANG; CHANG, 2007). Outro estudo demonstrou que esse derivado do ácido gálico apresenta também atividade neuroprotetora, por aumentar a expressão da proteína antiamiloidogênica APP α-secretase (ZHANG et al., 2013).

O efeito antitumoral do GO tem sido pesquisado em linhagem celular de leucemia (LOCATELLI et al., 2008), melanoma (LOCATELLI et al., 2009a) e linfoma de células B (SERRANO et al., 1998). Além disso, tem sido pesquisado em modelo animal de metástase pulmonar (CORDOVA et al., 2017). Os mecanismos de ação do GO incluem a indução de estresse oxidativo associado à ativação de NF-kB e apoptose (LOCATELLI et al., 2008), indução de apoptose como consequência do estresse oxidativo sem associação com NF-kB (LOCATELLI et al., 2009a), indução da apoptose como resultado da fragmentação do DNA (SERRANO et al., 1998) e aumento de espécies reativas de oxigênio associado ao aumento da atividade da caspase-3 (CORDOVA et al., 2017). Esse estudo mais recente mostrou o efeito antimetastático do GO em modelo animal de metástase pulmonar e redução dos efeitos adversos quando o GO foi introduzido em nanopartículas lipídicas sólidas (CORDOVA et al., 2017). Entretanto, não existem relatos na literatura da avaliação do efeito antiproliferativo do GO no CH.

1.3.1 Toxicidade do galato de octila

Os primeiros estudos de toxicidade com o GO foram realizados com o objetivo de determinar a ingesta diária aceitável (IDA) e regular o uso desse antioxidante como aditivo em alimentos. Esses estudos iniciais com ratos definiram a LD_{50} do GO como 4700 mg/kg de peso corporal e mostraram que dietas contendo 0,2% de galato de octila causavam leve anemia hipocrômica. Então, a IDA de galatos (somando propila, octila e dodecila) para humanos foi definida como 0,2 mg/kg de peso corporal (JOINT FAO/WHO EXPERT COMMITTEE, 1964).

Posteriormente, foram realizados estudos de reprodução em ratos, os quais mostraram que a mortalidade de ratos jovens amamentados foi maior devido ao efeito perinatal, e pode ter sido causada possivelmente pelo GO presente no leite materno. Em experimentos com sensibilização prévia através de contato cutâneo em humanos, foi observado que o GO causava reações de sensibilização na mucosa oral, tornando o uso desse antioxidante inaceitável em cervejas e outras bebidas consumidas em grandes quantidades (JOINT FAO/WHO EXPERT COMMITTEE, 1972).

Em uma reavaliação do Comitê da Organização das Nações Unidas para Agricultura e Alimentação e Organização Mundial da Saúde em 1997, foi decidido que não seria possível manter a definição da IDA para o GO e o galato de dodecila, devido

à falta de estudos sobre a farmacocinética e metabolismo desses aditivos alimentares (WORLD HEALTH ORGANIZATION, 1997). Desde então, não há definição da IDA para este composto. Alguns países utilizam o GO como aditivo em certos alimentos, e determinam a concentração máxima aceitável de aditivo para os tipos de alimentos que são autorizados (EUROPEAN PARLIAMENT AND THE COUNCIL OF THE EUROPEAN UNION, 2008; U.S. FOOD AND DRUG ADMINISTRATION, 2018). Nos Estados Unidos, o GO é aprovado somente como um aditivo em margarinas com concentração inferior a 0,0075% (U.S. FOOD AND DRUG ADMINISTRATION, 2018). Na Europa, o OG é autorizado como um aditivo em carne processada tratada termicamente, goma de mascar e produtos processados a base de batata (EUROPEAN PARLIAMENT AND THE COUNCIL OF THE EUROPEAN UNION, 2008).

A toxicidade hepática de aditivos alimentares e medicamentos é um dos efeitos colaterais mais investigados pelas indústrias que atuam nas áreas de nutrição e farmácia. Dentre os efeitos tóxicos hepáticos, a esteatose é uma das principais alterações que podem provocar danos ao fígado. A esteatose hepática é caracterizada pelo acúmulo excessivo de lipídeos nos hepatócitos e pode ser causada principalmente pelo abuso de álcool, dislipidemia, obesidade, Diabetes mellitus, síndrome metabólica e uso de alguns medicamentos. Pode permanecer estável por muitos anos, regredir se as causas forem controladas ou evoluir para esteatoepatite. Nessa fase, se associa à inflamação, morte celular, fibrose e tem maior potencial para progredir para cirrose e CH (COTRIM, 2018).

Existem relatos na literatura mostrando que algumas drogas utilizadas para o tratamento do câncer podem causar esteatose hepática, como tamoxifeno (ZHAO et al., 2014), 5-fluoruracil (GENTILUCCI et al., 2006) e metotrexato (MENTER et al., 2009). Além disso, estudos mostram que alguns aditivos alimentares podem causar alteração do metabolismo lipídico hepático, como a frutose (CHEN et al., 2017; JENSEN et al., 2018), glutamato monossódico (COLLISON et al., 2009, 2013) e aspartame (COLLISON et al., 2013). Entretanto, não há estudos que apontem para a interferência do GO no metabolismo lipídico e consequente geração de depósito de gordura no fígado.

2. JUSTIFICATIVA

Considerando a quantidade restrita de terapias curativas e paliativas para o carcinoma hepatocelular e, que esse tumor representa a segunda causa mais comum de morte por câncer no mundo (TORRE et al., 2016), torna-se necessária a pesquisa de novas drogas alvo que possam representar futuras terapias anticâncer. Além disso, é importante pesquisar novas opções terapêuticas que possam ser utilizadas como adjuvantes de quimioterapias tradicionais, possibilitando menor resistência terapêutica.

O interesse na utilização de componentes obtidos de plantas para o desenvolvimento de agentes terapêuticos tem crescido (LOCATELLI; FILIPPIN-MONTEIRO; CRECZYNSKI-PASA, 2013). Também há fortes investimentos em pesquisas que envolvam a síntese de derivados de moléculas naturais, com o objetivo de melhorar suas características físico-químicas e potencializar seus efeitos terapêuticos.

O galato de octila, derivado semi-sintético do ácido gálico tem demonstrado ser uma molécula potencial para pesquisa de terapias anticâncer. O principal motivo é a sua estrutura química, que é muito similar à de seu precursor, que apresenta efeito antitumoral e, ao mesmo tempo, sua maior lipofilicidade, o que aumenta a afinidade e a permeabilidade pela membrana plasmática (SAEKI et al., 2000). Além disso, tem apresentado efeito antineoplásico em estudos com outros tipos de tumores e em comparação com o ácido gálico tem demonstrado maior potência, possibilitando a utilização de menores doses (LOCATELLI et al., 2008; SERRANO et al., 1998).

O galato de octila é utilizado em alguns países como um aditivo de alimentos devido sua característica antioxidante (EUROPEAN PARLIAMENT AND THE COUNCIL OF THE EUROPEAN UNION, 2008; U.S. FOOD AND DRUG ADMINISTRATION, 2018), entretanto não há estudos que avaliem seu efeito no metabolismo lipídico. Uma vez que existem pesquisas mostrando que determinados aditivos alimentares e medicamentos anticâncer podem induzir a esteatose hepática (CHEN et al., 2017; COLLISON et al., 2009, 2013; JENSEN et al., 2018), faz-se necessária a pesquisa do possível efeito tóxico do GO sobre o metabolismo lipídico.

3. OBJETIVOS

3.1. Geral

Avaliar do efeito do galato de octila sobre a proliferação celular e metabolismo lipídico na linhagem celular de carcinoma hepatocelular HepG2 e determinar os mecanismos envolvidos.

3.2. Específicos

1. Determinar o efeito do galato de octila sobre a proliferação celular e investigar o mecanismo envolvido, incluindo avaliações de: citotoxicidade, ciclo celular, senescência, níveis da proteína Ki 67, expressão do p21, produção de ATP, estresse oxidativo, autofagia, alterações mitocondriais e apoptose.

2. Avaliar o efeito tóxico do galato de octila sobre o metabolismo lipídico das células HepG2 e determinar o mecanismo envolvido, incluindo avaliações de gotas lipídicas e expressão de reguladores do metabolismo lipídico.

3. Desenvolver um método para avaliação quantitativa de gotas lipídicas coradas com Oil Red associada à Análise Morfométrica Nuclear para uso em células cultivadas *in vitro* utilizando microscopia confocal de varredura a laser e estimação dos parâmetros morfológicos usando o método da contagem de pontos.

CAPÍTULO II

Artigo Original: Octyl gallate reduces ATP levels and Ki67 expression leading HepG2 cells to cell cycle arrest and mitochondria-mediated apoptosis

Os resultados do presente trabalho respondem ao objetivo específico 1 e foram publicados no periódico Toxicology in Vitro.

Fator de impacto: 2.866

Qualis Capes 2013-2016: B1 (Ciências Biológicas I)

Toxicology in Vitro 48 (2018) 11–25

Contents lists available at ScienceDirect

Toxicology in Vitro

journal homepage: www.elsevier.com/locate/toxinvit

Octyl gallate reduces ATP levels and Ki67 expression leading HepG2 cells to cell cycle arrest and mitochondria-mediated apoptosis

Kelly Goulart Lima[a,*], Gabriele Catyana Krause[a], Elisa Feller Gonçalves da Silva[a], Léder Leal Xavier[b], Léo Anderson Meira Martins[c], Laura Manzoli Alice[a], Luiza Bueno da Luz[a], Rodrigo Benedetti Gassen[d], Eduardo Cremonese Filippi-Chiela[e], Gabriela Viegas Haute[a], Maria Claudia Rosa Garcia[a], Giselle Afonso Funchal[f], Leonardo Pedrazza[a], Camille Kirinus Reghelin[a], Jarbas Rodrigues de Oliveira[a]

[a] Laboratório de Biofísica Celular e Inflamação, Pontifícia Universidade Católica do Rio Grande do Sul, Av. Ipiranga, 6681, prédio 12, bloco c, Partenon, Porto Alegre, Rio Grande do Sul 90619-900, Brazil
[b] Laboratório de Biologia Celular e Tecidual, Departamento de Ciências Morfofisiológicas, Pontifícia Universidade Católica do Rio Grande do Sul, Av. Ipiranga, 6681, prédio 12, bloco c, Partenon, Porto Alegre, Rio Grande do Sul 90619-900, Brazil
[c] Departamento de Bioquímica, ICBS, Universidade Federal do Rio Grande do Sul, Rua Ramiro Barcelos, 2600-Anexo I, Porto Alegre, Rio Grande do Sul 90035-003, Brazil
[d] Laboratório de Imunologia Celular e Molecular, Instituto de Pesquisas Biomédicas, Pontifícia Universidade Católica do Rio Grande do Sul, Av. Ipiranga, 6681, Partenon, Porto Alegre, Rio Grande do Sul 90619-900, Brazil
[e] Programa de Pós-Graduação em Gastroenterologia e Hepatologia, Faculdade de Medicina, Universidade Federal do Rio Grande do Sul, Rua Ramiro Barcelos, 2400, Santana, Porto Alegre, Rio Grande do Sul 90035-003, Brazil
[f] Laboratório de Imunosenescência, Instituto de Pesquisas Biomédicas, Pontifícia Universidade Católica do Rio Grande do Sul, Av. Ipiranga, 6681, Partenon, Porto Alegre, Rio Grande do Sul 90619-900, Brazil.

ARTICLE INFO

Keywords:
Octyl gallate
HepG2 cells
ATP
Mitochondria
Cell cycle arrest
Apoptosis

ABSTRACT

Octyl gallate (OG) is an antioxidant that has shown anti-tumor, anti-diabetic and anti-amyloidogenic activities. Mitochondria play an important role in hepatocellular carcinoma, mainly by maintaining accelerated cellular proliferation through the production of ATP. Thus, the mitochondria may be a target for antitumor therapies. Here, we investigated the effects of OG in the hepatocarcinoma cell line (HepG2) and the mechanisms involved. We report, for the first time, that treatment with OG for 24 h inhibited HepG2 cell growth by decreasing mitochondrial activity and mass, which led to the reduction of ATP levels. This reduction in the energy supply triggered a decrease in Ki67 protein expression, leading cells to cycle arrest. In addition, treatment with two doses of OG for 48 h induced loss of mitochondrial functionality, mitochondrial swelling and apoptosis. Finally, we report that HepG2 cells had no resistance to treatment after multiple doses. Collectively, our findings indicate that metabolic dysregulation and Ki67 protein reduction are key events in the initial anti-proliferative action of OG, whereas mitochondrial swelling and apoptosis induction are involved in the action mechanism of OG after prolonged exposure. This suggests that OG targets mitochondria, thus representing a candidate for further research on therapies for hepatocarcinoma.

1. Introduction

Liver cancer is the second leading cause of cancer death in men and the sixth in women worldwide. Hepatocellular carcinoma (HCC) represents about 70% to 90% of primary liver cancers and its development is related, in most cases, to chronic liver injury, such as cirrhosis. The main HCC risk factors are chronic infection with hepatitis B virus (HBV) or hepatitis C virus (HCV), consumption of food contaminated with aflatoxin, obesity, type 2 diabetes, cirrhosis related to heavy alcohol consumption, nonalcoholic fatty liver disease (associated with obesity) and smoking (Torre et al., 2016).

Although surgical resection, ablation and liver transplantation are

Abbreviations: 7-AAD, 7-Amino-actinomycin D; AIF, Apoptosis-inducing factor; AO, Acridine orange; AOIs, Areas of interest; AVOs, Acidic vesicular organelles; CPD, Cumulative population doubling; DAD, Diode array detector; DAPI, 40,6-diamidino-2-phenylindole; DCFH-DA, 2′, 7′-dichlorodihydrofluorescein diacetate; dNTP, Deoxyribonucleotide triphosphate; GA, Gallic acid; HBV, Hepatitis B virus; HCC, Hepatocellular carcinoma; HCV, Hepatitis C virus; MMP, Mitochondrial membrane permeabilization; MTG, MitoTracker™ Green; MTR, MitoTracker™ Red; OG, Octyl gallate; PD, Population doubling; PI, Propidium iodide; TBARS, Thiobarbiture acid reactive substances; TEM, Transmission electron microscopy

* Corresponding author.
E-mail address: kelly.lima@acad.pucrs.br (K.G. Lima).

https://doi.org/10.1016/j.tiv.2017.12.017
Received 30 September 2017; Received in revised form 9 December 2017; Accepted 22 December 2017
Available online 26 December 2017
0887-2333/

curative options, few patients are eligible for these therapies. The application of these therapeutic options is indicated only in the early stages of the disease and unfortunately most patients are diagnosed at advanced stages (Forner et al., 2012). The only approved drug for systemic treatment use is sorafenib, an oral multikinase inhibitor of serine/threonine-kinases (c-RAF and BRAF) (Ziogas and Tsoulfas, 2017). However, it is only indicated as a palliative treatment and there are reports on resistance acquisition to the drug (Zhai and Sun, 2013). Considering the restricted therapeutic options, the search for new drugs is increasingly necessary.

Several studies have evaluated the antitumor activity of compounds extracted from plants or semi-synthetic derivatives from natural compounds. Among them, gallic acid (GA), a natural plant phenolic acid, has shown anti-tumor effects in several cell lineages (Inoue et al., 1995; Lu et al., 2010; Yoshioka et al., 2000), including hepatocarcinoma cells (HepG2) as shown in our previous study (Lima et al., 2016). Octyl gallate (OG) can be semi-synthetically produced from GA or isolated from fruits of *Terminalia bellerica* (Latha and Daisy, 2013). Octyl gallate differs from the origin molecule only by having eight atoms of carbon in the aliphatic side chain. This structural difference increases its lipophilicity, affinity and permeability through the cell plasma membranes allowing its higher action potential when compared to GA (Locatelli et al., 2013).

Currently, OG is used in food manufacturing as an antioxidant, as well as in the pharmaceutical and cosmetic industries (Locatelli et al., 2013). Studies with OG have shown its antitumor effect in leukemia (Locatelli et al., 2008), melanoma (Locatelli et al., 2009) and B cell lymphoma (Serrano et al., 1998). The described action mechanisms of OG include the induction of oxidative stress associated to NF-kB activation and cell death by apoptosis (Locatelli et al., 2008), induction of apoptosis as a consequence of oxidative stress without association with NF-kB (Locatelli et al., 2009) and induction of apoptosis as a result of DNA fragmentation (Serrano et al., 1998). However, there is no report in the literature evaluating the effect of OG on HCC. Here, we used the HepG2 cell line to investigate the effects of OG and the underlying mechanisms involved. We found that a short treatment period with OG (one dose for 24 h) inhibited cell growth, reduced cellular ATP and Ki67 levels and triggered cell cycle arrest, while treatment with two doses for 48 h induced mitochondria-mediated apoptosis and necrosis.

2. Materials and methods

2.1. Materials

The human hepatocarcinoma cell line (HepG2) was obtained from Rio de Janeiro Cell Bank, UFRJ, Rio de Janeiro, Brazil. DMEM and FBS were obtained from Gibco, Life Technologies. Streptomycin (100 mg/mL) and penicillin (100 units/mL), MitoTracker™ Green and MitoTracker™ Red were obtained from Invitrogen, Carlsbad, CA. Octyl gallate, Trypan blue, DCFH-DA and araldite were supplied by Sigma-Aldrich, USA. The Lactate dehydrogenase kit was obtained from Labtest, Brazil. Transcription Factor Buffer Set was supplied by BD Biosciences, USA. Annexin V Fluorescein (FITC) and Propidium iodide (PI) double staining assay was obtained from Santa Cruz Biotechnology, USA. Antibody against p21 was supplied by Abcam, Cambridge. Antibody against GAPDH and rabbit anti-mouse secondary antibody was supplied by Invitrogen, Carlsbad, CA. Secondary antibody goat anti-rabbit was provided by Cell Signaling, USA.

2.2. Cell culture and treatment

HepG2 cells were cultivated in DMEM supplemented with 10% FBS, 1% streptomycin (100 mg/mL) and penicillin (100 units/mL), 2 g/L HEPES buffer and 3.7 g/L $NaHCO_3$ in humidified atmosphere with 5% CO_2 at 37 °C. Stock solutions of OG were prepared in DMSO and dilutions were prepared in DMEM supplemented with 10% FBS. Cells were cultured for 24 h before treatment in all assays. Control wells contained DMEM, 10% FBS and DMSO 0.2% (vehicle). Cells were treated with 5–100 μM OG for 24 h and 48 h for the trypan blue exclusion assay and 40 μM OG for 24 h for the following assays: Lactate dehydrogenase leakage (LDH), 2′, 7′-dichlorodihydrofluorescein diacetate (DCFH-DA), Thiobarbiture acid reactive substances (TBARS), Catalase, GSH, Cell cycle, Nuclear morphometric analysis (NMA), Ki67, ATP, Acidic vesicular organelle quantification (AVOs), Annexin V/propidium iodide (PI), MitoTracker™ Green (MTG), MitoTracker™ Red (MTR), Ultrastructural analysis by Transmission Electron Microscopy (TEM) and Western blot analysis. Cells were also treated with 40 μM OG for 48 h, replacing medium with OG every 24 h (two doses) for analysis of mitochondrial mass (MTG) and activity (MTR), Annexin V/PI assay and ultrastructural analysis by TEM. For the analysis of resistance to treatment, cells were initially treated with 20 μM OG and 40 μM OG for 24 h. After, cells were harvested, seeded and re-treated with 20 μM OG and 40 μM OG at days 1, 2, 3 and 4, for 24 h. Control wells and no re-treated wells received fresh DMEM with 10% FBS and DMSO 0.2% (vehicle) in the same time interval.

2.3. Trypan blue exclusion assay

Cell viability was evaluated using the Trypan blue exclusion assay. Cells were seeded into 96-well plates (2.5×10^4 cells/well) cultured and treated as aforementioned. For determination of cell number, cells were counted using a hemocytometer under a light microscope (Nikon Optiphot, Japan). Three replicate wells were used at each concentration tested, including control. The IC_{50} was estimated using linear regression with 24 h of treatment and the assay was repeated using the IC_{50}.

2.4. Lactate dehydrogenase (LDH) leakage assay

The LDH assay was used to assess the cytotoxicity of treatment, since leakage of the LDH (cytoplasmic located enzyme) into the extracellular medium is evidence of membrane disruption. Cells were seeded into 96-well plates (2.5×10^4 cells/well), while cultured and treated as aforementioned. Enzyme activity was measured in both supernatants and cell lysate using the colorimetric assay Lactate dehydrogenase kit. For the cell lysis control, DMEM with 5% Tween solution was used. The amount of LDH was calculated by measuring the absorbance at 492 nm using an ELISA microplate reader. The sum of the amount of LDH in the supernatant and in the cell lysate was considered to be 100% of the enzyme content. Then, we calculated the percentage released (i.e. present in the supernatant) based on the total enzyme content.

2.5. Cell cycle

The HepG2 cell cycle was evaluated by 7-AAD as previously described (Krause et al., 2017). Firstly, cells were seeded into 96-well plates at a density of 2.5×10^4 cells per well and cultured and treated as aforementioned. Cells were collected using trypsinization, washed twice with PBS and, while vortexing (to loosen the pellet), 2.5 mL/sample of 70% ethanol was added, drop by drop, into the cell pellet and then incubated for 2 h at − 20 °C. After, the cell pellet was washed twice to remove ethanol: the first wash in PBS and the second in Stain Buffer. Then, cells were centrifuged and the supernatant was discarded. Next, the pellet was re-suspended in 100 μL of Stain Buffer and 4 μL of 7-AAD was added prior to incubation for 15 min at room temperature. Flow cytometry was then used to analyze the samples and identify the cell cycle phases. Data were analyzed using FlowJo 7.6.5 software (Tree Star Inc., Ashland OR). Analysis allows discrimination between Sub-G1, G0/G1, S and G2/M.

2.6. Nuclear morphometric analysis (NMA)

Analysis of the nuclear size and irregularity was performed to

further investigate the mechanism of cellular toxicity related to the treatment. Cells were seeded at a cell density of 5×10^4 cells per well in 24-well plates and cultured and treated as aforementioned. Two replicate wells were used for both the tested concentration and control. Cells were fixed with 4% paraformaldehyde for 2 h. Then, fixed cells were permeabilized with 0.3% Triton X-100 in PBS for 30 min and subsequently marked with a solution containing 300 nM DAPI for 2 min. The incubations were performed at room temperature and images were acquired using Olympus Q Color 3 camera coupled to a fluorescence microscope (IX71, Olympus). The nuclear morphometric analysis was performed using the Image Pro Plus 6.0 software (IPP6–Media Cybernetics, Silver Spring, MD). The percentages of normal, small and regular, large and regular and irregular nuclei were determined by measuring the nucleus area and identifying the nuclear morphometry (aspect, area box, radius ratio and roundness), which were combined into a single nuclear irregularity index (NII). Different nuclear phenotypes were separated in an area versus NII plot and control cell nuclei were used to set the normal parameters (Filippi-Chiela et al., 2012).

2.7. Ki67 staining

Ki67 intracellular staining was performed using the Transcription Factor Buffer Set, according to the manufacturer's instructions. Cells were seeded into 96-well plates (2.5×10^4 cells/well), cultured and treated as aforementioned. A positive control with 40 μM cisplatin was used with the same treatment time. Two replicate wells were used for both the tested concentration and control. Cells were acquired on FACSCanto II (BD Biosciences) with BD FACSDiva software (BD Biosciences). The data obtained were analyzed using Flowjo software (version 10, TreeStar).

2.8. Western blot analysis

Approximately 5×10^5 cells were seeded in a 6-well plate, cultured and treated as aforementioned. Cells were rinsed twice with PBS and lysed with CHAPS lysis buffer. Aliquots from each sample containing 20 μg protein were run on a 10% sodium dodecylsulphate polyacrylamide gel, and transferred to a nitrocellulose membrane. After the transfer, blots were blocked with Tris buffered saline containing 0.05% Tween-20 and 5% non-fat dry milk for 1 h and subsequently incubated overnight at 4 °C with primary antibodies against p21 (ab7960, Abcam) at 1:200 and GAPDH (39-8600, Invitrogen) at 1:1000 dilution. Then, membranes were incubated with the appropriate horseradish peroxidase-conjugated secondary antibodies (1:1000) at room temperature for 1 h. Blots were revealed by chemiluminescence and digital images were taken in a Carestream Gel Logic 2200 PRO Imaging System. Protein expression was determined in NanoDrop Lite (Thermo Fisher Scientific®) and Image Studio Lite software (LI-COR). Quantitative densitometric values of all proteins were normalized to GAPDH (de Mesquita et al., 2017).

2.9. Measurement of ATP by HPLC

The culture medium was removed by aspiration after the treatment period, followed by immediate addition of 1 mL of ice-cold 0.4 M perchloric acid. The culture plates were tightly sealed with Parafilm and cooled at − 80 °C for 30 min. Cell lysates were thawed on ice, scraped off the plates thoroughly, and transferred to 1.5 mL microtubes. Samples were centrifuged at 14,000 rpm for 10 min at 4 °C. Pellets were set aside for protein measurements in NanoDrop Lite (Thermo Fisher Scientific®). The supernatants were neutralized with 10 μL of 4 M K_2CO_3 added to 100 μL of the supernatant, kept for 10 min on ice and for 1 h at − 80 °C to promote precipitation of the perchlorate, and then centrifuged again at 14,000 rpm for 10 min at 4 °C. Supernatants were stored at − 80 °C until the HPLC assay (Manfredi et al., 2002). Samples were thawed and twenty microliters was injected into the HPLC system (all HPLC components and software ChemStation were from Agilent Technologies®). Chromatographic separations were performed using a reverse-phase column (150 mm × 4 mm, 5 μm Agilent® 100 RP-18 ec). The column was protected by a guard column (4 × 4 mm, 5 μm Agilent® 100 RP-18 ec), and was maintained at room temperature. The flow ramp of methanol: 60 mM KH_2PO_4 with 5 mM tetrabutylammonium chloride (pH 6.0) (13:87, *v*/v) mobile phase was maintained between 1.2 and 2.0 mL/min according to the retention time of each compound. The mobile phase was prepared daily due to low stability. Absorbance was monitored at 260 nm with a diode array detector (DAD) (Leite et al., 2013). Results were expressed as cellular ATP percentage in relation to control (considered as 100%).

2.10. DCFH-DA assay

To measure the reactive species levels, we performed the DCFH-DA assay. The 2′,7′-dichlorofluorescin diacetate (DCFH-DA) is a non-fluorescent compound, which is converted to highly fluorescent 2′,7′-dichlorofluorescin upon oxidation by oxygen or nitrogen reactive species. For this, 2.5×10^4 cells were seeded in 96-well plates and cultured and treated as aforementioned. Cells were harvested, washed once with PBS and incubated with 10 μM DCFH-DA (in PBS) for 30 min at 37 °C. The fluorescence intensity was monitored with a VICTOR® microplate reader (PerkinElmer) at an excitation wavelength of 485 nm and an emission wavelength of 520 nm. Results were expressed as fluorescence/10,000 cell.

2.11. Thiobarbituric acid reactive substances

The cell lysate was used to determine the concentrations of thiobarbituric acid reactive substances (TBARS). Cells were seeded into 6-well plates at a density of 5.0×10^5 cells per well and cultured and treated as aforementioned. Cells were harvested, re-suspended in PBS and sonicated for 2 h. The compound resulting from the reaction between thiobarbituric acid and malondialdehyde was measured at 535 nm using Spectrophotometer (Draper and Hadley, 1990). Results were corrected by cell number and expressed as TBARS nM/10,000 cells.

2.12. Catalase assay

Catalase activity was measured using a reagent containing 102 μL of H_2O_2 at 30%, 100 μL of Triton × 100 and 100 mL of PBS. Cells were seeded into 6-well plates at a density of 5.0×10^5 cells per well and cultured and treated as aforementioned. Cells were harvested, re-suspended in PBS and sonicated for 2 h. The cell lysate was added to the reagent heated at 37 °C and the decrease in H_2O_2 was measured after 1 min at 240 nm using Spectrophotometer. Results were corrected by cells number and expressed as UCAT/10,000 cells.

2.13. GSH

The GSH concentration was measured in the lysate cell using the method recommended by (Beutler et al., 1963). In this method, reduced thiols (GSH represents 95% of these thiols) react with 2-dinitrobenzoic acid (DTNB) to form a yellowish thiolate measurable at 412 nm. Cells were seeded and lysed as described for the Catalase assay and the lysate kept on ice until analysis (performed on the same day). Cells were cultured and treated as aforementioned. The cell lysate was added to a precipitating solution (1.67 g metaphosphoric acid, 0.2 g disodium EDTA, 30 g NaCl and distilled water q.s 100 mL) and, after 5 min, centrifuged at 1500 rpm for 5 min. An aliquot of the supernatant was added to a solution of Na_2HPO_4 300 mmol·L^{-1}. After homogenization, 0.05% DTNB solution was added to the system and measured at 412 nm using a Spectrophotometer. The blank value of the reagent was

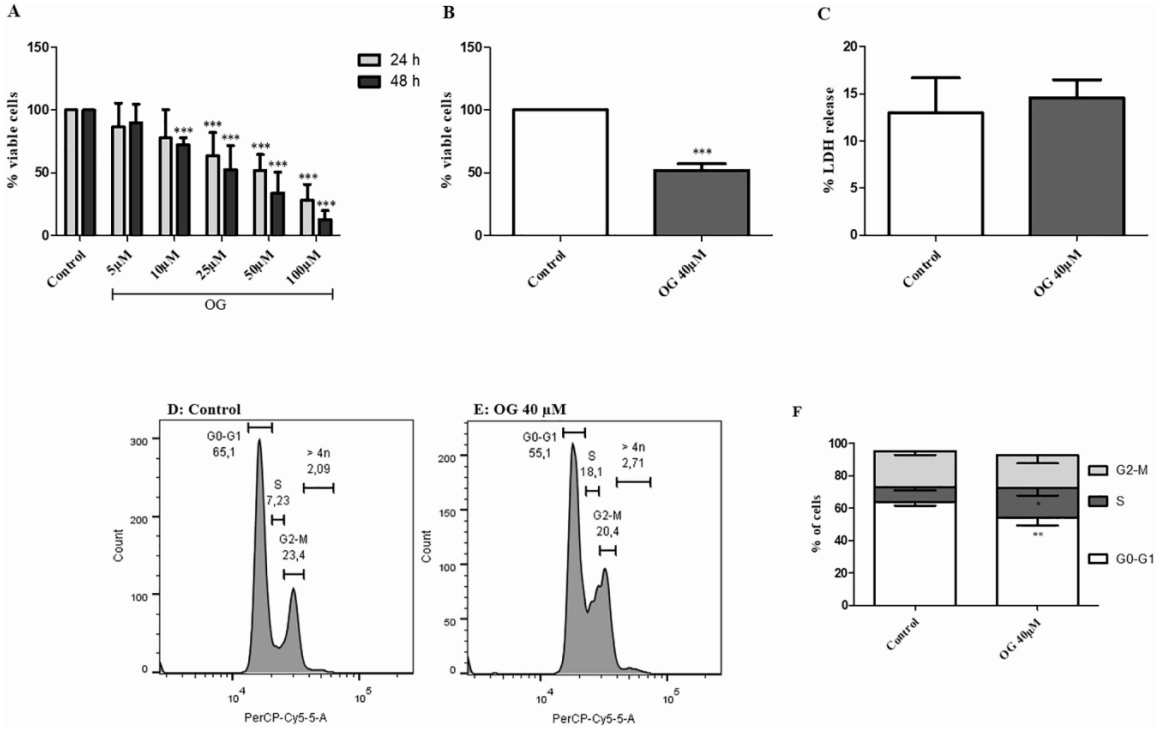

Fig. 1. Effect of OG on HepG2 cell viability at 24 h and 48 h (1A). Effect of OG IC50 on HepG2 cell viability at 24 h (1B). Cell number was assessed by direct cell counting. Results are expressed as number of cells in relation to control (considered as 100%). Data are represented as the mean ± SD from eight (A) and five (B) independent experiments (***$p < 0.0001$ vs control). Citotoxicity of OG treatment in HepG2 cells after 24 h (1C). Results are expressed as percent of lactate dehydrogenase release in the supernatant. Data are represented as the mean ± SD from four independent experiments. Effect of OG on the HepG2 cell cycle after 24 h (1D, 1E, 1F). Representative flow cytometric plots: control (1D) and OG 40 μM (1E). Cell cycle distribution (1F). Results are expressed as percentage of cells. Data are represented as the mean ± SD from four independent experiments (*$p < 0.05$, ** $p < 0.01$).

discounted from the sample measurement. The values obtained were corrected by the number of cells. GSH concentration was expressed as optical density/100,000 cells.

2.14. Acidic vesicular organelle (AVOs) quantification

Acridine orange (AO) is an AVO marker that fluoresces green in the whole cell except in the acidic compartments (mainly late autophagosomes), where it fluoresces red. Cells were seeded as described for the Lactate dehydrogenase (LDH) leakage assay. Cells were cultured and treated as aforementioned. To quantify the percentage of cells with AVOs and the intensity of red fluorescence, treated cells were detached from the plate, incubated with 2.7 μM of AO for 15 min at room temperature and analyzed using BD FACSCanto II flow cytometer (BD Biosciences, USA) and GUAVA software ExpressPlus (Guava Technologies, Hayward, CA) (Filippi-Chiela et al., 2013; Thomé et al., 2016).

2.15. Analysis of mitochondrial mass and activity by fluorometry

MitoTracker™ Red (MTR) and MitoTracker™ Green (MTG) are widely used to stain the mitochondria of live cells depending, respectively, on the oxidative activity (mitochondrial membrane potential) and organelle lipid content (mitochondrial mass). Therefore, it was possible to establish a relationship between MTR and MTG staining to assess the rate of mitochondrial function: if MTG fluorescence is higher than MTR fluorescence, this may represent the mitochondrial swelling that characterizes organelle function failure (Agnello et al., 2008). Briefly, after OG treatment (40 μM 1 dose and 2 doses), HepG2 cells were washed in PBS saline and harvested using trypsin. Then, cells were re-suspended and incubated for 20 min in the dark with 100 nM of MTG and MTR that were diluted into PBS. The cellular fluorescence was measured using BD FACSCanto II flow cytometer (BD Biosciences, USA). Then, two analyses were performed. Firstly, the mean of fluorescence of MTR and MTG were expressed as units of fluorescence compared to control (control = 1); then a ratio between MTR and MTG fluorescence was calculated to establish a correlation between them (Meira Martins et al., 2015). To illustrate these variations in fluorescence, three gates were superimposed on the flow cytometer dot plot and the percentage of cells inside them was measured. The “negative cells” gate included dead cells that were not stained with MTR or MTG; the “lower fluorescence” gate included live cells that were stained with MTR or MTG but presented lower fluorescence intensity; the “higher fluorescence” gate included live cells that were stained with MTR or MTG and presented higher fluorescence intensity. Finally, a diagonal gate was used as a parameter to evaluate the displacement of co-stained cells to the gate whose cells had higher MTG fluorescence intensity than MTR fluorescence intensity, which is an indication of mitochondrial swelling. All analyses were performed using Flowjo software (version 10, TreeStar).

2.16. Ultrastructural analysis by transmission electron microscopy (TEM)

To analyze the treated and control cells using transmission electron microscopy (TEM), semi-confluent HepG2 cells were collected using trypsinization. The cells were harvested by centrifugation and washed twice after phosphate buffered saline (pH 7.2) addition. Then, cells were fixed in a mixture of 4% paraformaldehyde and 2.5% glutaraldehyde buffered with 0.1 M phosphate (pH 7.3) at room temperature, and then postfixed in osmium tetroxide in the same buffer for 45 min

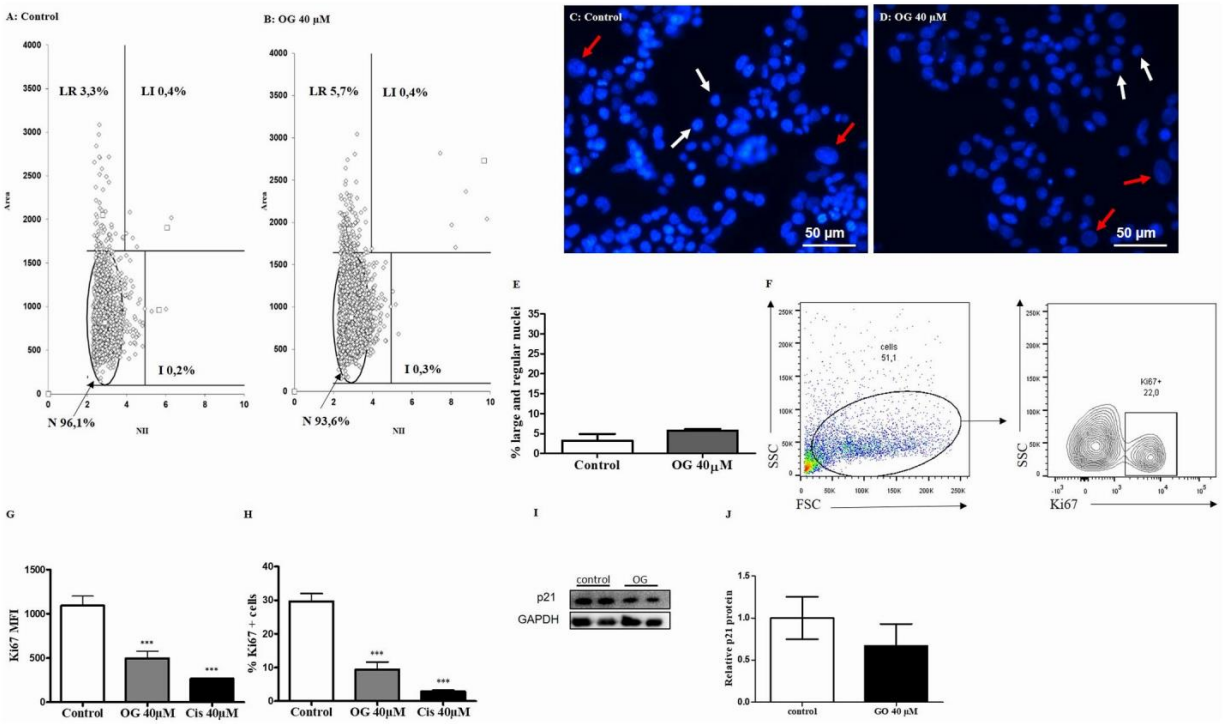

Fig. 2. Effect of OG on the nuclear morphometry of HepG2 cells after 24 h of treatment (2A, 2B). Images were obtained by fluorescence microscopy. At least 200 nuclei in four independent experiments were analyzed at each data point. DAPI-stained nuclei were analyzed for size and irregularity and the percentages of normal (N), large and regular (LR), large and irregular (LI) and irregular (I) nuclei are shown (2A, 2B). Representative images of nuclei from control cells (2C) and treated cells with OG (2D). The red arrows show the large and regular nuclei (LR) and white arrows show normal nuclei. Percentage of large and regular (LR) nuclei (2E). Data are represented as the mean ± SD from three independent experiments. Representative gate strategy for Ki67 expression as measured by flow cytometry (2F). The first gate was performed to exclude debris and the second gate to select the cells with high fluorescence (Ki67 +). Effect of OG on the Ki67 expression of HepG2 cells after 24 h (2G, 2H). Results are expressed as Ki67 mean fluorescence intensity (MFI) (2G) and percentage of Ki67 positive cells (2H). Data are represented as the mean ± SD from three independent experiments (***$p < 0.0001$). Expression of p21 protein in HepG2 cells after 24 h of treatment with 40 µM OG by Western blot analysis (2I). GAPDH was used to normalize protein expression. Protein levels (fold induction) of the expression of p21 in HepG2 cells after 24 h of treatment with 40 µM OG ($p = 0.12$) (2 J). Data are represented as the mean ± SD of 3 independent experiments. (For interpretation of the references to color in this figure legend, the reader is referred to the web version of this article.)

before dehydration. After, they were dehydrated in a graded acetone series (30–100%) and embedded in araldite (Durcupan ACM, Fluka) for 72 h at 60 °C. Thin sections (70 nm) were stained with 2% uranyl acetate followed by lead citrate (Meira Martins et al., 2015). Ultrastructural analysis was performed on the control (DMSO 0.2%) and treated cells (OG 40 µM 1 and 2 doses) using the Tecnai G2 T20, FEI transmission electron microscopy and Image Pro Plus software (Image Pro Plus 6.1, Media Cybernetics, Silver Spring, EUA). The analyses were performed by two blinded specialists in image analysis, planar morphometry and stereology. The morphological evaluation was performed using TEM images as described below.

2.16.1. Mitochondrial and autophagosome densities

To estimate Mitochondrial and autophagosome densities, a quantitative analysis, similar to the Neubauer chamber was performed. Briefly, randomized squares measuring 3.0 µm^2, named areas of interest (AOIs), were overlaid on each image (4500 ×), and mitochondria and autophagosomes located inside each square or intersected by the upper and/or left edges of the squares were counted. Mitochondria and autophagosomes intersected by the lower and/or right edges of the squares were not counted (de Senna et al., 2017). On average, 7 AOIs were analyzed in each cell and 10 cells were analyzed per group.

2.16.2. Mitochondrial area

The total mitochondrial area and the mitochondrial area without crests were calculated using a stereological tool, the point counting method (Fernandes et al., 2016; Ilha et al., 2008; Lazzarotto Rucatti et al., 2015; Weibel, 1979; Zacharová and Kubínová, 1995). A grid mask (a grid of crosses with equidistant intervals) with an area/point value of 6518.5 nm^2, was placed over the mitochondria images. When the upper right quadrant of the cross hit images of mitochondria and of mitochondrial crests they were counted. The difference between these two counts was used to estimate mitochondrial area without crests. Areas were obtained using the following equation: $\hat{A} = \Sigma p.a/p$, where $\hat{A}$ is the area, Σp is the sum of points counted, and a/p is the area/point value. On average, 12 mitochondria were analyzed in each cell, and 6 cells were analyzed per group.

2.16.3. Gray scale analysis of mitochondria

The electron density of mitochondria was measured using gray scale analysis (Xavier et al., 2005). The same images used for estimation of the mitochondrial area were used in the analysis of regional gray scale (255 shades of gray). One or two equal-sized areas of interest (AOIs) measuring 6849.5 nm^2 were overlaid on each mitochondria to measure gray scale. The image analysis software determines the gray scale of the AOIs based on the pixels in the digitized images. According to this method, 0 = absolute black and 255 = absolute white. Thus, an increase in gray scale indicates lower electron density that correlates with loss of mitochondrial crests.

2.16.4. Mitochondrial shape Z

The shape coefficient, also known as the shape Z (García-Fiñana

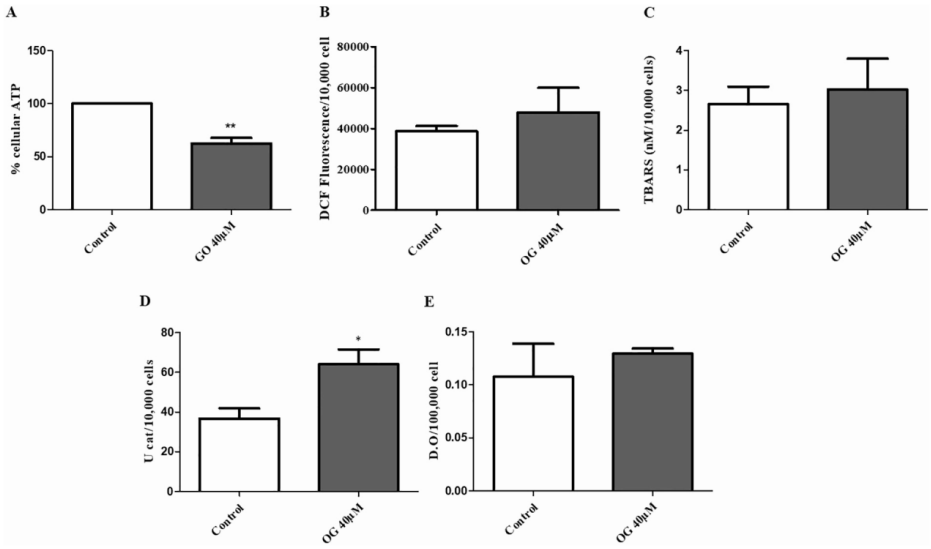

Fig. 3. Effect of OG on ATP in HepG2 cells after 24 h (3A). Cellular ATP was measured using HPLC. Results are expressed as % cellular ATP in relation to control (considered as 100%). Data are represented as the mean ± SD from three independent experiments (**$p < 0.01$). Effect of OG treatment on oxidative stress of HepG2 cells after 24 h (3B, 3C, 3D, 3E). Results are expressed as DCF Fluorescence/10^4 cells (3B); TBARS nmol/10^4 cells (3C); Unit of catalase (Ucat)/10^4 cells (3D); Optical density/1 × 10^5 cells (GSH) (3E). Data are represented as the mean ± SD from three independent experiments (*$p < 0.05$ vs control).

et al., 2003; Kiêu et al., 1999; Matheron, 1971; Mathieu et al., 1981), was used to determine the elongation of the mitochondria. This parameter is obtained using the following equation: Shape Z = P/√Â, where Shape Z is the shape coefficient, P is the perimeter, and Â is the area value. The same images used for estimation of the mitochondria area were used in the analysis of Shape Z. Mitochondria were delineated and the perimeter and area measurements were used to calculate Shape Z. Low Shape Z values indicate a more rounded mitochondria, while high values indicate more elongated mitochondria.

2.17. Apoptosis assay by Annexin V-FITC and PI staining

Annexin V Fluorescein (FITC) and Propidium iodide (PI) double staining assay was performed to quantify cell death by apoptosis or necrosis using BD FACSCanto II flow cytometer (BD Biosciences, USA). Cells were seeded into 96-well plates at a density of 2.5 × 10^4 cells per well. After, cells were cultured and treated as aforementioned. For positive controls, cells were treated with 40 µM cisplatin for 24 h and 20 µM cisplatin for 48 h. After treatment, cells were harvested, washed with ice-cold PBS, re-suspended in 100 µL of binding buffer (10 mM Hepes/NaOH (pH 7.4), 140 mM NaCl, 2.5 mM $CaCl_2$) at a cell density of 1 × 10^6 cells/mL. Then, cells were incubated with 4 µL of Annexin V FITC and 2 µL of PI for 15 min at room temperature in the dark. The samples were then analyzed using flow cytometry. Data were analyzed using FlowJo 7.6.5 software (Tree Star Inc., Ashland OR). Analysis allows discrimination between live cells (Annexin V-/PI-), early apoptotic cells (Annexin V + /PI-), late apoptotic cells (Annexin V + /PI +) and necrotic cells (Annexin V-/PI +).

2.18. Treatment resistance analysis

The cumulative population doubling (CPD) assay was used to evaluate the proliferation rate and the regrowth of HepG2 cells after OG treatment, as previously described (Filippi-Chiela et al., 2015). Approximately 5 × 10^5 cells were seeded in a 6-well plate, cultured and treated as aforementioned. After, the cells were harvested and seeded at a density of 12 × 10^4, 9 × 10^4, 6 × 10^4 and 3 × 10^4 cells per well in 24-well plates and incubated for 24 h at 37 °C in a 5% CO_2 incubator. The cells were retreated as previously described, and then counted. The number of viable cells was determined by mixing 25 µL of cell suspension and 25 µL of 0.4% trypan blue stain solution (Sigma-Aldrich, USA), using a hemocytometer under a light microscope (Nikon Optiphot, Japan). Trypan positive cells (blue) were counted as dead cells and the unstained cells were counted as live. The cells were counted on the second, third, fourth and fifth days after seeding. Population doubling (PD) at each interval was determined according to the formula PD = [log N(t) − log N(to)] / log 2, where N(t) is the number of cells at the time count, and N(to) is the number of cells seeded. The sum of PDs was then plotted against time of culture.

2.19. Data and statistical analysis

All results are presented as mean ± SD from three to eight independent experiments. The Student's *t*-test was used for comparisons between groups in the assays: Trypan blue exclusion (comparison between control and IC50), LDH release, Cell cycle, Nuclear Morphometric Analysis, ATP, DCFH-DA, TBARS, GSH, Catalase and Western blot. One-way analysis of variance (ANOVA) followed by Tukey's multiple comparison post-test was used for comparisons between groups in the assays: Trypan blue exclusion (dose curve), Ki67 expression, Acridine orange, MitoTracker™ Green, MitoTracker™ Red, Ultrastructural analysis (TEM), Annexin V/PI and treatment resistance analysis. A p value < 0.05 was considered statistically significant. Statistical analyses were performed using GraphPad Prism 5.0 (GraphPad Software, San Diego, CA).

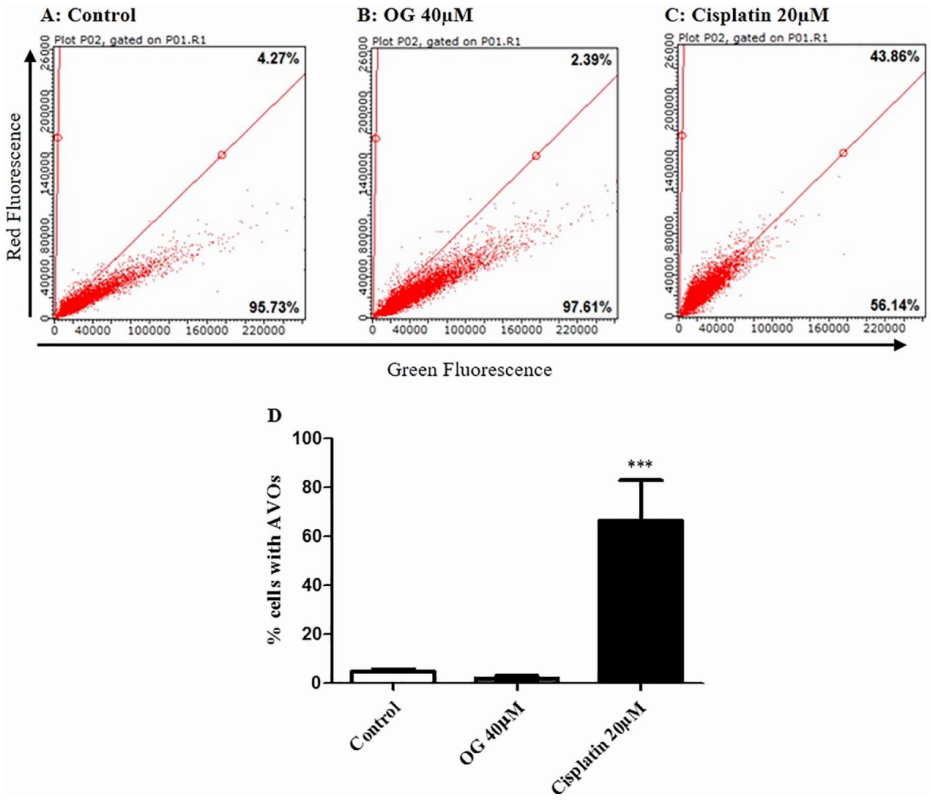

Fig. 4. Effect of OG in Autophagy. Representative flow cytometric plots Green Fluorescence/Red Fluorescence (4A, 4B, 4C). Control (4A), cells exposed to 40 µM OG for 24 h (4B), cells exposed to 20 µM cisplatin (positive control) for 24 h (4C). Results are expressed as percentage of cells with acidic vesicular organelles (AVOs) (4D). The AVOs are represented by autolysosomes and lysosomes. Data are represented as the mean ± SD from three independent experiments (***p < 0,001 vs control). (For interpretation of the references to color in this figure legend, the reader is referred to the web version of this article.)

3. Results

3.1. Octyl gallate decreases HepG2 cell viability

The treatment of HepG2 cells with different concentrations of OG decreased the percentage of viable cells in a time- and dose-dependent manner ($p < 0.0001$; Fig. 1A). After this initial experiment on cellular viability, we selected 40 µM of OG to continue the experiments, as this dose reduced cell viability by approximately 50% (IC_{50}) in 24 h ($p < 0.0001$; Fig. 1B).

3.2. OG did not cause necrosis following 24-h of treatment

LDH release is a typical feature of cell necrosis (Huang et al., 2013). The LDH release from HepG2 cells treated with 40 µM OG for 24 h was measured to determine whether necrosis was involved in the OG-induced decrease in cell viability. As shown in Fig. 1C, there was no significant difference in LDH release compared to the untreated control ($p = 0.45$).

3.3. Octyl gallate induces cell cycle arrest of HepG2 cells without producing senescence

Since OG reduced cell viability, the effects of OG on the cell cycle were examined. Representative histograms are shown in Fig. 1D (control) and Fig. 1E (OG 40 µM). Cell cycle analysis showed that OG increased the percentage of cells in the S phase after 24 h of treatment ($p < 0.05$; Fig. 1F), causing cell cycle arrest. Considering that cellular senescence is the state of permanent cell cycle arrest (Takahashi et al., 2007), we evaluated if senescence could be involved in the OG induced cell cycle arrest. The percentage of large and regular (LR) nuclei are shown in Fig. 2A (control) and Fig. 2B (OG 40 µM). Representative images of nuclei are shown in Fig. 2C (control) and Fig. 2D (treated cells). As shown in Fig. 2E, there was no significant difference in percentage of large and regular nuclei (indicative of senescence) compared to the untreated control ($p = 0.18$). These data suggest that the reduction in viable cells is related to the inhibition of proliferation by cell cycle arrest in the absence of senescence.

3.4. Octyl gallate reduces Ki67 expression in HepG2 cells

Since OG caused cell cycle arrest, the effects of OG on Ki67 protein expression were investigated. The representative gate strategy for Ki67

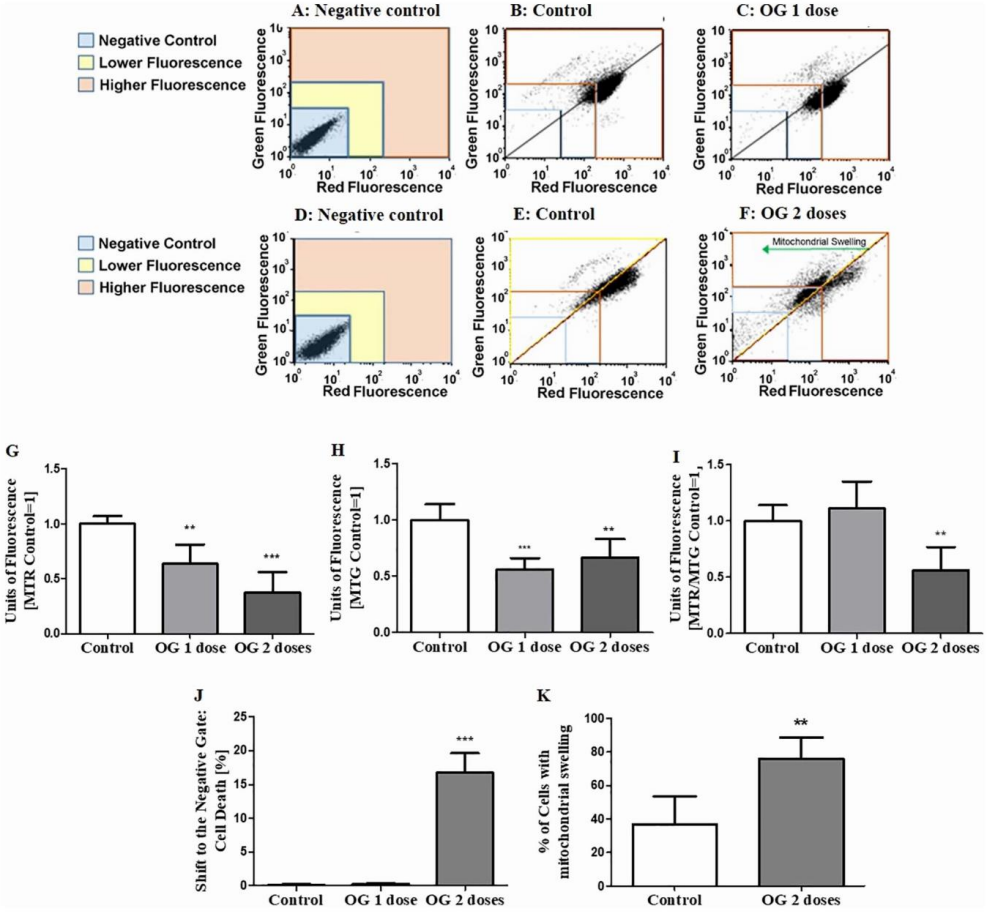

Fig. 5. The evaluation of mitochondrial function (MTR) and mass (MTG) after treatment with 40 μM OG (1 dose and 2 doses every 24 h). Representative flow cytometric plots: negative control without staining (5A, 5D), control (5B, 5E), OG 40 μM 1 dose (5C) and 40 μM OG 2 doses (5F). The increase in the percentage of cells present in the "lower fluorescence" gate (data not shown) in the HepG2 treated cells (1 and 2 doses) corroborated the results in the MTR and MTG units of fluorescence decrease (5G, 5H). The ratio between MTR and MTG units of fluorescence (5I) indicated the loss of mitochondrial function only in cells treated with 2 doses, indicating mitochondrial swelling (5 K). A shift to the negative gate (5J) indicated cell death with 2 doses of OG. Data are represented as the mean ± SD from three independent experiments (**$p < 0.01$, ***$p < 0.0001$).

expression is shown in Fig. 2F. As shown in Fig. 2G and H, OG reduced Ki67 protein expression and the percentage of Ki67 positive cells ($p < 0.0001$), confirming the inhibition of cell proliferation and the involvement of Ki67 in cell cycle arrest in the S phase.

3.5. Octyl gallate did not increase p21 expression

A previous study showed that decreased Ki67 expression can lead to increased p21 expression depending on the cell type (Sun et al., 2017). Thus, we investigated if increased p21 expression could be related to cell cycle arrest caused by OG. However, our findings showed no change in p21 expression after treatment with 1 dose of OG for 24 h. ($p = 0.12$; Fig. 2I and J).

3.6. Octyl gallate decreased cellular ATP

Since OG reduced the proliferation by inducing cell cycle arrest and decreasing Ki67 protein levels, we evaluated whether these effects could be involved with alteration of energetic metabolism. As shown in Fig. 3A, OG significantly reduced the cellular ATP levels after treatment for 24 h ($p < 0.01$). This data indicates that the cellular ATP decrease is involved in the cell cycle arrest.

3.7. Oxidative stress is not involved in the antiproliferative effects of octyl gallate

A previous study on OG showed that increased oxidative stress is involved in the loss of mitochondrial membrane potential and the consequent mitochondrial dysfunction (de Cordova et al., 2011). Thus, we investigated if oxidative stress could reduce ATP levels. Treatment with OG increased catalase levels ($p < 0.05$; Fig. 3D) without altering the levels of reactive species ($p = 0.25$; Fig. 3B), TBARS ($p = 0.51$; Fig. 3C) and GSH ($p = 0.32$; Fig. 3E).

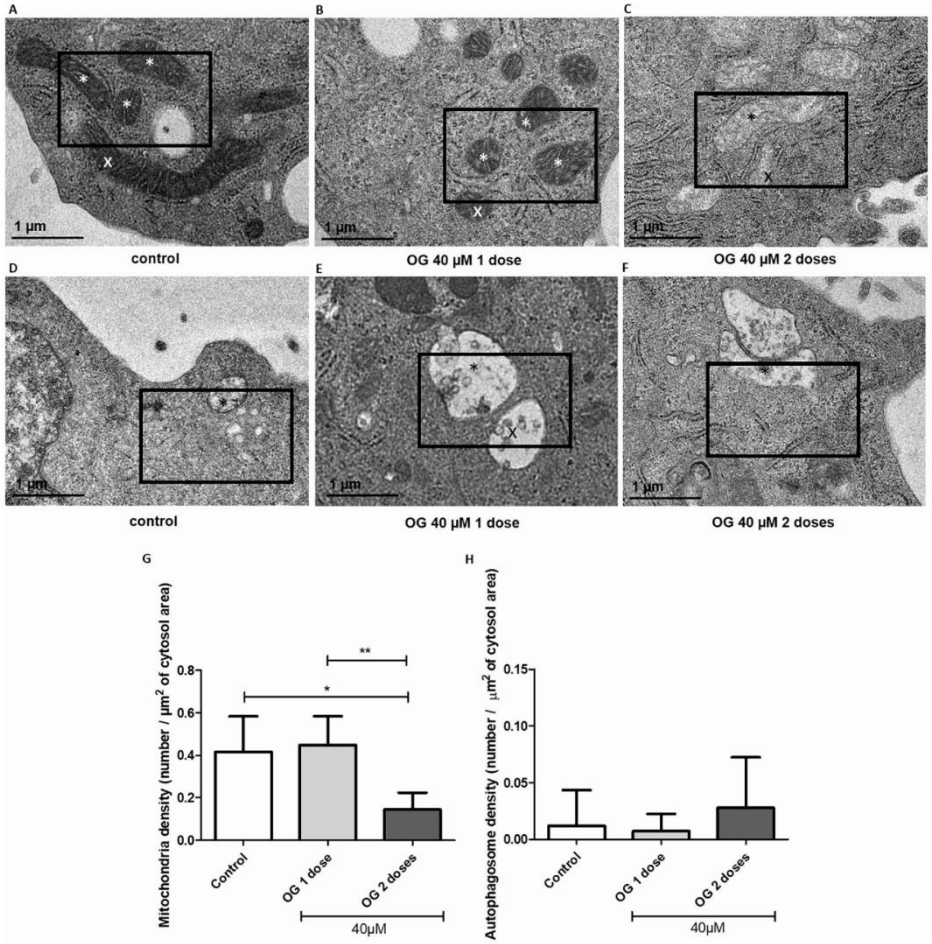

Fig. 6. Ultrastructural analysis of HepG2 (mitochondrial and autophagosome densities). Digitized images of HepG2 cells with and without treatment showing the arrangement of AOIs 3.0 µm² (black box) overlaying the images. Representation of one of the fields (AOIs) used in the study to evaluate mitochondrial and autophagosome densities (black box). The mitochondria and autophagosomes located inside this square or intersected by the upper and/or left edge of the AOI were counted (*); the mitochondria and autophagosome intersected by the lower and/or right edge of the AOI were not counted (x). Control (6A, 6D), OG 40 µM 1 dose (6B, 6E) and OG 40 µM 2 doses (6C,6F). (Calibration bar = 1 µm). Panels 6A, 6B and 6C show mitochondrial density estimation and panels 6D, 6E and 6F show autophagosome density estimation. Transmission electron microscopy images revealed that treatment with 2 doses 40 µM OG decreases mitochondrial density (6G) without changes in autophagosome density (6H). Results are expressed as number of mitochondria and autophagosome per µm² of cytosol area (6G, 6H). Data are represented as the mean ± SD from three independent experiments (*$p < 0.05$; **$p < 0.01$).

3.8. Autophagy is not involved in the antiproliferative effects of octyl gallate

Autophagy is generally induced by limitations in ATP availability or a lack of essential nutrients (Zhou et al., 2017). Thus, we evaluated whether the decrease in ATP could be involved in autophagy induction. Representative flow cytometric plots are shown in Fig. 4A (control), Fig. 4B (OG 40 µM) and 4C (cisplatin 20 µM). As shown in Fig. 4D, only the positive control (cisplatin 20 µM) showed autophagy induction ($p < 0.001$).

3.9. Octyl gallate induces mitochondrial swelling only in prolonged treatment

Since treatment with OG decreased cellular ATP levels, we evaluated the mitochondrial function in cells treated with one and two doses of 40 µM OG by staining organelles with MTR and MTG, two probes that have affinity for mitochondrial membrane potential and mitochondrial mass, respectively. Interestingly, treatment with one dose induced a decrease in the relative MTR ($p < 0.0001$; Fig. 5G) and MTG fluorescence ($p < 0.001$; Fig. 5H), but only treatment with two doses reduced the ratio between MTR and MTG ($p < 0.001$; Fig. 5I). These results suggest a reduction in the mitochondrial number in cells treated with one dose of OG (24 h) and an increase in the number of

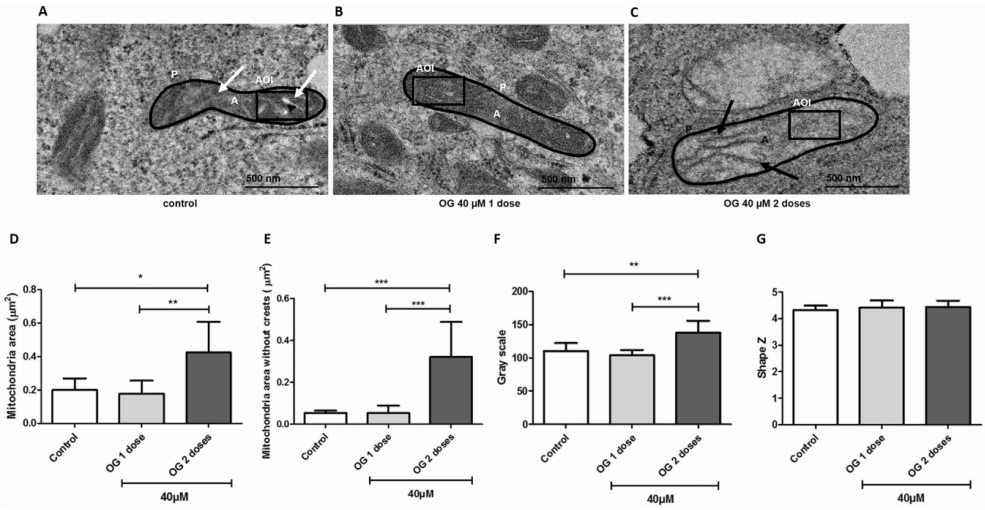

Fig. 7. Ultrastructural analysis of HepG2 cells (Mitochondrial area, Mitochondrial area without crests, Gray scale and Shape Z). Transmission electron microscopy images revealed that treatment with 2 doses 40 µM OG altered the organelle morphology by promoting cristae disruption and swelling (7C). Digitized images of HepG2 cells with and without treatment. Control (7A), OG 40 µM 1 dose (7B) and OG 40 µM 2 doses (7C). Legends: A: area, P: perimeter, AOI: areas of interest, white arrows (normal crests), black arrows (cristae disruption). Calibration bar = 500 nm. Results are expressed as mitochondrial area in μm^2 (7D), mitochondrial area without crests in μm^2 (7E), gray scale (7F) and Shape Z coefficient (Shape Z = P/$\sqrt{A}$, where Shape Z is the shape coefficient, P is the perimeter, and Â is the area value) (7G). Data are represented as the mean ± SD from three independent experiments. Note that to facilitate figure observation, the point grid used to estimate the mitochondrial area, mitochondrial area without crests is not presented in this figure (* $p < 0.05$, ** $p < 0.01$, *** $p < 0.001$).

swollen and non-functional mitochondria after prolonged treatment with OG (two doses, 48 h; Fig. 5K).

3.10. Ultrastructural analysis confirmed mitochondrial swelling and showed reduction of mitochondrial density only in prolonged treatment

To confirm mitochondrial swelling and to evaluate the effect of OG on the density of mitochondria and autophagosomes, we performed ultrastructural analysis of HepG2 cells. Transmission electron microscopy images revealed that treatment with 2 doses 40 µM OG decreased mitochondrial density ($p < 0.05$; Fig. 6G) without changes in autophagosome density ($p = 0.30$; Fig. 6H). Moreover, ultrastructural analysis of HepG2 cells confirmed the findings of the flow cytometry with MTR and MTG staining, since it revealed that treatment with 2 doses 40 µM OG altered the organelle morphology by promoting an increase in mitochondrial area ($p < 0.05$; Fig. 7D); cristae disruption, represented by mitochondrial area without crests ($p < 0.0001$; Fig. 7E); gray scale ($p < 0.001$; Fig. 7F) and mitochondria swelling (representative Fig. 7C). However, no change was found change in the Shape Z ($p = 0.53$; Fig. 7G).

3.11. Octyl gallate induces late apoptosis and necrosis in HepG2 cells only in prolonged treatment

Since our experiments showed mitochondrial dysfunction, we investigated whether cell death by apoptosis or necrosis could be the outcome of the OG mechanism. Representative flow cytometric plots (24-h of treatment) are shown in Fig. 8A (control), Fig. 8B (OG 40 µM) and Fig. 8C (cisplatin 40 µM). As shown in Fig. 8E and F, only the positive control (cisplatin 40 µM) induced at early apoptosis ($p < 0.05$) and late apoptosis ($p < 0.05$) at 24 h of treatment. Representative flow cytometric plots (2 doses OG every 24 h) are shown in Fig. 9A (control), Fig. 9B (OG 40 µM) and Fig. 9C (cisplatin 20 µM). Interestingly, longer treatment (2 doses OG every 24 h) induced late apoptosis ($p < 0.01$; Fig. 9F) and necrosis ($p < 0.05$; Fig. 9G), which is in accordance with the results of the ultrastructural analysis.

3.12. Chronic octyl gallate treatment suppresses the long-term regrowth of HepG2 cells

We evaluated the long-term response of HepG2 cells exposed to treatment with single or multiple doses of OG. The cells were counted on the second, third, fourth and fifth days after seeding, as shown in Fig. 10A. Treatment with either a single dose or half dose of 40 µM OG did not suppress HepG2 cell regrowth during the period of analysis. On the other hand, retreatment with either multiple doses of 40 µM or a half dose of 20 µM lead to a stable arrest of cell growth and a reduction of cumulative population doubling on the fifth day of analysis (*$p < 0.05$, **$p < 0.01$, *** $p < 0.0001$; Fig. 10b).

4. Discussion

The effects of the antioxidant octyl gallate have been studied in some in vitro and in vivo models considering the treatment of leukemia (Locatelli et al., 2008), melanoma (Locatelli et al., 2009), B-cell lymphoma (Serrano et al., 1998), diabetes (Latha and Daisy, 2013) and Alzheimer's disease (Zhang et al., 2013). These studies showed that OG was able to reduce the growth of tumor cells (Locatelli et al., 2009, 2008; Serrano et al., 1998), increase insulin secretion in the β cells of the pancreas (Latha and Daisy, 2013) and reduce amyloid-β peptide levels (Zhang et al., 2013). However, as far as we know, there are no reports in the literature regarding any investigation of the effects of OG on hepatocarcinoma.

In the present study, OG decreased the viability of HepG2 cells in a time and dose-dependent manner, with IC_{50} of 40 µM after 24 h of treatment. Our result agrees with a previous study that found an IC_{50} of 45 µM in a melanoma cell line, with the same treatment time (Locatelli et al., 2009). Another study with a leukemia cell line found an IC_{50} of

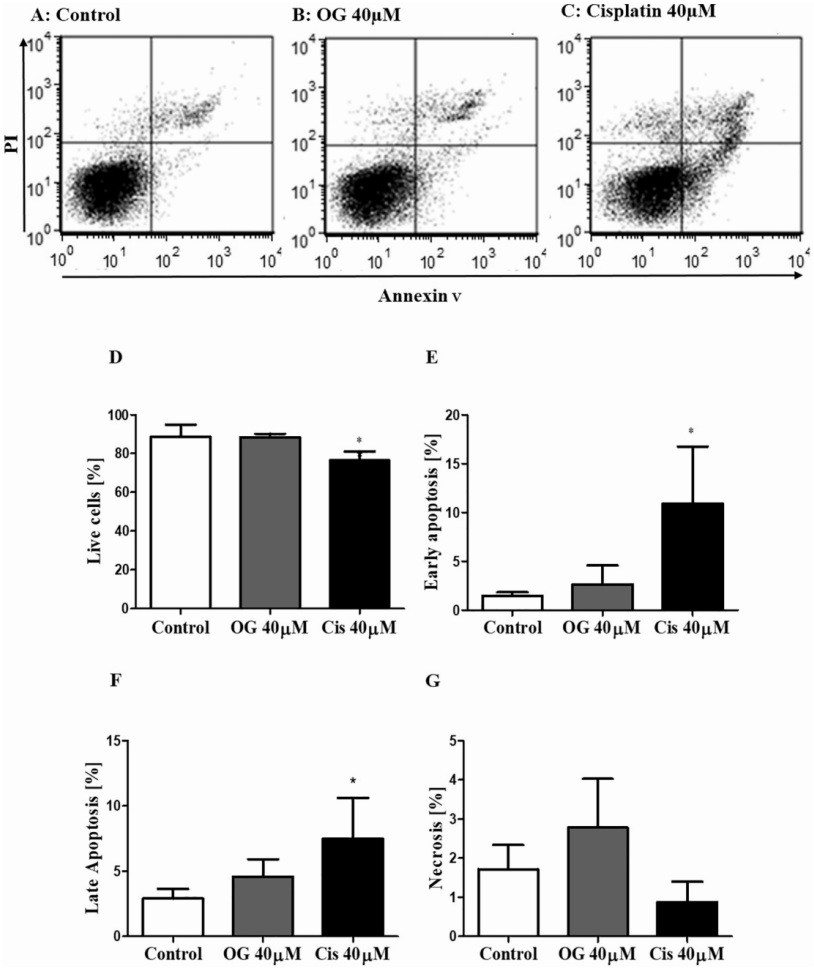

Fig. 8. Effect of OG on the induction of apoptosis and necrosis of HepG2 cells after 24 h. Representative flow cytometric plots: control (8A), OG 40 µM (8B) and Cisplatin 40 µM (8C). Results are expressed as percentage of cells. Live cells (8D), early apoptosis (8E), late apoptosis (8F) and necrosis (8G). Data are represented as the mean ± SD from four independent experiments (* $p < 0.05$).

50 µM with 48 h of treatment (Locatelli et al., 2008), whereas a study with B-cell lymphoma found an IC_{50} of 1.5 µM with 72 h of treatment (Serrano et al., 1998). These results show that different cell types have distinct sensitivities to OG treatment and the effects also depend on the time variable. Similar to other studies (de Cordova et al., 2011; Locatelli et al., 2009, 2008; Serrano et al., 1998), our results show that the reduction in cell viability with a short treatment of 24 h did not involve cell death by necrosis.

Cell cycle arrest is the action mechanism of some chemotherapeutics and it may be involved with the reduction of energy supply (Cantó and Auwerx, 2010); tumor suppressor signaling (Liu and Lozano, 2005); and the action of cell cycle control proteins such as Ki67 (Sun et al., 2017), among other events. Thus, we hypothesized that the reduction in cell proliferation could be related to cell cycle arrest. Our results show an increase in the percentage of cells in the S phase, corroborating our hypothesis. This suggests that OG caused genotoxic stress during DNA replication that may occur by dNTP depletion, chemical inhibition of DNA polymerases, induction of the synthesis of aberrant DNA structures, incomplete replication or DNA double-strand breaks (Bartek et al., 2004). Our study is the first report in the literature to show cell cycle arrest as part of the OG mechanism. In addition, OG did not induce senescence, which suggests that although senescent cells present a permanent state of cell cycle arrest (Takahashi et al., 2007), it is not part of the OG mechanism.

Ki67 protein has been used for many years as a marker of cell proliferation and an indicator for the prognosis of cancer patients, since it is generally strongly expressed in proliferating cells and poorly in quiescent cells (Gerdes et al., 1984), but its mechanism was not known (Scholzen and Gerdes, 2000). A recent study showed that Ki67 plays an important role in normal S phase progression and Xi heterochromatin maintenance, since it stimulates the expression of genes related to DNA replication and cell cycle progression. However, the contribution of

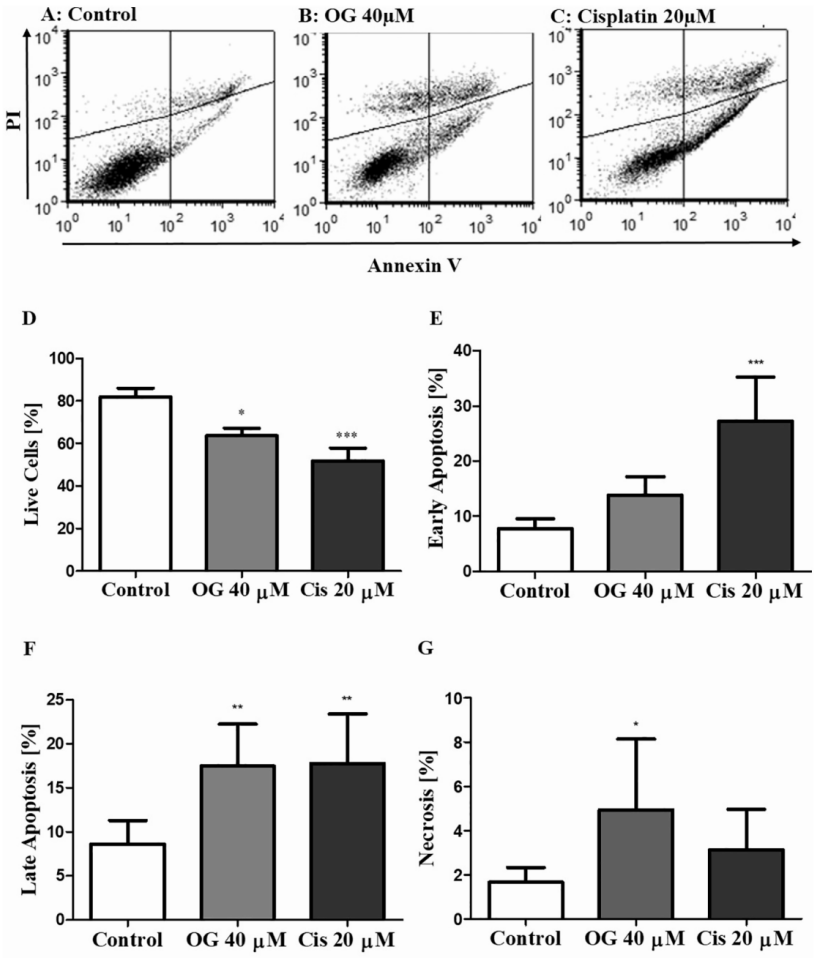

Fig. 9. Effect of OG on the induction of apoptosis and necrosis of HepG2 cells after 2 doses of OG every 24 h. Representative flow cytometric plots: control (9A), OG 40 µM (9B) and Cisplatin 20 µM (9C). Results are expressed as percentage of cells. Live cells (9D), early apoptosis (9E), late apoptosis (9F) and necrosis (9G). Data are represented as the mean ± SD from three independent experiments (*$p < 0.05$, **$p < 0.01$, ***$p < 0.0001$).

Ki67 to cell cycle progression is considered cell-type dependent (Sun et al., 2017). Our results show a significant reduction in the Ki67 levels after 24 h of treatment, indicating its involvement in cell cycle arrest.

The reduction in Ki67 protein expression also is related to the increase in p21 expression in some cell lines, such as MCF7 breast adenocarcinoma cells, according to a previous study (Sun et al., 2017). It is known that the induction of cell cycle arrest caused by p53 in the G1-S phases is involved with the increase in p21 (Harris and Levine, 2005). Thus, we evaluated the expression of p21 (direct target of transcriptional induction by the tumor suppressor p53) (Deng et al., 1995). If p53 were involved with OG-induced cell cycle arrest, an increase in p21 expression would be expected, since direct transcriptional activation of p21 by p53 is a key event leading to growth arrest (Eckner, 2012). As our results show S cell cycle arrest, we evaluated whether p21 signaling would be involved. Western blot assay showed that there was no significant difference in p21 expression after treatment of 1 dose for 24 h with OG, showing that cell cycle arrest did not involve p53/p21 signaling. Our findings are similar to another study that not found an increase in p21 in response to Ki67 depletion in HCT116 colorectal carcinoma and MDA-MB-231 breast adenocarcinoma cells (Sun et al., 2017). Other mechanisms of cell cycle control may be involved in the effects of OG, such as the signaling of other tumor suppressors; and the action of CDKs, cyclins, E3 ubiquitin ligases (Salazar-Roa and Malumbres, 2017; Williams and Stoeber, 2012). Therefore, further studies are needed to evaluate these hypotheses.

ATP is by far one of the most important molecules for cancer cells, being the principal material for phosphorylation reactions, DNA and RNA replication and repair, and the function of the MDR1 and ABC pumps on the cellular membrane, which are the major lines of defense of tumors against chemotherapy (Phan et al., 2014). The reduction in cellular ATP levels may be a target for antitumor therapies, due to the inhibition of cell proliferation, since the resultant cell regulation only

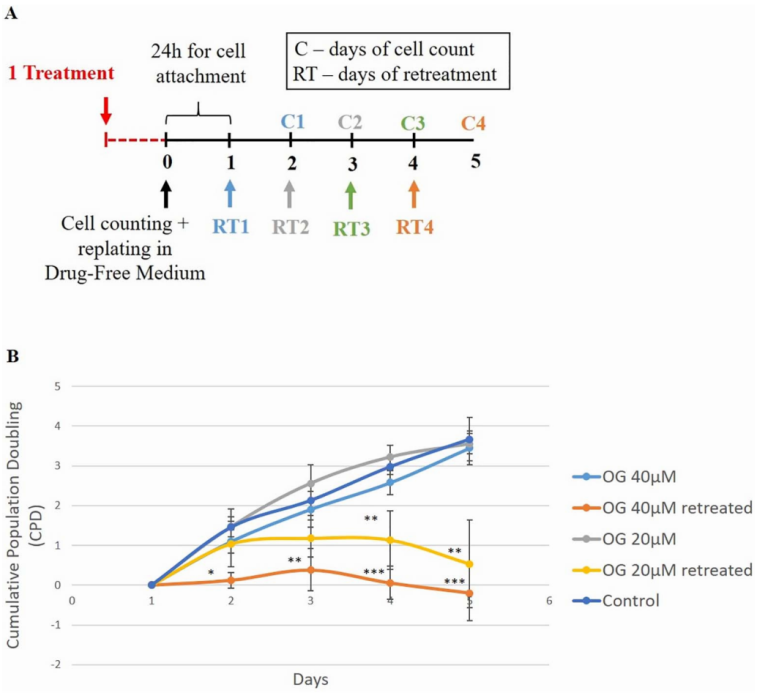

Fig. 10. Octyl gallate reduces tumor cell re-growth. The protocol of treatments is shown in panel 10A. Data are represented as the mean ± SD from three independent experiments (10B) (*p < 0.05, **p < 0.01, ***p < 0.001).

allows proliferation when cellular energy reserves are sufficient (Fogarty and Hardie, 2010). Our results show that the anti-proliferative effects of OG are mediated by the reduction in ATP levels, in agreement with a study using a melanoma cell line (Locatelli et al., 2009). These results suggest that the reduced energy supply resulting from the decreased ATP levels signals to the cell the necessity to stop proliferation. Thus, the expression of the Ki67 protein, which is important for normal progression of the S-phase cycle, is reduced. This signaling of the ATP and Ki67 protein, undoubtedly, plays a key role in the OG-induced halting of proliferation mechanisms. However, research into proteins that act as energy sensors, such as AMP-activated protein kinase (AMPK) and proteins involved in the cell-cycle progression (cyclins and CDK inhibitors), is also of great relevance to achieve a better understanding these mechanisms (Salazar-Roa and Malumbres, 2017).

An increase in oxidative stress has been reported as a part of the antitumor mechanism of OG in other cancer lines (de Cordova et al., 2011; Locatelli et al., 2009, 2008). One of these studies (de Cordova et al., 2011) showed that an increase in oxidative stress induced loss of mitochondrial membrane potential and consequent mitochondrial dysfunction, that could be one hypothesis to explain the reduction in ATP found herein. However, our findings show that the anti-proliferative effect of OG on HepG2 cells did not involve oxidative stress. Interestingly, OG increased catalase levels, suggesting that this enzyme may control an increase in the hydrogen peroxide levels in treated HepG2 cells.

Since autophagy may be induced by limitations in cellular ATP, we investigated whether OG treatment could lead to autophagy. Our results showed that the mechanism of OG did not involve the induction of autophagy, despite the reduction in cellular ATP. Previous studies with octyl gallate and gallic acid also found no involvement of autophagy in the action mechanism of these compounds (de Cordova et al., 2011; Locatelli et al., 2009; Lu et al., 2010).

Previous studies have shown that gallic acid and its derivatives can uncouple mitochondrial oxidative phosphorylation, thus influencing the energetic state of the cell (Nakagawa and Tayama, 1995; Serrano et al., 1998). Our results are in agreement with these studies, since the treatment of the HepG2 cells with OG reduced mitochondrial number and activity in the short treatment of 24 h (one dose) and induced mitochondrial failure and swelling after the longer treatment of 48 h (two doses). Our imaging analysis by transmission electron microscopy showed mitochondrial swelling in response to the prolonged OG-treatment and the non-involvement of autophagy, thus corroborating the results of flow cytometry with regard to these issues. Altogether, prolonged OG-treatment triggered a reduction in mitochondrial density that may suggest an inhibition of mitochondrial biogenesis and an increase in mitochondrial dysfunction.

The Shape Z is a mathematical tool used to quantitatively assess morphological changes (de Campos et al., 2012; García-Fiñana et al., 2003; Kiêu et al., 1999; Matheron, 1971; Mathieu et al., 1981). Different treatments influence mitochondrial shape (Hernández-Alvarez et al., 2013; Thaher et al., 2017). However, in general, these changes are qualitatively described (Hernández-Alvarez et al., 2013; Meira Martins et al., 2015; Thaher et al., 2017) or a simple quantitative evaluation is performed (Dietrich et al., 2013). Thus, the aim of our evaluation, using shape Z, was to complement our analysis of mitochondrial density and area, evaluating if our treatments were able to produce a more rounded or elongated mitochondria. Since swollen mitochondria are identified by their expanded matrix space (Sun et al., 2007), we hypothesized that mitochondrial swelling could reduce the elongation of the mitochondria with a possible reduction in the shape Z. However, no change was found in this parameter.

Studies that investigated the effects of OG on leukemia and

melanoma cell lines showed that this compound interfered in mitochondrial activity by reducing mitochondrial GSH levels and by increasing oxidative stress (Locatelli et al., 2009, 2008). Our findings show no increase in oxidative stress, but suggest a possible increase in reactive species, particularly hydrogen peroxide, may be compensated by antioxidant defenses, since we found an increase in catalase after treatment. Another hypothesis is that the mechanism of OG presents variations according to cell type.

The relationship between mitochondrial dysfunction and cell death by apoptosis is widely known. The main event involved is mitochondrial membrane permeabilization (MMP), which constitutes the goal of anticancer chemotherapy in tumor cells. Induction of MMP can lead to caspase activation in the intrinsic apoptosis pathway, irreversible loss of mitochondrial function, and mitochondrial release of caspase-independent death effectors including apoptosis-inducing factor (AIF), ultimately causing apoptosis (Kroemer et al., 2007). Our results show that OG-treatment induced late apoptosis/necrosis only with prolonged treatment (48 h, two doses), which is in accordance to the results of the ultrastructural analysis that showed morphological alterations in the mitochondria of prolonged-treated cells. Studies with other cancer models have shown that OG mechanism also involves the induction of apoptosis (de Cordova et al., 2011; Locatelli et al., 2009, 2008). The relationship between mitochondrial dysfunction and increased p53 is also well described (Schuler and Green, 2001). We believe that when we used one dose of OG, the mitochondrial alterations did not cause apoptosis, but cell cycle arrest via Ki67 without activation of p53, since there was no increase in p21 expression. However, when we used two doses, the mitochondria was severely affected, causing apoptosis.

The OG also showed antiproliferative effects in the chronic assay with several treatment doses, since the cells that received the retreatment with either multiple doses of 40 μM or a half dose of 20 μM OG initially showed stable CPD with a further reduction over time. This result agrees with the results of the cell cycle and Annexin V/PI assays, which showed a reduction in proliferation and the induction of apoptosis. The long-term evaluation and retreatment allowed the in vitro assay to be more similar to the clinical regimens, in which patients usually receive several chemotherapeutic doses. This is clinically relevant since chronic in vitro results strongly correlate with in vivo results, in contrast to acute in vitro assays (Augustine et al., 2009).

5. Conclusions

Altogether, these results suggest that octyl gallate, when in contact for 24 h with HepG2 cells, inhibits its growth by decreasing mitochondrial activity, which results in the reduction of ATP levels. This reduction of energy supply leads to decreased expression of the Ki67 protein, which is important for cell cycle normality, without increasing p21 expression, thus producing S phase cell cycle arrest. Nevertheless, this stimulus for 24 h does not induce cell death. When cells are exposed to one more dose of octyl gallate, its effects are more potent, causing loss of mitochondrial functionality, mitochondrial swelling and consequent apoptosis, while there is no resistance to treatment with multiple doses. This suggests that the initial treatment with OG did not select resistant HepG2 cells, which may not have stable resistance to OG. Thus, octyl gallate could be a strong candidate for further research targeting the discovery of new therapeutic options for hepatocarcinoma.

Transparency document

The Transparency document associated with this article can be found, in online version.

Acknowledgments

Special thanks to the colleagues from the Immunodiagnostic Laboratory, Cellular and Molecular Immunology Laboratory and Central Laboratory of Microscopy and Microanalysis (LabCEMM) at the Pontifical Catholic University of Rio Grande do Sul, as well colleagues from the Biochemistry Laboratory of the Federal University of Rio Grande do Sul. K. G. Lima is the recipient of a fellowship from CAPES (Coordenação de Aperfeiçoamento de Pessoal de Nível Superior - Brazil).

Conflict of interest statement

The authors declare no conflict of interest.

References

Agnello, M., Morici, G., Rinaldi, A.M., 2008. A method for measuring mitochondrial mass and activity. Cytotechnology 56, 145–149. http://dx.doi.org/10.1007/s10616-008-9143-2.

Augustine, C.K., Yoo, J.S., Potti, A., Yoshimoto, Y., Zipfel, P.A., Friedman, H.S., Nevins, J.R., Ali-Osman, F., Tyler, D.S., 2009. Genomic and molecular profiling predicts response to temozolomide in melanoma. Clin. Cancer Res. 15, 502–510. http://dx.doi.org/10.1158/1078-0432.CCR-08-1916.

Bartek, J., Lukas, C., Lukas, J., 2004. Checking on DNA damage in S phase. Nat. Rev. Mol. Cell Biol. 5, 792–804. http://dx.doi.org/10.1038/nrm1493.

Beutler, E., Duron, O., B.M., K., 1963. Improved method for the determination of blood glutathione. J. Lab. Clin. Med. 61, 882–888.

de Campos, D., do Nascimento, P.S., Ellwanger, J.H., Gehlen, G., Rodrigues, M.F., Jotz, G.P., Xavier, L.L., 2012. Histological organization is similar in human vocal muscle and tongue—a study of muscles and nerves. J. Voice 26, 811.e19–811.e26. http://dx.doi.org/10.1016/j.jvoice.2011.12.006.

Cantó, C., Auwerx, J., 2010. AMP-activated protein kinase and its downstream transcriptional pathways. Cell. Mol. Life Sci. 67, 3407–3423. http://dx.doi.org/10.1007/s00018-010-0454-z.

de Cordova, C.A.S., Locatelli, C., Assunção, L.S., Mattei, B., Mascarello, A., Winter, E., Nunes, R.J., Yunes, R.A., Creczynski-Pasa, T.B., 2011. Octyl and dodecyl gallates induce oxidative stress and apoptosis in a melanoma cell line. Toxicol. in Vitro 25, 2025–2034. http://dx.doi.org/10.1016/j.tiv.2011.08.003.

Deng, C., Pumin Zhang, tS, Wade Harper, J., Elledge, S.J., Leder, P., 1995. Mice lacking p21 c~P7/wAF7 undergo normal development, but are defective in Gl checkpoint control. Cell 82, 875–884.

Dietrich, M.O., Liu, Z.-W., Horvath, T.L., 2013. Mitochondrial dynamics controlled by Mitofusins regulate Agrp neuronal activity and diet-induced obesity. Cell 155, 188–199. http://dx.doi.org/10.1016/j.cell.2013.09.004.

Draper, H.H., Hadley, M., 1990. Malondialdehyde determination as index of lipid peroxidation. Methods Enzymol. 186, 421–431.

Eckner, R., 2012. p53-dependent growth arrest and induction of p21: a critical role for PCAF-mediated histone acetylation. Cell Cycle 11, 2591–2592. http://dx.doi.org/10.4161/cc.21235.

Fernandes, R.O., De Castro, A.L., Bonetto, J.H.P., Ortiz, V.D., Müller, D.D., Campos-Carraro, C., Barbosa, S., Neves, L.T., Xavier, L.L., Schenkel, P.C., Singal, P., Khaper, N., da Rosa Araujo, A.S., Belló-Klein, A., 2016. Sulforaphane effects on postinfarction cardiac remodeling in rats: modulation of redox-sensitive prosurvival and proapoptotic proteins. J. Nutr. Biochem. 34, 106–117. http://dx.doi.org/10.1016/j.jnutbio.2016.05.004.

Filippi-Chiela, E.C., Oliveira, M.M., Jurkovski, B., Callegari-Jacques, S.M., da Silva, V.D., Lenz, G., 2012. Nuclear morphometric analysis (NMA): screening of senescence, apoptosis and nuclear irregularities. PLoS One 7, e42522. http://dx.doi.org/10.1371/journal.pone.0042522.

Filippi-Chiela, E.C., Thomé, M.P., de Silva, M.M., Pelegrini, A.L., Ledur, P.F., Garicochea, B., Zamin, L.L., Lenz, G., 2013. Resveratrol abrogates the temozolomide-induced G2 arrest leading to mitotic catastrophe and reinforces the temozolomide-induced senescence in glioma cells. BMC Cancer 13, 147. http://dx.doi.org/10.1186/1471-2407-13-147.

Filippi-Chiela, E.C., Silva, M.M.B., Thomé, M.P., Lenz, G., 2015. Single-cell analysis challenges the connection between autophagy and senescence induced by DNA damage. Autophagy 11, 1099–1113. http://dx.doi.org/10.1080/15548627.2015.1009795.

Fogarty, S., Hardie, D.G., 2010. Development of protein kinase activators: AMPK as a target in metabolic disorders and cancer. Biochim. Biophys. Acta 1804, 581–591. http://dx.doi.org/10.1016/j.bbapap.2009.09.012.

Forner, A., Llovet, J.M., Bruix, J., 2012. Hepatocellular carcinoma. Lancet 379, 1245–1255. http://dx.doi.org/10.1016/S0140-6736(11)61347-0.

García-Fiñana, M., Cruz-Orive, L.M., Mackay, C.E., Pakkenberg, B., Roberts, N., 2003. Comparison of MR imaging against physical sectioning to estimate the volume of human cerebral compartments. NeuroImage 18, 505–516.

Gerdes, J., Lemke, H., Baisch, H., Wacker, H.H., Schwab, U., Stein, H., 1984. Cell cycle analysis of a cell proliferation-associated human nuclear antigen defined by the monoclonal antibody Ki-67. J. Immunol. 133, 1710–1715.

Harris, S.L., Levine, A.J., 2005. The p53 pathway: positive and negative feedback loops. Oncogene 24, 2899–2908. http://dx.doi.org/10.1038/sj.onc.1208615.

Hernández-Alvarez, M.I., Paz, J.C., Sebastián, D., Muñoz, J.P., Liesa, M., Segalés, J., Palacín, M., Zorzano, A., 2013. Glucocorticoid modulation of mitochondrial function

in hepatoma cells requires the mitochondrial fission protein Drp1. Antioxid. Redox Signal. 19, 366–378. http://dx.doi.org/10.1089/ars.2011.4269.
Huang, C.Y., Kuo, W.T., Huang, Y.C., Lee, T.C., Yu, L.C., 2013. Resistance to hypoxia-induced necroptosis is conferred by glycolytic pyruvate scavenging of mitochondrial superoxide in colorectal cancer cells. Cell Death Dis. 4, e622. http://dx.doi.org/10.1038/cddis.2013.149.
Ilha, J., Araujo, R.T., Malysz, T., Hermel, E.E.S., Rigon, P., Xavier, L.L., Achaval, M., 2008. Endurance and resistance exercise training programs elicit specific effects on sciatic nerve regeneration after experimental traumatic lesion in rats. Neurorehabil. Neural Repair 22, 355–366. http://dx.doi.org/10.1177/1545968307313502.
Inoue, M., Suzuki, R., Sakaguchi, N., Li, Z., Takeda, T., Ogihara, Y., Jiang, B.Y., Chen, Y., 1995. Selective induction of cell death in cancer cells by gallic acid. Biol. Pharm. Bull. 18, 1526–1530.
Kiêu, K., Souchetb, S., Istasc, J., 1999. Precision of systematic sampling and transitive methods. J. Stat. Plan. Inference 77, 263–279.
Krause, G.C., Lima, K.G., Dias, H.B., da Silva, E.F.G., Haute, G.V., Basso, B.S., Gassen, R.B., Marczak, E.S., Nunes, R.S.B., de Oliveira, J.R., 2017. Liraglutide, a glucagon-like peptide-1 analog, induce autophagy and senescence in HepG2 cells. Eur. J. Pharmacol. 809, 32–41. http://dx.doi.org/10.1016/j.ejphar.2017.05.015.
Kroemer, G., Galluzzi, L., Brenner, C., 2007. Mitochondrial membrane permeabilization in cell death. Physiol. Rev. 87, 99–163. http://dx.doi.org/10.1152/physrev.00013.2006.
Latha, R.C., Daisy, P., 2013. Therapeutic potential of octyl gallate isolated from fruits of Terminalia bellerica in streptozotocin-induced diabetic rats. Pharm. Biol. 51, 798–805. http://dx.doi.org/10.3109/13880209.2013.766894.
Lazzarotto Rucatti, A., Jaenisch, R.B., Rossato, D.D., Bonetto, J.H.P., Ferreira, J., Xavier, L.L., Sonza, A., Dal Lago, P., 2015. Skeletal muscle electrical stimulation improves baroreflex sensitivity and heart rate variability in heart failure rats. Auton. Neurosci. 193, 92–96. http://dx.doi.org/10.1016/j.autneu.2015.08.008.
Leite, C.E., Maboni, L.O., Cruz, F.F., Rosemberg, D.B., Zimmermann, F.F., Pereira, T.C., Bogo, M.R., Bonan, C.D., Campos, M.M., Morrone, F.B., Battastini, A.M., 2013. Involvement of purinergic system in inflammation and toxicity induced by copper in zebrafish larvae. Toxicol. Appl. Pharmacol. 272, 681–689. http://dx.doi.org/10.1016/j.taap.2013.08.001.
Lima, K.G., Krause, G.C., Schuster, A.D., Catarina, A.V., Basso, B.S., De Mesquita, F.C., Pedrazza, L., Marczak, E.S., Martha, B.A., Nunes, F.B., Chiela, E.C., Jaeger, N., Thomé, M.P., Haute, G.V., Dias, H.B., Donadio, M.V., De Oliveira, J.R., 2016. Gallic acid reduces cell growth by induction of apoptosis and reduction of IL-8 in HepG2 cells. Biomed Pharmacother 84, 1282–1290. http://dx.doi.org/10.1016/j.biopha.2016.10.048.
Liu, G., Lozano, G., 2005. p21 stability: linking chaperones to a cell cycle checkpoint. Cancer Cell 7, 113–114. http://dx.doi.org/10.1016/j.ccr.2005.01.019.
Locatelli, C., Rosso, R., Santos-Silva, M.C., de Souza, C.A., Licínio, M.A., Leal, P., Bazzo, M.L., Yunes, R.A., Creczynski-Pasa, T.B., 2008. Ester derivatives of gallic acid with potential toxicity toward L1210 leukemia cells. Bioorg. Med. Chem. 16, 3791–3799. http://dx.doi.org/10.1016/j.bmc.2008.01.049.
Locatelli, C., Leal, P.C., Yunes, R.A., Nunes, R.J., Creczynski-Pasa, T.B., 2009. Gallic acid ester derivatives induce apoptosis and cell adhesion inhibition in melanoma cells: the relationship between free radical generation, glutathione depletion and cell death. Chem. Biol. Interact. 181, 175–184. http://dx.doi.org/10.1016/j.cbi.2009.06.019.
Locatelli, C., Filippin-Monteiro, F.B., Creczynski-Pasa, T.B., 2013. Alkyl esters of gallic acid as anticancer agents: a review. Eur. J. Med. Chem. 60, 233–239. http://dx.doi.org/10.1016/j.ejmech.2012.10.056.
Lu, Y., Jiang, F., Jiang, H., Wu, K., Zheng, X., Cai, Y., Katakowski, M., Chopp, M., To, S.S, 2010. Gallic acid suppresses cell viability, proliferation, invasion and angiogenesis in human glioma cells. Eur. J. Pharmacol. 641, 102–107. http://dx.doi.org/10.1016/j.ejphar.2010.05.043.
Manfredi, G., Yang, L., Gajewski, C.D., Mattiazzi, M., 2002. Measurements of ATP in mammalian cells. Methods 26, 317–326.
Matheron, G., 1971. The Theory of Regionalized Variables and Its Applications, 5th ed. Les cahiers du Centre de Morphologie Mathematique de Fontainebleau, Fontainebleau, France.
Mathieu, O., Cruz-Orive, L.M., Hoppeler, H., Weibel, E.R., 1981. Measuring error and sampling variation in stereology: comparison of the efficiency of various methods for planar image analysis. J. Microsc. 121, 75–88.
Meira Martins, L.A., Vieira, M.Q., Ilha, M., de Vasconcelos, M., Biehl, H.B., Lima, D.B., Schein, V., Barbé-Tuana, F., Borojevic, R., Guma, F.C., 2015. The interplay between apoptosis, mitophagy and mitochondrial biogenesis induced by resveratrol can determine activated hepatic stellate cells death or survival. Cell Biochem. Biophys. 71, 657–672. http://dx.doi.org/10.1007/s12013-014-0245-5.
de Mesquita, F.C., Guixé-Muntet, S., Fernández-Iglesias, A., Maeso-Díaz, R., Vila, S., Hide, D., Ortega-Ribera, M., Rosa, J.L., García-Pagán, J.C., Bosch, J., de Oliveira, J.R., Gracia-Sancho, J., 2017. Liraglutide improves liver microvascular dysfunction in cirrhosis: evidence from translational studies. Sci. Rep. 7, 3255. http://dx.doi.org/10.1038/s41598-017-02866-y.
Nakagawa, Y., Tayama, S., 1995. Cytotoxicity of propyl gallate and related compounds in rat hepatocytes. Arch. Toxicol. 69, 204–208.
Phan, L.M., Yeung, S.C., Lee, M.H., 2014. Cancer metabolic reprogramming: importance, main features, and potentials for precise targeted anti-cancer therapies. Cancer Biol. Med. 11, 1–19. http://dx.doi.org/10.7497/j.issn.2095-3941.2014.01.001.
Salazar-Roa, M., Malumbres, M., 2017. Fueling the cell division cycle. Trends Cell Biol. 27, 69–81. http://dx.doi.org/10.1016/j.tcb.2016.08.009.
Scholzen, T., Gerdes, J., 2000. The Ki-67 protein: from the known and the unknown. J. Cell. Physiol. 182, 311–322. http://dx.doi.org/10.1002/(SICI)1097-4652(200003)182:3<311::AID-JCP1>3.0.CO;2-9.
Schuler, M., Green, D.R., 2001. Mechanisms of p53-dependent apoptosis. Biochem. Soc. Trans. 29, 684–688. http://dx.doi.org/10.1042/BST0290684.
de Senna, P.N., Bagatini, P.B., Galland, F., Bobermin, L., do Nascimento, P.S., Nardin, P., Tramontina, A.C., Gonçalves, C.A., Achaval, M., Xavier, L.L., 2017. Physical exercise reverses spatial memory deficit and induces hippocampal astrocyte plasticity in diabetic rats. Brain Res. 1655, 242–251. http://dx.doi.org/10.1016/j.brainres.2016.10.024.
Serrano, A., Palacios, C., Roy, G., Cespón, C., Villar, M.L., Nocito, M., González-Porqué, P., 1998. Derivatives of gallic acid induce apoptosis in tumoral cell lines and inhibit lymphocyte proliferation. Arch. Biochem. Biophys. 350, 49–54.
Sun, M.G., Williams, J., Munoz-Pinedo, C., Perkins, G.A., Brown, J.M., Ellisman, M.H., Green, D.R., Frey, T.G., 2007. Correlated three-dimensional light and electron microscopy reveals transformation of mitochondria during apoptosis. Nat. Cell Biol. 9, 1057–1072. http://dx.doi.org/10.1038/ncb1630.
Sun, X., Bizhanova, A., Matheson, T.D., Yu, J., Zhu, J.L., Kaufman, P.D., 2017. Ki-67 contributes to normal cell cycle progression and inactive X heterochromatin in p21 checkpoint-proficient human cells. Mol. Cell. Biol. http://dx.doi.org/10.1128/MCB.00569-16.
Takahashi, A., Ohtani, N., Hara, E., 2007. Irreversibility of cellular senescence: dual roles of p16INK4a/Rb-pathway in cell cycle control. Cell Div 2, 10. http://dx.doi.org/10.1186/1747-1028-2-10.
Thaher, O., Wolf, C., Dey, P.N., Pouya, A., Wüllner, V., Tenzer, S., Methner, A., 2017. The thiol switch C684 in Mitofusin-2 mediates redox-induced alterations of mitochondrial shape and respiration. Neurochem. Int. http://dx.doi.org/10.1016/J.NEUINT.2017.05.009.
Thomé, M.P., Filippi-Chiela, E.C., Villodre, E.S., Migliavaca, C.B., Onzi, G.R., Felipe, K.B., Lenz, G., 2016. Ratiometric analysis of Acridine Orange staining in the study of acidic organelles and autophagy. J. Cell Sci. 129, 4622–4632. http://dx.doi.org/10.1242/jcs.195057.
Torre, L.A., Siegel, R.L., Ward, E.M., Jemal, A., 2016. Global cancer incidence and mortality rates and trends–an update. Cancer Epidemiol. Biomark. Prev. 25, 16–27. http://dx.doi.org/10.1158/1055-9965.EPI-15-0578.
Weibel, E.R., 1979. Stereological Methods. Practical Methods for Biological Morphometry. London.
Williams, G.H., Stoeber, K., 2012. The cell cycle and cancer. J. Pathol. 226, 352–364. http://dx.doi.org/10.1002/path.3022.
Xavier, L.L., Viola, G.G., Ferraz, A.C., Da Cunha, C., Deonizio, J.M., Netto, C.A., Achaval, M., 2005. A simple and fast densitometric method for the analysis of tyrosine hydroxylase immunoreactivity in the substantia nigra pars compacta and in the ventral tegmental area. Brain Res. Brain Res. Protoc. 16, 58–64. http://dx.doi.org/10.1016/j.brainresprot.2005.10.002.
Yoshioka, K., Kataoka, T., Hayashi, T., Hasegawa, M., Ishi, Y., Hibasami, H., 2000. Induction of apoptosis by gallic acid in human stomach cancer KATO III and colon adenocarcinoma COLO 205 cell lines. Oncol. Rep. 7, 1221–1223.
Zacharová, G., Kubínová, L., 1995. Stereological methods based on point counting and unbiased counting frames for two-dimensional measurements in muscles: comparison with manual and image analysis methods. J. Muscle Res. Cell Motil. 16, 295–302.
Zhai, B., Sun, X.Y., 2013. Mechanisms of resistance to sorafenib and the corresponding strategies in hepatocellular carcinoma. World J. Hepatol. 5, 345–352. http://dx.doi.org/10.4254/wjh.v5.i7.345.
Zhang, S.Q., Sawmiller, D., Li, S., Rezai-Zadeh, K., Hou, H., Zhou, S., Shytle, D., Giunta, B., Fernandez, F., Mori, T., Tan, J., 2013. Octyl gallate markedly promotes anti-amyloidogenic processing of APP through estrogen receptor-mediated ADAM10 activation. PLoS One 8, e71913. http://dx.doi.org/10.1371/journal.pone.0071913.
Zhou, L., Liu, S., Han, M., Feng, S., Liang, J., Li, Z., Li, Y., Lu, H., Liu, T., Ma, Y., Cheng, J., 2017. MicroRNA-185 induces potent autophagy via AKT signaling in hepatocellular carcinoma. Tumour Biol. 39. http://dx.doi.org/10.1177/1010428317694313.
Ziogas, I.A., Tsoulfas, G., 2017. Evolving role of Sorafenib in the management of hepatocellular carcinoma. World J. Clin. Oncol. 8, 203–213. http://dx.doi.org/10.5306/wjco.v8.i3.203.

CAPÍTULO III

Short Communication: Octyl gallate induces hepatic steatosis in HepG2 cells through mTOR/SREBP-1c-independent pathway

Os resultados do presente trabalho respondem ao objetivo específico 2 e foram submetidos ao periódico Food and Chemical Toxicology.

Fator de impacto: 3.778
Qualis Capes 2013-2016: A2 (Ciências Biológicas I)

Octyl gallate induces hepatic steatosis in HepG2 cells through mTOR/SREBP-1c-independent pathway

Author Information

Kelly Goulart Lima[a], Vitor Giancarlo Schneider Levorse[a], Maria Claudia Rosa Garcia[a], Bruno de Souza Basso[a], Gabriela Viegas Haute[a], Léder Leal Xavier[b], Márcio Vinícius Fagundes Donadio[a] and Jarbas Rodrigues De Oliveira[a]

a Laboratório de Biofísica Celular e Inflamação, Escola de Ciências, Pontifícia Universidade Católica do Rio Grande do Sul. Av. Ipiranga, 6681, prédio 12, bloco C, Partenon, Porto Alegre, Rio Grande do Sul, Brazil. CEP: 90619-900.

b Laboratório de Biologia Celular e Tecidual, Escola de Ciências, Pontifícia Universidade Católica do Rio Grande do Sul. Av. Ipiranga, 6681, prédio 12, bloco C, Sala 104, Partenon, Porto Alegre, Rio Grande do Sul, Brazil. CEP: 90619-900.

Corresponding author

Kelly Goulart Lima

Laboratório de Biofísica Celular e Inflamação, Escola de Ciências, Pontifícia Universidade Católica do Rio Grande do Sul.

Complete postal address: Av. Ipiranga, 6681, prédio 12, bloco C, Partenon, Porto Alegre, Rio Grande do Sul, Brazil. CEP: 90619-900. Phone number: +555133534147

e-mail address: kelly.lima@acad.pucrs.br

Abstract

Octyl gallate (OG) is an antioxidant used in some foods, although there is no definition of its acceptable daily intake. There are reports *in vitro* and *in vivo* showing that both food additives and drugs can alter lipid metabolism. The accumulation of lipid droplets in hepatic cells is one of the main findings in the deregulated lipid metabolism and is strongly related to the development of nonalcoholic fatty liver disease (NAFLD). Here, we investigated the effects of OG on lipid metabolism in the hepatocellular carcinoma cell line (HepG2). Results show, for the first time, that treatment with OG increased the overall amount of lipids, the triglyceride concentration and the lipid droplets area. Moreover, it decreased mTOR protein expression without modifying SREBP-1c, PPAR-α and PPAR-γ gene expression. Considering that the ability of OG to inhibit mitochondrial activity and to induce apoptosis is well-known, it is very likely that reduction of mitochondrial fatty acid b-oxidation is involved in this mechanism. Taken together, our findings indicate that OG induces lipid droplets accumulation in HepG2 cells without involving the regulation of mTOR/SREBP-1c signaling or modification of PPAR-α and PPAR-γ gene expression and may contribute to NAFLD when used as a food additive.

Keywords

Octyl gallate; HepG2 cells; Lipid droplets; Lipid metabolism, mTOR.

Abbreviations

ACC, acetyl CoA carboxylase; ADI, acceptable daily intake; AOIs, Areas of interest; DMEM, Dulbecco's Modified Eagle Medium; DMSO, dimetilsulfoxido; ELOVL6, elongation of long-chain fatty acids family member 6; FAS, fatty acid synthase; FBS, fetal bovine serum; GA, Gallic acid; HC, Hepatocellular carcinoma; HEPES, 4-(2-hydroxyethyl)-1-piperazineethanesulfonic acid; JECFA, Joint Expert Committee on Food Additives; LD50, median lethal dose; mTOR, mechanistic target of rapamycin; NAFL, non-alcoholic fatty liver; NAFLD, Non-alcoholic fatty liver disease; NASH, non-alcoholic steatohepatitis; OA, oleic acid; O.D, optical density; OG, octyl gallate; PBS, phosphate buffered saline; SCD1, stearoyl-CoA desaturase 1; PPAR-α, Peroxisome proliferator-activated receptor alpha; PPAR-γ, Peroxisome proliferator-activated receptor gamma; PPAR-δ, Peroxisome proliferator-activated receptor delta; SREBP-1c, Sterol regulatory element binding protein 1c; TEM, Transmission electron microscopy; TG, triglyceride.

1. Introduction

Non-alcoholic fatty liver disease (NAFLD) includes from simple steatosis (deposition of adipose tissue in the liver) to more progressive steatosis with associated hepatitis, fibrosis, cirrhosis, and in some cases hepatocellular carcinoma (Sayiner et al., 2016). Thus, NAFLD is comprised of non-alcoholic fatty liver (NAFL), that does not present hepatocyte injury, and non-alcoholic steatohepatitis (NASH), that is a necroinflammatory process (Kanwar and Kowdley, 2016). The main NAFLD risk factors are metabolic disorders, type 2 diabetes mellitus, genetic predisposition, high-fat diet, use of tobacco, lower physical activity levels, polycystic ovarian syndrome and obstructive sleep apnea (Benedict and Zhang, 2017). The incidence of NAFLD is estimated that to be 20-30% in Western countries and 5-18% in Asia (Sayiner et al., 2016).

There are reports that the use of drugs such as tamoxifen (Zhao et al., 2014), aspirin (Deschamps et al., 1991), glucocorticoids (Letteron et al., 1997), 5-fluoruracil (Gentilucci et al., 2006) and methotrexate (Menter et al., 2009) can lead to NAFLD. Furthermore, several studies show that food additives can also induce NAFLD, including fructose (Chen et al., 2017; Jensen et al., 2018), monosodium glutamate (Collison et al., 2013, 2009) and aspartame (Collison et al., 2013).

Octyl gallate (OG) is an ester of gallic acid (GA), which can be produced semi-synthetically from it or isolated from *Terminalia bellerica* fruits (Latha and Daisy, 2013). It is an antioxidant used in some foods, although there is no current definition of its acceptable daily intake (ADI), considering the lack of studies on its pharmacokinetics and metabolism (World Health Organization, 1997). In the United States, OG is approved only as a margarine additive with a concentration of less than 0.0075% (U.S. Food and Drug Administration, 2018), while in Europe it is authorized as a food additive in heat-treated processed meat, chewing gum and processed potato products (EUROPEAN PARLIAMENT AND THE COUNCIL OF THE EUROPEAN UNION, 2008).

Study using an animal model showed that the biodegradation of OG yields n-octyl alcohol and gallic acid (Koss and Koransky, 1982), although it did not clarify the difference in toxicological potency between gallates (propyl, octyl and dodecyl), preventing the establishment of its ADI by FAO/WHO Joint Expert Committee on Food Additives (JECFA) (World Health Organization, 1997). Another animal model study

showed that OG at high doses was able to induce strong inhibition of gluconeogenesis, which could be considered as harmful (Eler et al., 2015). However, no studies have evaluated its effect on lipid metabolism. Here, we used HepG2 cell line to investigate the effects of OG on lipid metabolism and the underlying mechanisms involved.

2. Materials and methods

2.1. Materials

The human hepatocarcinoma cell line (HepG2) was obtained from Rio de Janeiro Cell Bank (UFRJ, Rio de Janeiro, Brazil). DMEM and FBS were obtained from Gibco, Life Technologies. Streptomycin (100 mg/mL) and penicillin (100 units/mL), octyl gallate, trypan blue, Oil Red and araldite were supplied by Sigma-Aldrich, USA. Antibody against mTOR and secondary antibody goat anti-rabbit were supplied by Cell Signaling, USA. Antibody against GAPDH, rabbit anti-mouse secondary antibody, Trizol reagent, Superscript III First-Strand Synthesis SuperMix and SYBR Green I were supplied by Invitrogen, Carlsbad, CA. Primer sequences were supplied by Integrated DNA Technologies (Iowa, USA). Oleic acid (OA) was supplied by Synth, Brazil and isopropanol was supplied by Nuclear, Brazil.

2.2. Cell culture and treatment

HepG2 cells were cultivated in DMEM supplemented with 10% FBS, 1% streptomycin (100 mg/mL) and penicillin (100 units/mL), 2 g/L HEPES buffer and 3.7 g/L $NaHCO_3$ in humidified atmosphere with 5% CO_2 at 37 °C. Stock solutions of OG were prepared in DMSO and dilutions were prepared in DMEM supplemented with 10% FBS. Stock solutions of OA were prepared in isopropanol and dilutions were prepared in DMEM supplemented with 10% FBS. Cells were cultured for 24 hours before treatment in all assays. Control wells contained DMEM, 10% FBS and DMSO 0.2% (vehicle). Cells were treated with 40 µM OG and positive controls were treated with 100 µM OA for 24 hours.

2.3. Morphological analysis

Cells were seeded into 24-well plates (12 × 10^4 cells/well) cultured and treated as aforementioned. Cell morphological changes were evaluated after 24 h of treatment under phase contrast inverted microscope at 400× magnification and photographed using Bel Photonics camera.

2.4. Oil Red Staining

Cells were seeded as described for the Morphological analysis and treated as aforementioned. After the treatment period, culture medium was discarded and cells were washed twice with PBS. Afterwards, cells were fixed with 4% paraformaldehyde for 30 min, washed thrice with PBS and subsequently rinsed with propylene glycol. Then, cells were stained with freshly prepared solution of propylene glycol containing 0.5% Oil Red (previously filtered with a 0.45 µm filter) for 15 min. Thus, cells were rinsed with 60% propylene glycol and washed with distilled water. Images of cells with lipid droplets stained were acquired under phase contrast inverted microscope at 400× magnification using Bel Photonics camera.

2.5. Trypan blue exclusion assay

Cell viability was evaluated using the Trypan blue exclusion assay to correct the reading of the lipids optical density by number of cells. Cells were seeded as described for morphological analysis and treated as aforementioned. For determination of cell number, cells were counted using a hemocytometer under a light microscope (Nikon Optiphot, Japan). Two replicate wells were used at each concentration tested, including control.

2.6. Lipid Measurement

After image acquisition of cells with Oil Red stained lipid droplets, 200 µL of isopropanol was added to each plate well for the lipid dissolution. Optical density (O.D) was monitored with a VICTOR® microplate reader (PerkinElmer) at a wavelength of 490 nm. Results were expressed as O.D Lipids / 100,000 cell.

2.7 Triglyceride Assay

Cells were seeded into 60.8 cm^2 plates (5 × 10^6 cells/well) cultured and treated as aforementioned. After, cells were scraped and transferred into an Eppendorf tube (1.5 mL) and centrifuged at 3000 rpm for 5 min. Cell pellets were washed with Phosphate-Buffered Saline (PBS) once, resuspended in 400 µL PBS buffer and submitted to ultrasonication. The concentration of cellular TG was determined using an TG Color assay kit (Wiener lab, Argentina) and normalized with protein concentration, according to the protocol provided by the manufacturer. Absorbance was measured at 505 nm using CT300i Chemistry Analyzer (Wiener lab, Argentina).

2.8. Ultrastructural Analysis by Transmission Electron Microscopy (TEM)

To analyze the treated and control cells using transmission electron microscopy (TEM), semi-confluent HepG2 cells were collected using trypsinization. Cells were harvested by centrifugation and washed twice after phosphate buffered saline (pH 7.2) addition. Then, cells were fixed in a mixture of 4 % paraformaldehyde and 2.5 % glutaraldehyde buffered with 0.1 M phosphate (pH 7.3) at room temperature, and postfixed in osmium tetroxide in the same buffer for 45 min before dehydration. Afterwards, they were dehydrated in a graded acetone series (30–100%) and embedded in araldite (Durcupan ACM, Fluka) for 72 h at 60°C. Thin sections (70 nm) were stained with 2% uranyl acetate followed by lead citrate (Meira Martins et al., 2015). Ultrastructural analysis was performed on the control (DMSO 0.2%) and treated cells (OG 40µM) using the Tecnai G2 T20, FEI transmission electron microscopy and Image Pro Plus software (Image Pro Plus 6.1, Media Cybernetics, Silver Spring, EUA). The analyses were performed by two blinded specialists in image analysis, planar morphometry and stereology. The morphological evaluation was performed using TEM images as described below.

2.8.1. Lipid droplet density

In order to estimate lipid droplet density, a quantitative analysis, similar to the Neubauer chamber, was performed. Briefly, randomized squares measuring 3.0 $µm^2$, named areas of interest (AOIs), were overlaid on each image (4500×) and lipid droplets

located inside each square or intersected by the upper and/or left edges of the squares were counted. On the contrary, lipid droplets intersected by the lower and/or right edges of the squares were not counted (de Senna et al., 2017). On average, 7 AOIs were analyzed in each cell and 10 cells were analyzed per group.

2.8.2. Lipid droplet area

The lipid droplet area were calculated using a stereological tool, the point counting method (Fernandes et al., 2016; Ilha et al., 2008; Lazzarotto Rucatti et al., 2015; Weibel, 1979; Zacharová and Kubínová, 1995). A grid mask (a grid of crosses with equidistant intervals) with an area/point value of 6518.5 nm^2, was placed over the lipid droplets image. When the upper right quadrant of the cross hit images of lipid droplets they were counted. Areas were obtained using the following equation: $\hat{A} = \sum p.a/p$, where $\hat{A}$ is the area, $\sum p$ is the sum of points counted, and a/p is the area/point value. On average, 5 lipid droplets were analyzed in each cell, and 6 cells were analyzed per group.

2.9. Western blot analysis

Approximately 5×10^5 cells were seeded in a 6-well plate, cultured and treated as aforementioned. Cells were rinsed twice with PBS and lysed with CHAPS lysis buffer. Aliquots from each sample containing 20µg protein were run on a 10% sodium dodecylsulphate polyacrylamide gel, and transferred to a nitrocellulose membrane. After the transfer, blots were blocked with Tris buffered saline containing 0.05% Tween-20 and 5% non-fat dry milk for 1 hour and subsequently incubated overnight at 4 °C with primary antibodies against mTOR (2972, Cell Signaling) at 1:500 and GAPDH (39-8600, Invitrogen) at 1:1000 dilution. Then, membranes were incubated with the appropriate horseradish peroxidase-conjugated secondary antibodies (1:1000) at room temperature for 1 hour. Blots were revealed by chemiluminescence and digital images were taken in a Carestream Gel Logic 2200 PRO Imaging System. Protein expression was determined in NanoDrop Lite (Thermo Fisher Scientific®) and Image Studio Lite software (LI-COR). Quantitative densitometric values of all proteins were normalized to GAPDH (de Mesquita et al., 2017).

2.10. RNA isolation and quantitative PCR

Approximately 2.5 × 10^5 cells were seeded in a 6-well plate, cultured and treated as aforementioned. Total RNA was extracted from cells using Trizol reagent (Invitrogen) according to the manufacturer's instructions. RNA was reverse transcribed into cDNA, using Superscript III First-Strand Synthesis SuperMix (Invitrogen) according to the manufacturer's instructions. Primer sequences used were synthesized by Integrated DNA Technologies (Iowa, USA) with sequences described in Table 1. The quantity of cDNA was examined by NanoDrop 2000 (Thermo Fisher Scientific). The expression level of SREBP1c, PPAR-α, PPAR-γ and β-actin was quantified by qRT-PCR, which was conducted on Step One Applied Biosystems. The reaction was catalyzed by SYBR Green I (Applied Biosystems- Thermo Fisher Scientific) kit according to the manufacturer´s instructions. Data were analyzed with β-actin as a reference gene (control).

Table 1. Primer sequences used for qRT-PCR

Genes	Primer sequences (5'-3')	GenBank accession number
SREBP-1c	Forward CGGAACCATCTTGGCAACAGT Reverse CGCTTCTCAATGGCGTTGT	NM_001005291
PPAR-γ	Forward ACCAAAGTGCAATCAAAGTGGA Reverse ATGAGGGAGTTGGAAGGCTCT	NM_138711
PPAR-α	Forward TGCAAACTTGGACTTGAACG Reverse TGATGTCACAGAACGGCTTC	NM_001001928.2
β-actin	Forward TATGCCAACACAGTGCTGTCTG Reverse TACTCCTGCTTGCTGATCCACATG	NM_001101.4

2.11. Data and statistical analysis

All results are presented as mean ± SD from three independent experiments. The Student's t-test was used for comparisons between groups in Ultrastructural analysis (TEM), Western blot and quantitative PCR assays. One-way analysis of variance (ANOVA) followed by Tukey's multiple comparison post-test were used for comparisons between groups in the Lipid Measurement and TG Assay. A p-value < 0.05 was considered statistically significant. Statistical analyses were performed using GraphPad Prism 5.0 (GraphPad Software, San Diego, CA).

3. Results

3.1. Octyl gallate induces lipid accumulation in HepG2 cells

Treatment with OG induced vesicles accumulation in the cell cytoplasm, as observed in figure 1B. The positive control for induction of lipid droplets accumulation (treatment with oleic acid) also led to cytoplasmic vesicle accumulation as shown in figure 1C, although with greater intensity. In order to confirm that these were lipid droplets, we have performed the Oil Red Staining assay. This assay revealed that treatment with OG significantly increased lipid accumulation, as shown in figure 2D with a representative image in figure 2B. As expected, the positive control increased lipid accumulation with greater intensity (Fig. 2C and Fig. 2D). As shown in the figure 2E, our results also showed an increase in the TG concentration after OG treatment, corroborating the accumulation of lipids demonstrated in the Oil Red assay.

3.2. Ultrastructural analysis showed that OG increase lipid droplet area without modify the lipid droplet density

To confirm the effect of OG on lipid accumulation and to evaluate lipid droplet area and density, we have performed ultrastructural analysis of HepG2 cells. Transmission electron microscopy images revealed that treatment with 40 µM OG increased lipid droplet area ($p < 0.05$; Fig. 3C) without changing lipid droplet density ($p = 0.97$; Fig. 3D). Representative images were shown in Fig. 3A (control) and Fig. 3B (40 µM OG).

3.3. Octyl gallate decrease expression mTOR protein

Previous studies showed that lipid accumulation is mainly regulated by mTOR/SREBP1c signaling (Porstmann et al., 2008; Yin et al., 2017). Thus, we have investigated if increased mTOR expression could be related to lipid accumulation caused by OG. Interestingly, our findings showed that treatment with OG decreased mTOR expression ($p < 0.05$; Figures 4A and 4B).

3.4. Octyl gallate did not increase expression gene SREBP1c

In order to confirm the non-involvement of mTOR/SREBP-1c signaling in lipid accumulation, we have evaluated SREBP-1c gene expression. As expected, our findings showed that treatment with OG did not modify SREBP-1c gene expression (Fig. 4C).

3.5 Octyl gallate did not modify the PPAR-α and PPAR-γ gene expression.

In order to investigate whether the modification of PPAR-α and PPAR-γ gene expression could be related to lipid accumulation induced by OG, we have evaluated the expression of these genes. However, our findings show no changes in PPAR-α (Fig. 4D) and PPAR-γ (Fig. 4E) expression after treatment with OG.

4. Discussion

The initial toxicity studies performed with OG aimed to determine the acceptable daily intake (ADI) in order to regulate the use of this antioxidant as an additive in food. These initial studies with rats defined median lethal dose (LD50) as 4700mg/kg body weight and showed that diets containing 0.2% octyl gallate caused a slight hypochromic anaemia. Thus, at that time, an ADI for man of 0.2 mg/kg body weight (as a sum of propyl, octyl and dodecyl gallates) was defined (Joint FAO/WHO Expert Committee, 1964).

Subsequent reproduction studies in rats evaluating the effects of OG showed high mortality levels in young pups, probably due to a perinatal effect related to a mechanism transmitted by the mother's milk. In addition, there were observations that OG caused reactions of sensitization in the oral mucosa of individuals previously sensitized by cutaneous contact with OG, which made its use not acceptable in beer and other beverages consumed in large amounts (Joint FAO/WHO Expert Committee, 1972).

In a re-evaluation of the committee in 1997, a decision that it would not be possible to maintain the definition of the ADI for octyl and dodecyl gallates was taken, considering the lack of studies on pharmacokinetics and metabolism (World Health Organization, 1997). Ever since, there is no definition of the ADI for OG. Some

countries use the OG as additive in certain foods, although restricted to specific foods and with its maximum acceptable concentration determined for the types of foods that are authorized (EUROPEAN PARLIAMENT AND THE COUNCIL OF THE EUROPEAN UNION, 2008; U.S. Food and Drug Administration, 2018). As far as we know, there are no reports in the literature regarding any investigation of the effects of OG on hepatic lipid metabolism.

Our results show, for the first time, that OG has the capacity to induce lipid accumulation in an in vitro model of hepatic steatosis. Studies with other food additives (Chen et al., 2017; Collison et al., 2013; Jensen et al., 2018) or therapeutic drugs (Gentilucci et al., 2006; Menter et al., 2009; Zhao et al., 2014) also found lipid accumulation in liver, showing the connection between the use of certain compounds and the induction of NAFLD.

Since the regulation of lipid metabolism via Akt/mTOR/SREBP-1c signaling is widely known (Li et al., 2015; Porstmann et al., 2008), we have investigated whether the mechanism of lipid accumulation induction by OG could be related to increased mTOR expression. Interestingly, we have observed a reduction in the expression of this protein, which is in agreement with our previous study that showed reduction of cellular growth through reduction of Ki 67 protein (cell proliferation marker) (Lima et al., 2018).

The transcription factor SREBP-1c is the major isoform that controls fatty acid synthesis in the liver (Pettinelli et al., 2011). SREBP-1c promotes transcription of lipogenic genes including fatty acid synthase (FAS), stearoyl-CoA desaturase 1 (SCD1), elongation of long chain fatty acids family member 6 (ELOVL6), and acetyl CoA carboxylase (ACC) (Sanders and Griffin, 2016). One previous study showed that tamoxifen-induced hepatocyte steatosis involved the upregulation of SREBP-1c gene (Zhao et al., 2014). However, our findings have shown no changes in SREBP-1c gene expression, probably due to differences in the mechanism of action of tamoxifen and OG.

The peroxisome proliferator-activated receptors (PPARs) are a set of three nuclear hormone receptors (PPAR-α, PPAR-γ and PPAR-δ) that act mainly in the regulation of metabolic pathways involving fatty-acid oxidation and lipid metabolism (Ament et al., 2012). PPAR-α regulates a number of catabolic pathways; PPAR-γ appears to be key in lipid storage and synthesis, as well as in adipogenesis (Andrew Clayton et al., 2006; Kirschenlohr et al., 2006); and PPAR-δ has a role in adipocyte

differentiation, lipoprotein metabolism, atherosclerosis and β-oxidation in adipocytes, skeletal muscle and heart (Takahashi et al., 2006). Thus, we have investigated if any changes in PPAR-α and PPAR-γ expression could be related to lipid accumulation induced by OG. However, our findings showed no changes in the expression of these genes. Our results are in agreement with another study that showed no involvement of PPAR-γ gene in the mechanism of induction of lipid accumulation by tamoxifen (Zhao et al., 2014). On the other hand, our data differed from another study that showed reduction of PPAR-α after treatment with oleic acid (Cui et al., 2010).

A study with murine lymphoma cells (EL4), prostate cancer cell lines C4-2b and DU145, human colon adenocarcinoma (HCT116) and mouse embryo fibroblasts showed that induction of apoptosis and decrease of mitochondrial membrane potential leads to an early increase in cytoplasmic lipid droplet formation by reducing mitochondrial fatty acid b-oxidation (Boren and Brindle, 2012). In our previous study, we have shown that the OG, when in contact for 24 h with HepG2 cells, inhibited its growth by decreasing mitochondrial activity, as well as a prolonged exposure (2 treatments every 24h) promoted loss of mitochondrial functionality, mitochondrial swelling and consequent apoptosis (Lima et al., 2018). Thus, induction of apoptosis can be a trigger for lipid accumulation.

5. Conclusion

Altogether, these results suggest that OG induces lipid droplets accumulation in HepG2 cells without the regulation of mTOR/SREBP-1c signaling or modification of PPAR-α and PPAR-γ gene expression. Since the ability of OG to inhibit mitochondrial activity and to induce apoptosis is well-known, it is very likely that reduction of mitochondrial fatty acid b-oxidation is involved in this mechanism. Our results suggest that the use of OG as an additive in food can lead to NAFLD, although further studies are needed to clarify the effects of OG in the lipid metabolism in vivo and the mechanisms involved.

Acknowledgments

Special thanks the colleagues from the Immunodiagnostic Laboratory, Central Laboratory of Microscopy and Microanalysis (LabCEMM) at the Pontifical Catholic University of Rio Grande do Sul. K. G. Lima is the recipient of a fellowship from CAPES (Coordenação de Aperfeiçoamento de Pessoal de Nível Superior - Brazil).

Conflict of Interest Statement

The authors declare no conflict of interest.

References

Ament, Z., Masoodi, M., Griffin, J.L., 2012. Applications of metabolomics for understanding the action of peroxisome proliferator-activated receptors (PPARs) in diabetes, obesity and cancer. Genome Med. 4, 32. doi:10.1186/gm331

Andrew Clayton, T., Lindon, J.C., Cloarec, O., Antti, H., Charuel, C., Hanton, G., Provost, J.-P., Le Net, J.-L., Baker, D., Walley, R.J., Everett, J.R., Nicholson, J.K., 2006. Pharmaco-metabonomic phenotyping and personalized drug treatment. Nature 440, 1073–1077. doi:10.1038/nature04648

Benedict, M., Zhang, X., 2017. Non-alcoholic fatty liver disease: An expanded review. World J. Hepatol. 9, 715–732. doi:10.4254/wjh.v9.i16.715

Boren, J., Brindle, K.M., 2012. Apoptosis-induced mitochondrial dysfunction causes cytoplasmic lipid droplet formation. Cell Death Differ. 19, 1561–1570. doi:10.1038/cdd.2012.34

Chen, Q., Wang, T., Li, J., Wang, S., Qiu, F., Yu, H., Zhang, Y., Wang, T., 2017. Effects of Natural Products on Fructose-Induced Nonalcoholic Fatty Liver Disease (NAFLD). Nutrients 9, 96. doi:10.3390/nu9020096

Collison, K.S., Makhoul, N.J., Zaidi, M.Z., Inglis, A., Andres, B.L., Ubungen, R., Saleh, S., Al-Mohanna, F.A., 2013. Prediabetic changes in gene expression induced by aspartame and monosodium glutamate in Trans fat-fed C57Bl/6 J mice. Nutr. Metab. (Lond). 10, 44. doi:10.1186/1743-7075-10-44

Collison, K.S., Maqbool, Z., Saleh, S.M., Inglis, A., Makhoul, N.J., Bakheet, R., Al-Johi, M., Al-Rabiah, R., Zaidi, M.Z., Al-Mohanna, F.A., 2009. Effect of dietary monosodium glutamate on trans fat-induced nonalcoholic fatty liver disease. J. Lipid Res. 50, 1521–1537. doi:10.1194/jlr.M800418-JLR200

Cui, W., Chen, S.L., Hu, K.-Q., 2010. Quantification and mechanisms of oleic acid-induced steatosis in HepG2 cells. Am. J. Transl. Res. 2, 95–104.

de Mesquita, F.C., Guixé-Muntet, S., Fernández-Iglesias, A., Maeso-Díaz, R., Vila, S., Hide, D., Ortega-Ribera, M., Rosa, J.L., García-Pagán, J.C., Bosch, J., de Oliveira, J.R., Gracia-Sancho, J., 2017. Liraglutide improves liver microvascular dysfunction in cirrhosis: Evidence from translational studies. Sci. Rep. 7, 3255. doi:10.1038/s41598-017-02866-y

de Senna, P.N., Bagatini, P.B., Galland, F., Bobermin, L., do Nascimento, P.S., Nardin, P., Tramontina, A.C., Gonçalves, C.A., Achaval, M., Xavier, L.L., 2017. Physical exercise reverses spatial memory deficit and induces hippocampal astrocyte plasticity in diabetic rats. Brain Res 1655, 242–251. doi:10.1016/j.brainres.2016.10.024

Deschamps, D., Fisch, C., Fromenty, B., Berson, A., Degott, C., Pessayre, D., 1991. Inhibition by salicylic acid of the activation and thus oxidation of long chain fatty acids. Possible role in the development of Reye's syndrome. J. Pharmacol. Exp. Ther. 259, 894–904.

Eler, G.J., Santos, I.S., de Moraes, A.G., Comar, J.F., Peralta, R.M., Bracht, A., 2015. n -Octyl Gallate as Inhibitor of Pyruvate Carboxylation and Lactate Gluconeogenesis. J. Biochem. Mol. Toxicol. 29, 157–164. doi:10.1002/jbt.21680

EUROPEAN PARLIAMENT AND THE COUNCIL OF THE EUROPEAN UNION, 2008. REGULATION (EC) No 1333/2008 OF THE EUROPEAN PARLIAMENT AND OF THE COUNCIL of 16 December 2008 on food additives [WWW Document]. URL http://eur-lex.europa.eu/legal-content/EN/TXT/?uri=CELEX:32008R1333 (accessed 2.19.18).

Fernandes, R.O., De Castro, A.L., Bonetto, J.H.P., Ortiz, V.D., Müller, D.D., Campos-Carraro, C., Barbosa, S., Neves, L.T., Xavier, L.L., Schenkel, P.C., Singal, P., Khaper, N., da Rosa Araujo, A.S., Belló-Klein, A., 2016. Sulforaphane effects on postinfarction cardiac remodeling in rats: modulation of redox-sensitive prosurvival and proapoptotic proteins. J. Nutr. Biochem. 34, 106–117. doi:10.1016/j.jnutbio.2016.05.004

Gentilucci, U.V., Santini, D., Vincenzi, B., Fiori, E., Picardi, A., Tonini, G., 2006. Chemotherapy-induced steatohepatitis in colorectal cancer patients. J. Clin. Oncol. 24, 5467; author reply 5467-8. doi:10.1200/JCO.2006.08.1828

Ilha, J., Araujo, R.T., Malysz, T., Hermel, E.E.S., Rigon, P., Xavier, L.L., Achaval, M., 2008. Endurance and Resistance Exercise Training Programs Elicit Specific Effects on Sciatic Nerve Regeneration After Experimental Traumatic Lesion in Rats. Neurorehabil. Neural Repair 22, 355–366. doi:10.1177/1545968307313502

Jensen, T., Abdelmalek, M.F., Sullivan, S., Nadeau, K.J., Green, M., Roncal, C., Nakagawa, T., Kuwabara, M., Sato, Y., Kang, D.-H., Tolan, D.R., Sanchez-Lozada, L.G., Rosen, H.R., Lanaspa, M.A., Diehl, A.M., Johnson, R.J., 2018. Fructose and Sugar: A Major Mediator of Nonalcoholic Fatty Liver Disease. J. Hepatol. doi:10.1016/j.jhep.2018.01.019

Joint FAO/WHO Expert Committee, 1972. EVALUATION OF MERCURY, LEAD, CADMIUM AND THE FOOD ADDITIVES AMARANTH, DIETHYLPYROCARBONATE, AND OCTYL GALLATE [WWW Document]. URL http://www.inchem.org/documents/jecfa/jecmono/v004je07.htm (accessed 2.16.18).

Joint FAO/WHO Expert Committee, 1964. SPECIFICATIONS FOR IDENTITY AND PURITY AND TOXICOLOGICAL EVALUATION OF SOME ANTIMICROBIALS AND ANTIOXIDANTS [WWW Document]. URL http://www.inchem.org/documents/jecfa/jecmono/v38aje04.htm (accessed 2.16.18).

Kanwar, P., Kowdley, K. V., 2016. The Metabolic Syndrome and Its Influence on Nonalcoholic Steatohepatitis. Clin. Liver Dis. 20, 225–243. doi:10.1016/j.cld.2015.10.002

Kirschenlohr, H.L., Griffin, J.L., Clarke, S.C., Rhydwen, R., Grace, A.A., Schofield, P.M., Brindle, K.M., Metcalfe, J.C., 2006. Proton NMR analysis of plasma is a weak predictor of coronary artery disease. Nat. Med. 12, 705–710. doi:10.1038/nm1432

Koss, G., Koransky, W., 1982. Enteral absorption and biotransformation of the food additive octyl gallate in the rat. Food Chem. Toxicol. 20, 591–594. doi:10.1016/S0278-6915(82)80069-0

Latha, R.C., Daisy, P., 2013. Therapeutic potential of octyl gallate isolated from fruits of Terminalia bellerica in streptozotocin-induced diabetic rats. Pharm Biol 51, 798–805. doi:10.3109/13880209.2013.766894

Lazzarotto Rucatti, A., Jaenisch, R.B., Rossato, D.D., Bonetto, J.H.P., Ferreira, J., Xavier, L.L., Sonza, A., Dal Lago, P., 2015. Skeletal muscle electrical stimulation improves baroreflex sensitivity and heart rate variability in heart failure rats. Auton. Neurosci. 193, 92–6. doi:10.1016/j.autneu.2015.08.008

Letteron, P., Brahimi-Bourouina, N., Robin, M.A., Moreau, A., Feldmann, G., Pessayre, D., 1997. Glucocorticoids inhibit mitochondrial matrix acyl-CoA dehydrogenases and fatty acid beta-oxidation. Am. J. Physiol. Liver Physiol. 272, G1141–G1150. doi:10.1152/ajpgi.1997.272.5.G1141

Li, J., Huang, Q., Long, X., Zhang, J., Huang, X., Aa, J., Yang, H., Chen, Z., Xing, J., 2015. CD147 reprograms fatty acid metabolism in hepatocellular carcinoma cells through Akt/mTOR/SREBP1c and P38/PPARα pathways. J. Hepatol. 63, 1378–1389. doi:10.1016/J.JHEP.2015.07.039

Lima, K.G., Krause, G.C., da Silva, E.F.G., Xavier, L.L., Martins, L.A.M., Alice, L.M., da Luz, L.B., Gassen, R.B., Filippi-Chiela, E.C., Haute, G.V., Garcia, M.C.R., Funchal, G.A., Pedrazza, L., Reghelin, C.K., de Oliveira, J.R., 2018. Octyl gallate reduces ATP levels and Ki67 expression leading HepG2 cells to cell cycle arrest and mitochondria-mediated apoptosis. Toxicol. Vitr. 48, 11–25. doi:10.1016/j.tiv.2017.12.017

Meira Martins, L.A., Vieira, M.Q., Ilha, M., de Vasconcelos, M., Biehl, H.B., Lima, D.B., Schein, V., Barbé-Tuana, F., Borojevic, R., Guma, F.C., 2015. The interplay between apoptosis, mitophagy and mitochondrial biogenesis induced by resveratrol can determine activated hepatic stellate cells death or survival. Cell Biochem Biophys 71, 657–672. doi:10.1007/s12013-014-0245-5

Menter, A., Korman, N.J., Elmets, C.A., Feldman, S.R., Gelfand, J.M., Gordon, K.B., Gottlieb, A.B., Koo, J.Y.M., Lebwohl, M., Lim, H.W., Van Voorhees, A.S., Beutner, K.R., Bhushan, R., 2009. Guidelines of care for the management of psoriasis and psoriatic arthritis. J. Am. Acad. Dermatol. 61, 451–485. doi:10.1016/j.jaad.2009.03.027

Pettinelli, P., Obregón, A.M., Videla, L.A., 2011. Molecular mechanisms of steatosis in nonalcoholic fatty liver disease. Nutr. Hosp. 26, 441–50. doi:10.1590/S0212-16112011000300003

Porstmann, T., Santos, C.R., Griffiths, B., Cully, M., Wu, M., Leevers, S., Griffiths, J.R., Chung, Y.-L., Schulze, A., 2008. SREBP Activity Is Regulated by mTORC1 and Contributes to Akt-Dependent Cell Growth. Cell Metab. 8, 224–236. doi:10.1016/j.cmet.2008.07.007

Sanders, F.W.B., Griffin, J.L., 2016. De novo lipogenesis in the liver in health and disease: more than just a shunting yard for glucose. Biol. Rev. Camb. Philos. Soc. 91, 452–68. doi:10.1111/brv.12178

Sayiner, M., Koenig, A., Henry, L., Younossi, Z.M., 2016. Epidemiology of Nonalcoholic Fatty Liver Disease and Nonalcoholic Steatohepatitis in the United States and the Rest of the World. Clin. Liver Dis. 20, 205–214. doi:10.1016/j.cld.2015.10.001

Takahashi, S., Tanaka, T., Kodama, T., Sakai, J., 2006. Peroxisome proliferator-activated receptor δ (PPARδ), a novel target site for drug discovery in metabolic syndrome. Pharmacol. Res. 53, 501–507. doi:10.1016/j.phrs.2006.03.019

U.S. Food and Drug Administration, 2018. Food Additives & Ingredients - Food Additive Status List.

Weibel, E.R., 1979. Stereological methods. Practical methods for biological morphometry. London.

World Health Organization, 1997. Evaluation of Certain Food Additives and Contaminants.

Yin, F., Sharen, G., Yuan, F., Peng, Y., Chen, R., Zhou, X., Wei, H., Li, B., Jing, W., Zhao, J., 2017. TIP30 regulates lipid metabolism in hepatocellular carcinoma by regulating SREBP1 through the Akt/mTOR signaling pathway. Oncogenesis 6, e347. doi:10.1038/oncsis.2017.49

Zacharová, G., Kubínová, L., 1995. Stereological methods based on point counting and unbiased counting frames for two-dimensional measurements in muscles: comparison with manual and image analysis methods. J Muscle Res Cell Motil 16, 295–302.

Zhao, F., Xie, P., Jiang, J., Zhang, L., An, W., Zhan, Y., 2014. The Effect and Mechanism of Tamoxifen-Induced Hepatocyte Steatosis in Vitro. Int. J. Mol. Sci. 15, 4019–4030. doi:10.3390/ijms15034019

Figure legends

Fig. 1. Effects of OG on HepG2 cell morphology after 24 h. Images were obtained by phase contrast inverted microscopy. Representative images of control cells (1A), OG-treated cells (1B) and OA-treated cells (1C) are presented. Black arrows show lipid droplets. Treatment with OG induced lipid droplets accumulation in the cell cytoplasm (1B). The positive control (OA) led to lipid droplets accumulation with greater intensity (1C). OA: oleic acid. Calibration bar = 50 µm.

Fig.2. Effects of OG on steatosis induction in HepG2 cells determined by Oil Red staining and TG assay. Results are expressed as Optical density/1×10^5cells (2D) and TG accumulation (mg/100mg protein) (2E). Data are represented as the mean + SD from three independent experiments (*p < 0.05, **pn< 0.01). Representative images of control cells (2A), OG-treated cells (2B) and OA-treated cells (2C) are presented. Black arrows show lipid droplets. Treatment with OG induced lipid droplets accumulation in the cell cytoplasm (2B). The positive control (OA) led to lipid droplets accumulation with greater intensity (2C). Treatment with OG increased overall amount of lipids (2D) and TG concentration (2E). OA: oleic acid. Calibration bar = 50 µm.

Fig. 3. Ultrastructural analysis of HepG2 (lipid droplet area and lipid droplet density). Representative images of control cells (3A) and OG-treated cells (3B) are presented. LD: lipid droplet. Calibration bar = 500 nm. Transmission electron microscopy images revealed that treatment with OG increased lipid droplet area (3C) without changing lipid droplet density (3D). Results are expressed as lipid droplet area in μm^2 (3C) and number of lipid droplet per μm^2 of cytosol area (3D). Data are represented as the mean + SD from three independent experiments (* p< 0.05).

Fig. 4. Expression of mTOR protein in HepG2 cells after 24 h of treatment with OG by Western blot analysis (4A). GAPDH was used to normalize protein expression. Results are expressed as protein levels (fold induction) of the mTOR expression (4B). Treatment with OG decreased the expression of mTOR in HepG2 cells (p<0.05). In 4C, D and E the effect of OG on mRNA expression of genes (SREBP-1c, PPAR-α and PPAR-γ) regulating lipid metabolism in HepG2 is shown. Results are expressed as relative expression rate. OG did not change SREBP-1c (p = 0.61, 4C), PPAR-α (p =

0.42, 4D) and PPAR-γ (p = 0.13, 4E) mRNA expression. All data are represented as the mean ± SD of 3 independent experiments.

Figures

Fig. 1.

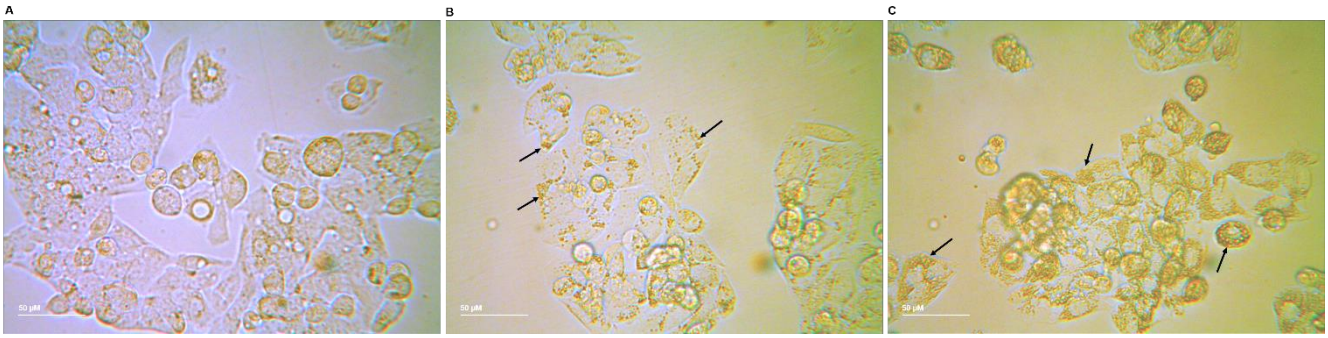

Fig.2.

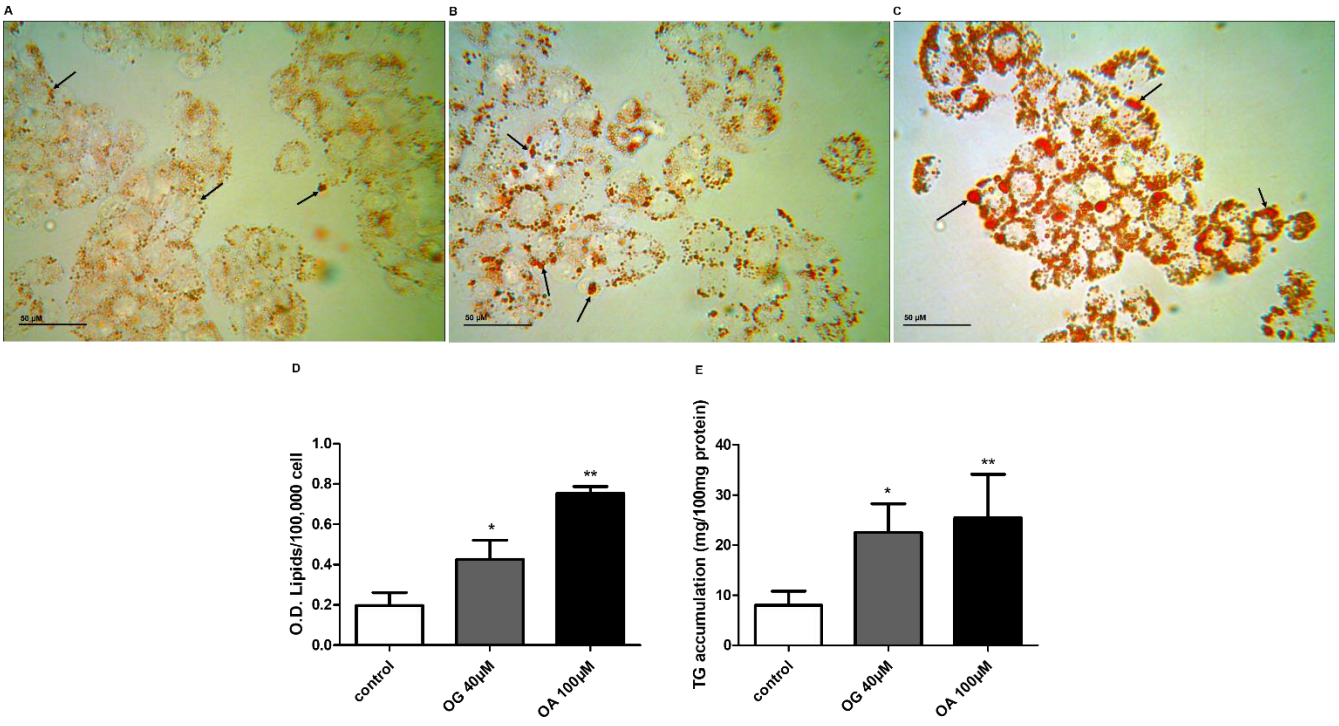

Fig. 3.

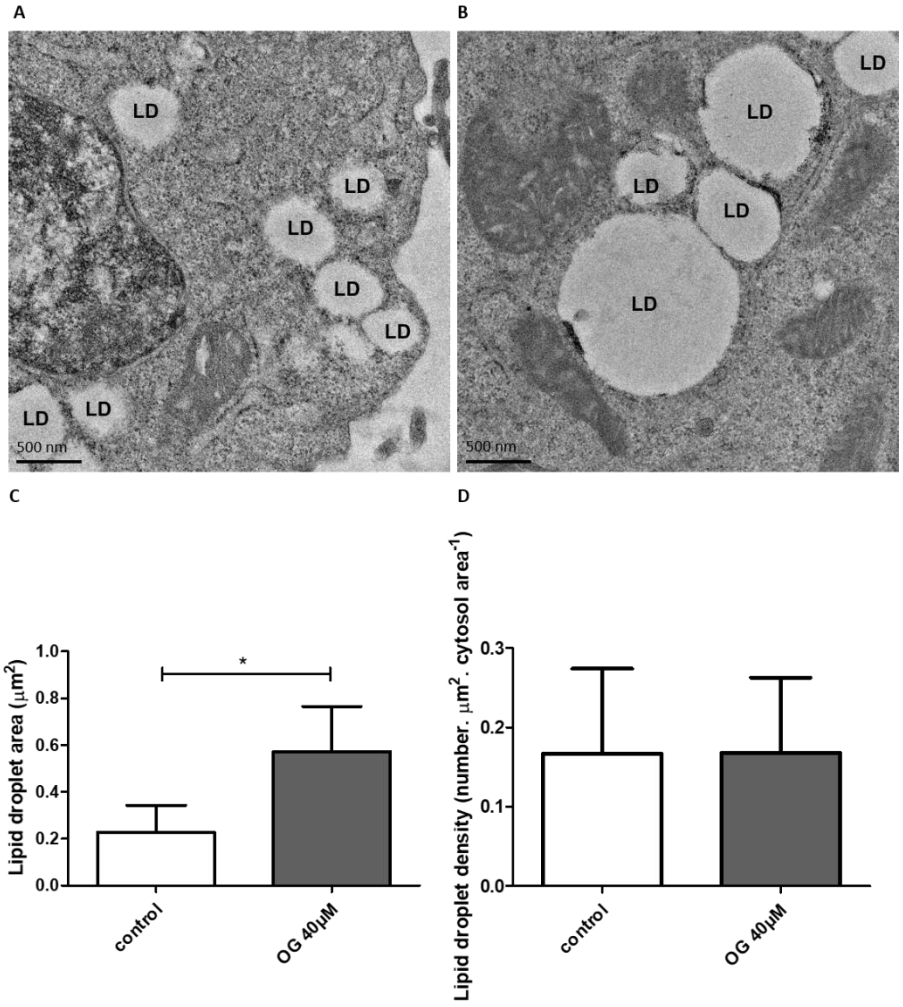
A
B
LD
500 nm
C
D
Lipid droplet area (μm²)
Lipid droplet density (number. μm². cytosol area⁻¹)
control
OG 40μM
*

Fig. 4.

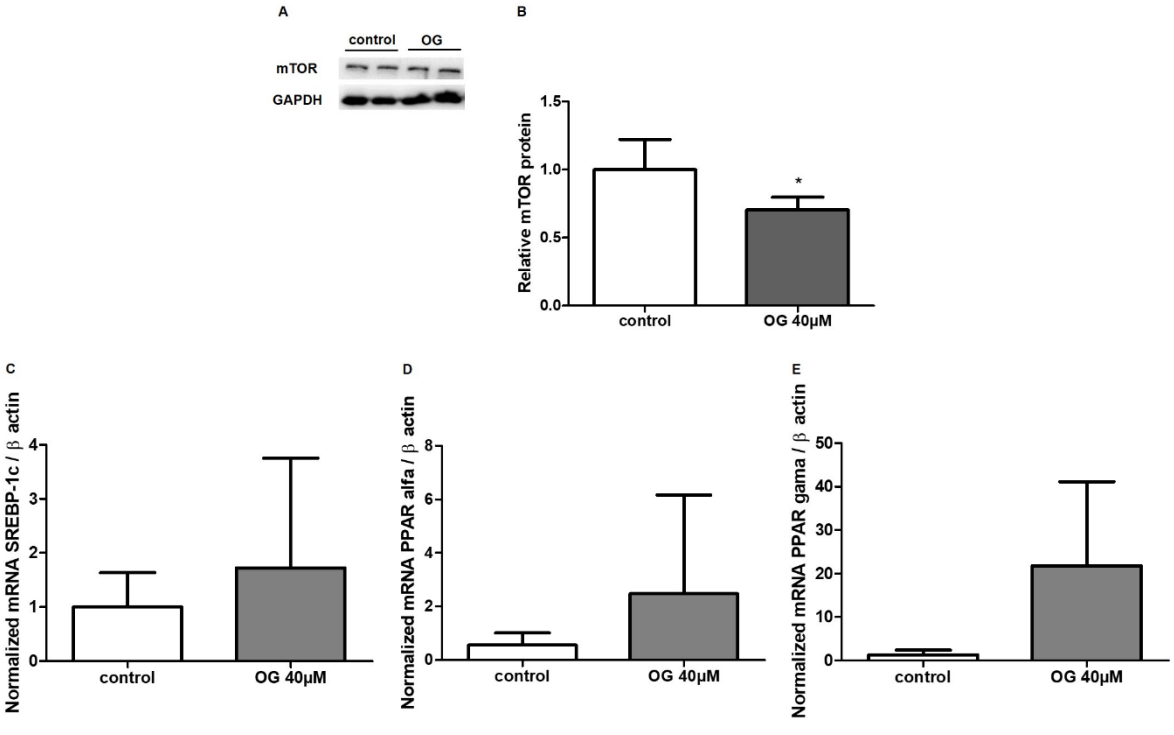
A
control
OG
mTOR
GAPDH
B
Relative mTOR protein
control
OG 40μM
*
C
Normalized mRNA SREBP-1c / β actin
D
Normalized mRNA PPAR alfa / β actin
E
Normalized mRNA PPAR gama / β actin

CAPÍTULO IV

Short Communication: A simple, fast, precise and unbiased method of analyzing lipid droplets combining Oil Red staining, nuclear morphometric analysis and confocal laser scanning microscopy

Os resultados do presente trabalho respondem ao objetivo específico 3 e foram submetidos ao periódico Histochemistry and Cell Biology.

Fator de impacto: 2.553

Qualis Capes 2013-2016: B1 (Ciências Biológicas I)

A simple, fast, precise and unbiased method of analyzing lipid droplets combining Oil Red staining, nuclear morphometric analysis and confocal laser scanning microscopy

Author Information

Kelly Goulart Lima[a], Léder Leal Xavier[b], Angélica Regina Cappellari[c], Fernanda Bueno Morrone[c], Vitor Giancarlo Schneider Levorse[a], Eduardo Cremonese Filippi-Chiela[d], Maria Claudia Rosa Garcia[a], and Jarbas Rodrigues de Oliveira[a]

a Laboratório de Biofísica Celular e Inflamação, Escola de Ciências, Pontifícia Universidade Católica do Rio Grande do Sul. Av. Ipiranga, 6681, prédio 12, bloco C, Partenon, Porto Alegre, Rio Grande do Sul, Brazil. CEP: 90619-900.

b Laboratório de Biologia Celular e Tecidual, Escola de Ciências, Pontifícia Universidade Católica do Rio Grande do Sul. Av. Ipiranga, 6681, prédio 12, bloco C, Sala 104, Partenon, Porto Alegre, Rio Grande do Sul, Brazil. CEP: 90619-900.

c Laboratório de Farmacologia Aplicada, Escola de Ciências da Saúde, Pontifícia Universidade Católica do Rio Grande do Sul. Av. Ipiranga, 6681, prédio 12, bloco C, Partenon, Porto Alegre, Rio Grande do Sul, Brazil. CEP: 90619-900.

d Programa de Pós-Graduação em Gastroenterologia e Hepatologia, Faculdade de Medicina, Universidade Federal do Rio Grande do Sul. Rua Ramiro Barcelos, 2400, Santana, Porto Alegre, Rio Grande do Sul, Brazil. CEP: 90035-003.

Corresponding author

Kelly Goulart Lima

Laboratório de Biofísica Celular e Inflamação, Escola de Ciências, Pontifícia Universidade Católica do Rio Grande do Sul.

Complete postal address: Av. Ipiranga, 6681, prédio 12, bloco C, Partenon, Porto Alegre, Rio Grande do Sul, Brazil. CEP: 90619-900. Phone number: +555133534147

e-mail address: kelly.lima@acad.pucrs.br

Abstract

Quantifying, localizing and identifying the shape of lipid droplets (LD) are important features to be assessed in the research of mechanisms involved in diseases such as steatosis, obesity, diabetes, myopathies, and arteriosclerosis. Lipid-droplet staining with Oil Red (OR) is widely used together with either light field or conventional fluorescence microscopy, although, image quality and lipid-droplet quantitation are limited. Nuclear Morphometric Analysis (NMA) indicates the proportion of cells in senescence, apoptosis or with nuclear irregularities based on nuclear morphology. These cellular mechanisms may underlie several clinical aspects of abovementioned illnesses. Thus, by combining a quantitative LD evaluation and NMA it is possible to relate any excessive or deficient LD with several cellular mechanisms. Here, for the first time, we report an easy, fast, precise and unbiased protocol for the quantitative evaluation of LD staining with OR combined with NMA in cultured cells in vitro using confocal laser scanning microscopy (CLSM). Additionally, our method substantially enhanced the quality of the images of LD compared to conventional fluorescence microscopy by eliminating out-of-focus light, increasing contrast and enhancing lipid droplet definition. We hope this protocol, and any adaptations of it, could be used by other researchers in future studies to obtain more detailed and reliable results.

Keywords

Lipid droplets; Oil Red; Nuclear Morphometric Analysis; confocal laser scanning microscopy; point counting method.

Introduction

Lipid droplets (LD) are active organelles that play a central role in cellular metabolism through lipids collection, storage, and supply according to the cellular need. Cells release LD-Free fatty acids to the microenvironment, which are used as substrates for energy metabolism, membrane synthesis, and the production of lipid-derived molecules (Herms et al. 2013). However, when there is an excess of fatty acids, progressive lipotoxicity occurs, characterized by organelle membrane destruction, stress pathway activation, metabolic dysregulation and apoptosis (Brookheart et al. 2009). Several diseases, such as steatosis, obesity, diabetes, myopathies, and arteriosclerosis, are related to the accumulation of lipids (Herms et al. 2013; Daemen et al. 2016).

Apoptosis as a consequence of lipotoxicity plays an important role in the pathogenesis of steatosis and has diagnostic and therapeutic implications (Walsh et al. 2004; Alkhouri et al. 2011). On the other hand, the inhibition of mitochondrial fatty acid β-oxidation that occurs after induction of apoptosis has also been related to accumulation of LD (Boren and Brindle 2012), showing that apoptosis may be a consequence of lipotoxicity or trigger for lipid accumulation. Another important mechanism, the cellular senescence, also has been related to the induction of steatosis. A recent study showed that cellular senescence drives hepatic steatosis and elimination of senescent cells may be a novel therapeutic strategy to reduce steatosis (Ogrodnik et al. 2017). Thus, quantifying, localizing and identifying the shape of LDs are important features to be assessed in the study of the mechanisms involved in diseases that have as characteristic the accumulation of lipids, mainly steatosis. (Herms et al. 2013; Daemen et al. 2016). However, there is no analyzing images methodology capable of measuring LDs and these cellular mechanisms simultaneously.

Nuclear Morphometric Analysis (NMA) can be used to indicate the proportion of cells in senescence, apoptosis or with nuclear irregularities based on nuclear morphology (Filippi-Chiela et al. 2012). This tool has been used in cultured cells to study the cellular mechanisms modulated by certain compounds, such as senescence (Menegotto et al. 2017), mitotic catastrophe (Filippi-Chiela et al. 2013), and apoptosis (Lima et al. 2016; Mandelkow et al. 2017; Krai et al. 2017). By combining LD quantification and NMA, it is possible to relate excessive or deficient lipid levels with

cellular mechanisms like apoptosis, senescence and mitotic catastrophe, which has being shown as playing a role in the pathogenesis, diagnosis and therapy of LD-associated diseases (Walsh et al. 2004; Alkhouri et al. 2011; Boren and Brindle 2012; Ogrodnik et al. 2017). Therefore, data obtained regarding this relationship can be used to conduct specific assays to discover cellular mechanisms with involved lipid metabolism.

Experiments using cell-culture models enable the controlled analysis of the effects of substances that can interfere in the accumulation or reduction of LD and their role in cellular mechanisms and cell fates. HepG2 Cells are widely used as an *in vitro* model for steatosis research, since, similarly to hepatocytes, they accumulate lipids in the cytoplasm (Cui et al. 2010; Zeng et al. 2016; ALKHATATBEH et al. 2016). Oleic acid (OA) is a monosaturated omega-9 fatty acid that is widely used to induce LD accumulation in HepG2 cells (Cui et al. 2010; Zeng et al. 2016; Cao et al. 2016). Among the available methods, staining lipids with the classic Oil Red (OR) dye represents a low-cost, easy-to-prepare method of visualizing and quantifying LD. OR stains neutral lipids (mainly triglycerides) with an orange-red tint (Lillie and Ashburn 1943). OR-stained LD are commonly visualized and quantified using either light field or conventional fluorescence microscopy (Koopman et al. 2001; Daemen et al. 2016), although, in both cases image quality and lipid-droplet quantitation are limited.

Capturing images using a light field microscope has some disadvantages: low resolution (0.2 µm), out-of-focus information which often blurs the image (Wright and Wright 2002) and the inability to combine its use with other fluorescent labeling techniques, such as the protein immunostaining involved in lipid metabolism (Koopman et al. 2001). Wide-field fluorescence microscopes provide better resolution, contrast, sensitivity, and acquisition speeds. However, they have limitations to analyze thick samples, since any out-of-focus feature produces a blurry haze in each image plane, reducing contrast (Jonkman and Brown 2015).

Therefore, the confocal laser scanning microscope represents an important tool in this field, since it can be used to produce optical sections of the specimen at relatively shallow depths of field (0.5–1.5 µm). Thus eliminating or reducing the background (which leads to loss of image quality) allows the collection of the information from a well-defined plane, rather than from the entire thickness of the specimen. Moreover, eliminating out-of-focus light results in increased contrast, clarity, and detection sensitivity. Another advantage of confocal microscopy is that cells can

be scanned in depth (z axis). These advantages make it possible to obtain high quality images with optimum resolution (Wright and Wright 2002). Here, we describe a method for quantitatively assessing LD by combining Oil Red staining with nuclear morphometric analysis on cultured cells in vitro using CLSM and estimating morphological parameters using the point counting method.

Materials and methods

Materials

The human hepatocarcinoma cell line (HepG2) was obtained from Rio de Janeiro Cell Bank, UFRJ, Rio de Janeiro, Brazil. DMEM and FBS were obtained from Gibco, Life Technologies. Streptomycin (100 mg/mL) and penicillin (100 units/mL), 40,6-diamidino-2-phenylindole (DAPI) and Clearmount solution were obtained from Invitrogen, Carlsbad, CA. Oil Red was supplied by Sigma-Aldrich, USA. Oleic acid (OA) was supplied by Synth, Brazil and isopropanol were supplied by Nuclear, Brazil. Coverslips were obtained from Assistent, Germany.

Cellular Culture and Treatment

HepG2 cells were cultivated in DMEM supplemented with 10% FBS, 1% streptomycin (100 mg/mL) and penicillin (100 units/mL), 2 g/L HEPES buffer and 3.7 g/L $NaHCO_3$ in a humidified atmosphere with 5% CO_2 at 37 °C. Stock solutions of OA were prepared in isopropanol and dilutions were prepared in DMEM supplemented with 10% FBS. Round 18-mm diameter coverslips were first washed with detergent solution Extran® 2%, after with distilled water three times and posteriorly sterilized in an autoclave. Cells were cultured for 24 hours before treatment under sterile coverslips placed in 6-well culture plates (6.0×10^4 cells/well). Cells were treated with 100 µM OA for 24 hours. Control wells contained DMEM and 10% FBS.

Oil Red and DAPI Staining

The protocol described below was adapted (Lillie and Ashburn 1943). After the treatment period, culture medium was discarded and cells were washed twice with

PBS. Posteriorly, the cells were fixed with 4% paraformaldehyde for 30 min. Then, fixed cells were washed thrice with PBS and subsequently rinsed with 60% isopropanol. After, the cells were stained with freshly prepared 0.3% Oil Red solution (previously filtered with a filter 0.22 µm) for 15 min. Thus, cells were rinsed with 60% isopropanol, washed thrice with PBS and subsequently stained with a solution containing 300 nM DAPI for 30 min. After, cells were washed once with PBS and Milli Q water. The coverslips were removed from the culture plates and dried at room temperature protected from light. Glass slides 26 mm × 76 mm were assembled with overlapping coverslips and Clearmount solution mounting medium.

Image Acquisition

Images were captured under a confocal laser scanning microscope (Leica TCS SP8, Leica Microsystems, Germany). Fifty single confocal sections with a z-step size of 0.1 µM were acquired with a 63× (numeric aperture 1.40) oil-immersion objective (HC PL APO CS2 63×/1.40 OIL, Leica Germany). For each sample, images of four fields were acquired and processed with Leica Application Suite X (LASX) software. The Oil Red fluorescence was measured after being excited by a 552 nm laser beam and emission scan collected at 660 nM. The DAPI fluorescence was measured after laser exciting at 390 nm and emission collected at 460 nm. Following image acquisition, all fifty z sections were projected from each acquired field of the sample, using Leica Application Suite X (LASX) software.

Lipid Droplets Quantification

The percentage of area covered by LD (pALD) was calculated using a stereological tool, the point counting method (Fernandes et al. 2016; Lima et al. 2018). The maximum projection images (projection of fifty z sections) were analyzed using Image Pro Plus 6.0 software (IPP6– Media Cybernetics, Silver Spring, MD). To quantify the percentage of area covered by LD, a grid mask (a grid of crosses with equidistant intervals) was placed over the images, each cross corresponding to one counting point, as shown in figure 1. When the upper right quadrant of the cross hit images of LD they were counted. The mean of counted points in the control samples was considered as 100%. To quantify the cell number, a quantitative analysis, similar to the Neubauer

chamber was performed (de Senna et al. 2017). Briefly, the overall area of the image was named the area of interest (AOI), nuclei located inside each image or intersected by the upper and/or left edges of the AOIs were counted. Nuclei intersected by the lower and/or the right edges of the AOIs were not counted. The mean number of nuclei in the control samples was considered as 100%.

Thus, the following morphometric parameters were calculated: (1) Percentage of area covered by LD in relation to control group (pALD); (2) Percentage of area covered by LD per cell (cALD); (3) Percentage of cells also in relation to control group (% cells). In these 3 morphometric parameters, controls were considered as 100%. Below, these 3 morphological parameters are briefly explained.

The pALD in relation to the control group was calculated for each image as follows: number of crosses (from grid mask) that hit LD in treated sample divided by the mean number of crosses (also from grid mask) that hit LD in control samples multiplied by 100. Thus, values of 130% in the treated group indicate that the area covered by LD in the treated group is 30% larger than in the control group.

The percentage of cells in the treated group in relation to the control group was calculated for each image as follows: number of cells counted in the AOI of the treated sample image divided by the average number of cells counted in the AOIs of the control samples images; this result is multiplied by 100. In this case, values of 130% in the treated group indicate that in treated group, the number of cells counted is 30% higher than in the control group.

The cALD was calculated for each image as follows: In the treated and controls groups, the number of crosses that hit LD in the AOI placed on the image is divided by the number of cells counted in the same AOI, the value obtained in the treated group is divided by the value obtained in the control group and the result obtained is multiplied by 100. In this parameter, values of 130% in the treated group indicate an increase of 30% in the area covered by LD per cell in the treated group.

In total, 10 images by group were analyzed. The analyses were performed by two blinded researchers specialized in image analysis, planar morphometry and stereology.

Nuclear morphometric analysis (NMA)

The NMA was performed with the same maximum projection images used to quantify the LDs and the same Image Pro Plus 6.0 software (IPP6– Media Cybernetics, Silver Spring, MD). The percentages of normal, small and regular, large and regular and irregular nuclei were determined by measuring the nucleus area and identifying the nuclear morphometry (aspect, area box, radius ratio and roundness), which were combined into a single nuclear irregularity index (NII). Different nuclear phenotypes were separated in an area versus NII plot and control cell nuclei were used to set the normal parameters (Filippi-Chiela et al. 2012)

Data and statistical analysis

All results are presented as mean ± SD from three independent experiments. The Unpaired Student's t-test was used for comparisons between groups. A p value < 0.05 was considered statistically significant. Statistical analyses were performed using GraphPad Prism 5.0 (GraphPad Software, San Diego, CA).

Results and Discussion

The maximum projections of the sections obtained with the confocal laser scanning microscope provided high resolution images, with excellent definition of the LD as shown in figure 2, which facilitated the quantification of LD by image analysis. Our study is the first in the literature to report a method of quantifying LD by combining Oil Red staining with confocal laser scanning microscopy and applying the point counting method of image analysis. A study that described a protocol for conventional fluorescence microscopy using OR staining obtained better results in comparison to bright-field microscopy. The advantages were elimination of phospholipid interference in the automated quantification of LD and possibility of performing multi-immunofluorescence staining on a single section (Koopman et al. 2001), although with the limitations in term of image quality inherent to conventional fluorescence microscope. Another study using a Nile Red lipophilic dye and conventional fluorescence microscopy also obtained images with low contrast and poor definition of

the LD (Yao et al. 2011), showing the need a more suitable method to improve the LD image quality and quantification.

Most studies that use OR staining do not involve quantitative assessment of the images (Cui et al. 2010; Zhao et al. 2014; Cao et al. 2016). Some use the staining protocol only to show representative images of LD stained with OR (Zhao et al. 2014) or dissolve the LD with subsequent reading of the optical density in a Microplate Reader (Cui et al. 2010; Cao et al. 2016). Our study proposed the application of the point counting method to directly quantify the pALD in each image, eliminating possible limitations regarding dissolution and lipid stability or low sensitivity for samples with small amounts of LD. The point counting method is highly accurate and allows the exclusion of possible artifacts in the image, which is often impossible using automated protocols in image analysis software (Xavier et al. 2005). The point counting method is widely used for distinct applications, such as estimating the percentage area in histological images (Fernandes et al. 2016) and mitochondrial area in cell cultures (Lima et al. 2018).

As shown in figure 3, it was possible to quantify three morphometric parameters in relation to the control group (considered 100%), the pALD (Fig. 3C), the percentage of cells (Fig. 3D) and the cALD (Fig. 3E). The results showed that, as expected, oleic acid was able to increase approximately 4-fold the pALD and the cALD, as shown in figures 3C and 3E. Interestingly, there was an increase in the percentage of cells after treatment with oleic acid. Our results are in agreement with another study that showed that Nonalcoholic fatty liver disease in an animal model correlates with an increase in the number of proliferating hepatocytes in the liver (VanSaun et al. 2013). A study that used HepG2 cells treated with the oleic acid (0.1-2mM) for 24h showed an excellent correlation of the measured optical density using the OR-based colorimetric quantitative assay (Cui et al. 2010). However, no image analysis was performed in that study. Image-based quantification of LD is important to corroborate the results obtained by colorimetric assays, since they have limits of detection affecting the sensitivity of the assay.

The treatment with oleic acid did not cause nuclear alterations, according to data obtained with the nuclear morphometry, as shown in figure 4. Our results are in agreement with another study that showed that apoptosis was induced in Hepg2 cells only with doses of oleic acid higher than 600 µM (Cui et al. 2010). Therefore, it was expected that our treatment with 100 µM of oleic acid would induce the accumulation

of LD without increasing the percentage of small and regular nuclei (characteristic of apoptosis) or other changes in nuclear morphology. However, our main interest in double staining was to verify the compatibility of OR and DAPI, which was confirmed.

In conclusion, the present study developed a simple, fast, precise and unbiased method of quantifying LD by combining Oil Red staining with DAPI for nuclear analysis using confocal laser scanning microscopy. This method provided great gains in the quality of the images of LD compared to conventional fluorescence microscopy due to the elimination of out-of-focus light, increased contrast and enhanced definition of the LD. We hope that this protocol, and any adaptations of it, might be accepted for use by other researchers in future studies to obtain more detailed and reliable results.

References

ALKHATATBEH MJ, LINCZ LF, THORNE RF (2016) Low simvastatin concentrations reduce oleic acid-induced steatosis in HepG2 cells: An in vitro model of non-alcoholic fatty liver disease. Exp Ther Med 11:1487–1492 . doi: 10.3892/etm.2016.3069

Alkhouri N, Carter-Kent C, Feldstein AE (2011) Apoptosis in nonalcoholic fatty liver disease: diagnostic and therapeutic implications. Expert Rev Gastroenterol Hepatol 5:201–12 . doi: 10.1586/egh.11.6

Boren J, Brindle KM (2012) Apoptosis-induced mitochondrial dysfunction causes cytoplasmic lipid droplet formation. Cell Death Differ 19:1561–1570 . doi: 10.1038/cdd.2012.34

Brookheart RT, Michel CI, Schaffer JE (2009) As a Matter of Fat. Cell Metab 10:9–12 . doi: 10.1016/j.cmet.2009.03.011

Cao P, Huang G, Yang Q, et al (2016) The effect of chitooligosaccharides on oleic acid-induced lipid accumulation in HepG2 cells. Saudi Pharm J SPJ Off Publ Saudi Pharm Soc 24:292–8 . doi: 10.1016/j.jsps.2016.04.023

Cui W, Chen SL, Hu K-Q (2010) Quantification and mechanisms of oleic acid-induced steatosis in HepG2 cells. Am J Transl Res 2:95–104

Daemen S, van Zandvoort MAMJ, Parekh SH, Hesselink MKC (2016) Microscopy tools for the investigation of intracellular lipid storage and dynamics. Mol Metab 5:153–163 . doi: 10.1016/J.MOLMET.2015.12.005

de Senna PN, Bagatini PB, Galland F, et al (2017) Physical exercise reverses spatial memory deficit and induces hippocampal astrocyte plasticity in diabetic rats. Brain Res 1655:242–251 . doi: 10.1016/j.brainres.2016.10.024

Fernandes RO, De Castro AL, Bonetto JHP, et al (2016) Sulforaphane effects on postinfarction cardiac remodeling in rats: modulation of redox-sensitive prosurvival and proapoptotic proteins. J Nutr Biochem 34:106–117 . doi: 10.1016/j.jnutbio.2016.05.004

Filippi-Chiela EC, Oliveira MM, Jurkovski B, et al (2012) Nuclear morphometric analysis (NMA): screening of senescence, apoptosis and nuclear irregularities. PLoS One 7:e42522 . doi: 10.1371/journal.pone.0042522

Filippi-Chiela EC, Thomé MP, e Silva MM, et al (2013) Resveratrol abrogates the temozolomide-induced G2 arrest leading to mitotic catastrophe and reinforces the temozolomide-induced senescence in glioma cells. BMC Cancer 13:147 . doi: 10.1186/1471-2407-13-147

Herms A, Bosch M, Ariotti N, et al (2013) Cell-to-Cell Heterogeneity in Lipid Droplets Suggests a Mechanism to Reduce Lipotoxicity. Curr Biol 23:1489–1496 . doi: 10.1016/j.cub.2013.06.032

Jonkman J, Brown CM (2015) Any Way You Slice It-A Comparison of Confocal Microscopy Techniques. J Biomol Tech 26:54–65 . doi: 10.7171/jbt.15-2602-003

Koopman R, Schaart G, Hesselink MK (2001) Optimisation of oil red O staining permits combination with immunofluorescence and automated quantification of lipids. Histochem Cell Biol 116:63–8

Krai J, Beckenkamp A, Gaelzer MM, et al (2017) Doxazosin nanoencapsulation improves its in vitro antiproliferative and anticlonogenic effects on breast cancer cells. Biomed Pharmacother 94:10–20 . doi: 10.1016/j.biopha.2017.07.048

Lillie R, Ashburn L (1943) Supersaturated solutions of fat stains in dilute isopropanol for demonstration of acute fatty degeneration not shown by Herxheimer's technique. Arch Pathol 36:432–440

Lima KG, Krause GC, da Silva EFG, et al (2018) Octyl gallate reduces ATP levels and Ki67 expression leading HepG2 cells to cell cycle arrest and mitochondria-mediated apoptosis. Toxicol Vitr 48:11–25 . doi: 10.1016/j.tiv.2017.12.017

Lima KG, Krause GC, Schuster AD, et al (2016) Gallic acid reduces cell growth by induction of apoptosis and reduction of IL-8 in HepG2 cells. Biomed Pharmacother 84:1282–1290 . doi: 10.1016/j.biopha.2016.10.048

Mandelkow R, Gümbel D, Ahrend H, et al (2017) Detection and Quantification of Nuclear Morphology Changes in Apoptotic Cells by Fluorescence Microscopy and Subsequent Analysis of Visualized Fluorescent Signals. Anticancer Res 37:2239–2244 . doi: 10.21873/anticanres.11560

Menegotto PR, da Costa Lopez PL, Souza BK, et al (2017) Gastrin-Releasing Peptide Receptor Knockdown Induces Senescence in Glioblastoma Cells. Mol Neurobiol 54:888–894 . doi: 10.1007/s12035-016-9696-6

Ogrodnik M, Miwa S, Tchkonia T, et al (2017) Cellular senescence drives age-dependent hepatic steatosis. Nat Commun 8:15691 . doi: 10.1038/ncomms15691

VanSaun MN, Mendonsa AM, Lee Gorden D (2013) Hepatocellular Proliferation Correlates with Inflammatory Cell and Cytokine Changes in a Murine Model of Nonalchoholic Fatty Liver Disease. PLoS One 8:e73054 . doi: 10.1371/journal.pone.0073054

Walsh MJ, Vanags DM, Clouston AD, et al (2004) Steatosis and liver cell apoptosis in chronic hepatitis C: A mechanism for increased liver injury. Hepatology 39:1230–1238 . doi: 10.1002/hep.20179

Wright SJ, Wright DJ (2002) Introduction to Confocal Microscopy. Methods Cell Biol 70:1–85 . doi: 10.1016/S0091-679X(02)70002-2

Xavier LL, Viola GG, Ferraz AC, et al (2005) A simple and fast densitometric method for the analysis of tyrosine hydroxylase immunoreactivity in the substantia nigra pars compacta and in the ventral tegmental area. Brain Res Brain Res Protoc 16:58–64 . doi: 10.1016/j.brainresprot.2005.10.002

Yao H-R, Liu J, Plumeri D, et al (2011) Lipotoxicity in HepG2 cells triggered by free fatty acids. Am J Transl Res 3:284–91

Zeng L, Tang W, Yin J, et al (2016) Alisol A 24-Acetate Prevents Hepatic Steatosis and Metabolic Disorders in HepG2 Cells. Cell Physiol Biochem 40:453–464 . doi: 10.1159/000452560

Zhao F, Xie P, Jiang J, et al (2014) The Effect and Mechanism of Tamoxifen-Induced Hepatocyte Steatosis in Vitro. Int J Mol Sci 15:4019–4030 . doi: 10.3390/ijms15034019

Figure Legends

Fig. 1. Representative digitized images of the maximum projections of nuclei and LD from HepG2 cells through confocal laser scanning microscopy. The grid mask used to estimate the percent of LD is presented in this figure. Control cells (1A) and cells treated with 100µM oleic acid (1B). LDs were stained with Oil Red and the nuclei with DAPI. Calibration bar = 25 µm.

Fig. 2. The maximum projections of the sections obtained with the confocal laser scanning microscope provided high resolution images, with excellent definition of the LD. Representative digitized images of the maximum projections of nuclei and LD from HepG2 cells through confocal laser scanning microscopy. Control cells (1A) and cells treated with 100µM oleic acid (1B). LD were stained with Oil Red and the nuclei with DAPI. Calibration bar = 25 µm.

Fig. 3. Representative digitized images of the maximum projections of nuclei and LD from HepG2 cells through confocal laser scanning microscopy. Control cells (3A) and cells treated with 100µM oleic acid (3B). Percentage area covered by LD (pALD, 3C), percentage of cells (% cells, 3D) and the percentage area covered by LD per cell (cALD, 3E). In these 3 morphometric parameters, controls were considered to be 100%. OA: cells treated with 100µM oleic acid for 24 hours. The results showed that oleic acid was able to increase approximately 4-fold the percentage area covered by LD, promote increases in the percentage of cells and in the percentage area covered by LD per cell. Data are represented as the mean + SD from three independent experiments. (** $p < 0.01$, ***$p < 0.0001$). OA: oleic acid.

Fig. 4. Effect of OA on the nuclear morphometry of HepG2 cells after 24 h of treatment. At least 90 nuclei in three independent experiments were analyzed from each group. DAPI-stained nuclei were analyzed for size and irregularity and the percentages of normal (N), large and regular (LR), large and irregular (LI) and irregular (I) nuclei are shown (4A, 4B). The treatment with oleic acid did not cause nuclear alterations, since 95.7% of the nuclei from the treated group were classified as normal, similar to the control group. OA: oleic acid, N: normal, S: small, SR: small and regular, SI: small and

irregular, LR: large and regular, LI: large and irregular and I: irregular. Data are represented as the mean + SD from three independent experiments.

Figures

Fig. 1.

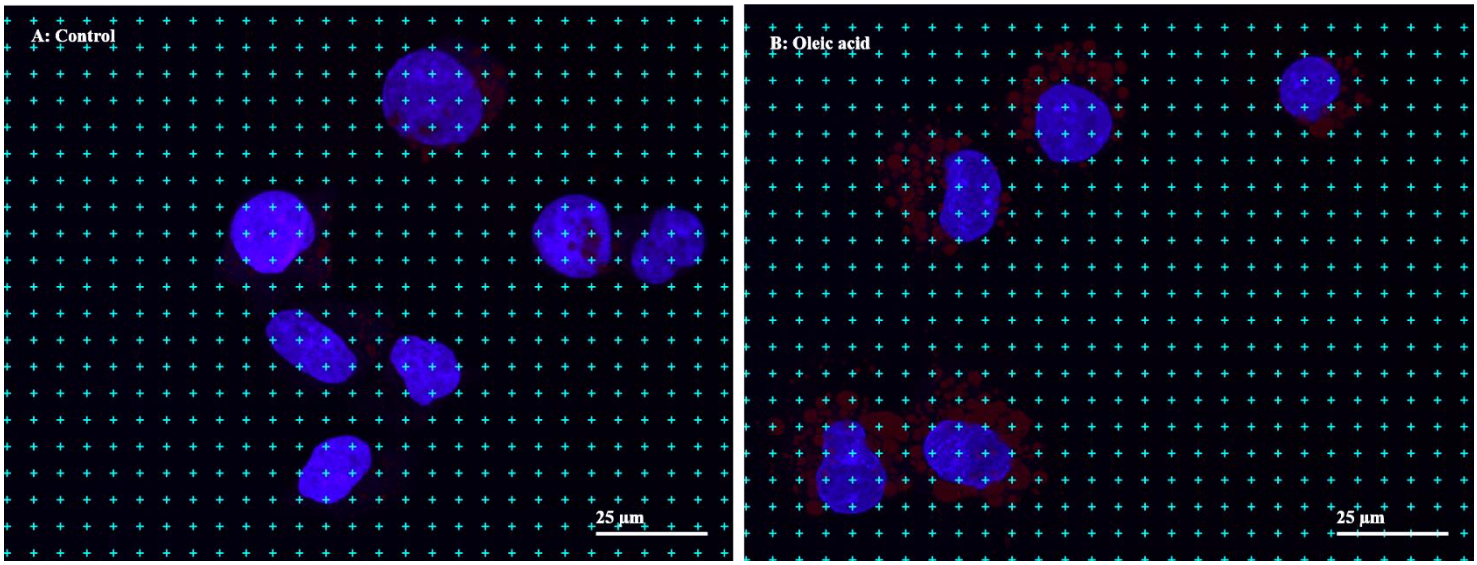

Fig. 2.

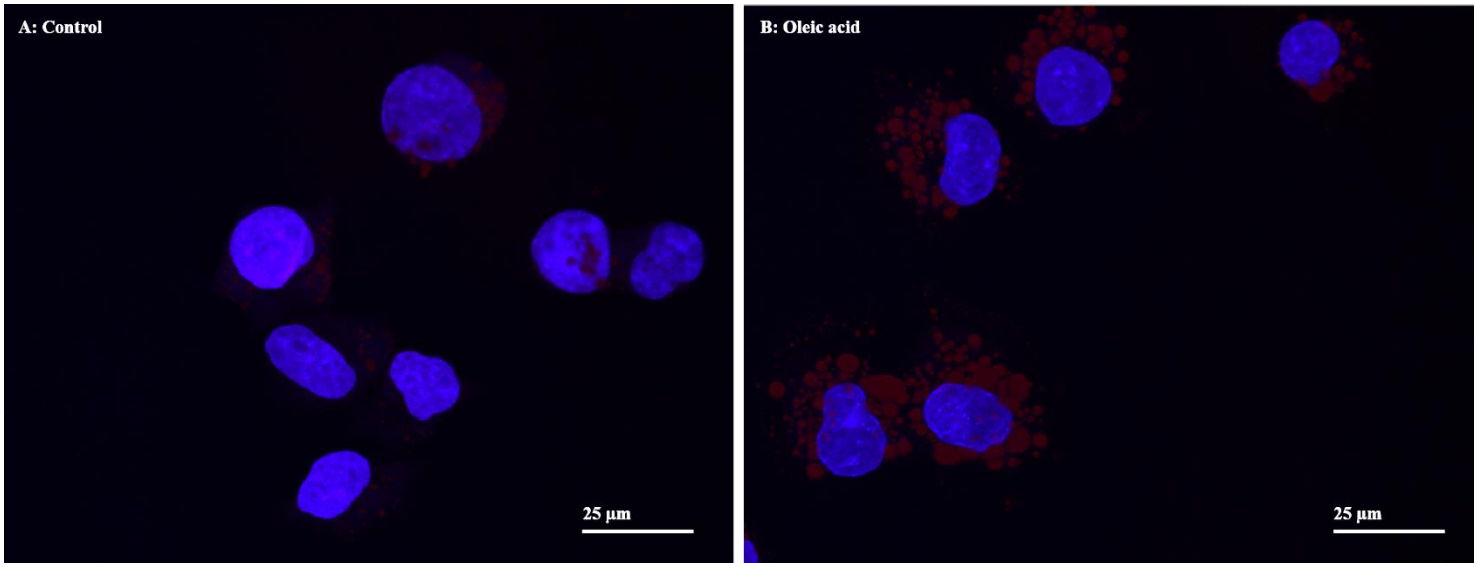

Fig. 3.

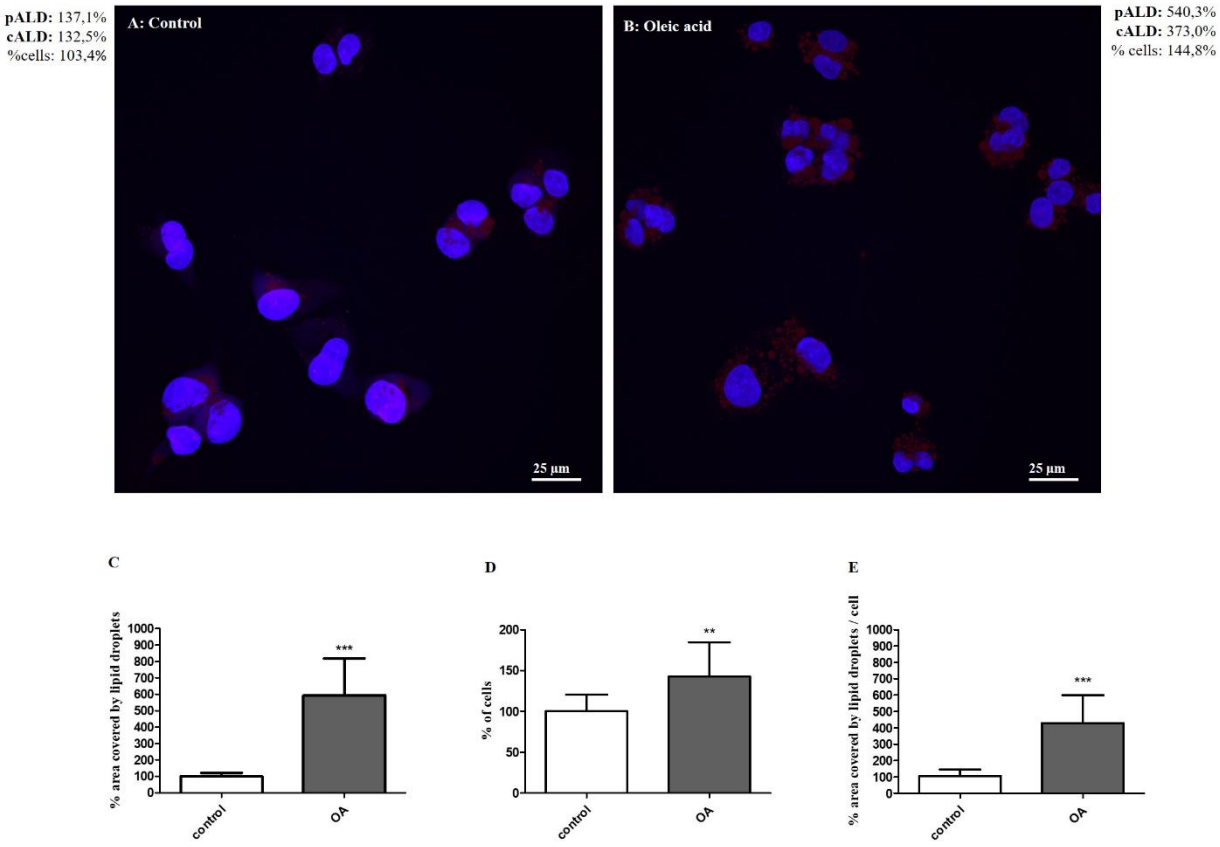
pALD: 137,1%
cALD: 132,5%
%cells: 103,4%
A: Control
B: Oleic acid
pALD: 540,3%
cALD: 373,0%
% cells: 144,8%
25 µm
25 µm
C
% area covered by lipid droplets
***
control
OA
D
% of cells
**
control
OA
E
% area covered by lipid droplets / cell
***
control
OA

Fig. 4.

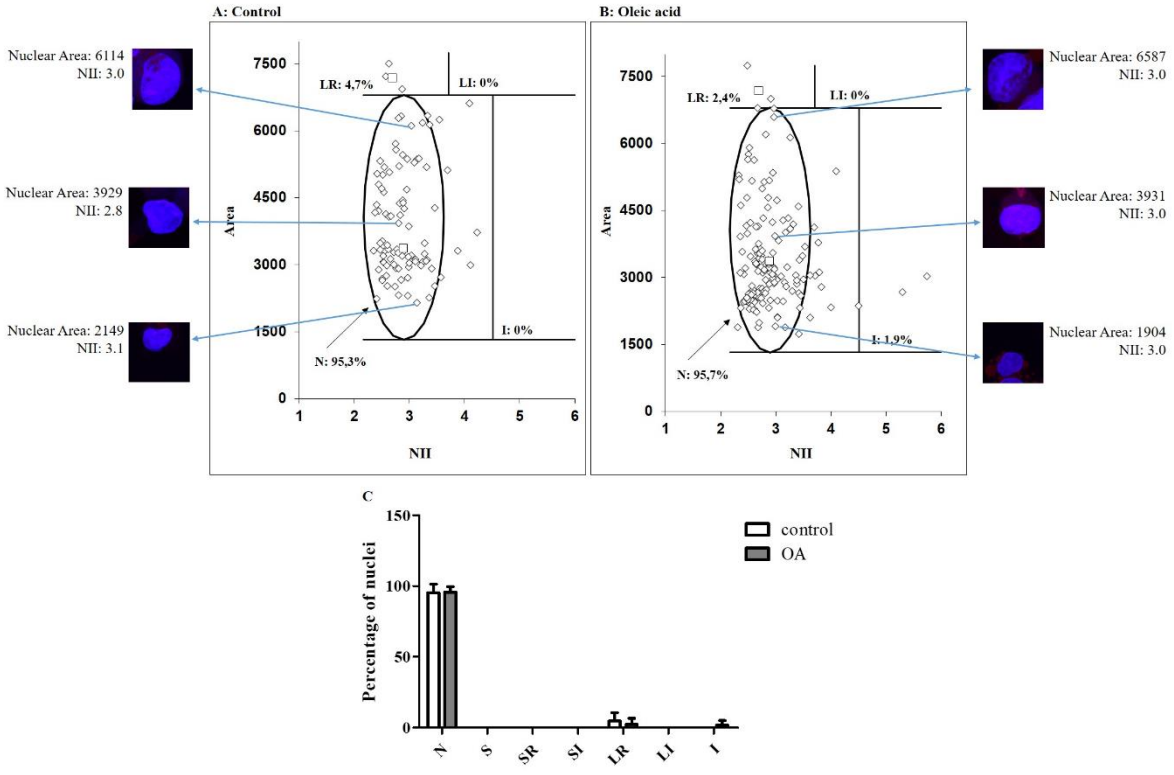
A: Control
B: Oleic acid
Nuclear Area: 6114
NII: 3.0
Nuclear Area: 3929
NII: 2.8
Nuclear Area: 2149
NII: 3.1
LR: 4,7%
LI: 0%
I: 0%
N: 95,3%
LR: 2,4%
LI: 0%
I: 1,9%
N: 95,7%
Area
NII
Nuclear Area: 6587
NII: 3.0
Nuclear Area: 3931
NII: 3.0
Nuclear Area: 1904
NII: 3.0
C
Percentage of nuclei
control
OA
N
S
SR
SI
LR
LI
I

CAPÍTULO V

1. CONSIDERAÇÕES FINAIS

As opções terapêuticas atuais para o Carcinoma Hepatocelular (CH) são restritas, de alto custo e em sua maioria invasivas. Ao mesmo tempo, o câncer de fígado (80% dos casos correspondem ao CH) é a segunda causa de morte por câncer em homens e a sexta em mulheres no mundo, segundo os últimos dados publicados pela Organização Mundial da Saúde, referente ao ano de 2012 (TORRE et al., 2016). Dessa forma, a busca por novas opções de tratamento para o CH apresenta alta relevância e vem crescendo nos últimos anos.

Muitos estudos têm avaliado o efeito antiproliferativo de moléculas de origem natural em modelos de CH *in vitro* e *in vivo* (LIMA et al., 2016; MAIOLI et al., 2018; MAURYA; TRIGUN, 2017). O galato de octila (GO), o qual pode ser obtido dos frutos da *Terminalia bellerica* ou semi-sinteticamente a partir do ácido gálico, tem sido aplicado em estudos com outros tipos de câncer, como melanoma (DE CORDOVA et al., 2011), leucemia (LOCATELLI et al., 2008), linfoma de células B (SERRANO et al., 1998) e recentemente em modelo de metástase pulmonar (CORDOVA et al., 2017) com resultados satisfatórios. Entretanto, antes da publicação do nosso primeiro artigo (LIMA et al., 2018), não havia relato na literatura sobre o efeito do GO em modelo de CH.

Em nosso estudo anterior (dissertação de mestrado) pesquisamos o efeito do ácido gálico nas células HepG2. Nossos resultados mostraram que essa molécula de origem natural tinha a capacidade de induzir à apoptose com uma dose de 550 µM com tratamento de 48 horas (LIMA et al., 2016). Então, resolvemos pesquisar a ação de algum derivado do ácido gálico que pudesse apresentar efeito semelhante com menor dose, com o objetivo de facilitar futuras pesquisas com modelo animal. Uma vez que o GO é um derivado do ácido gálico que apresenta maior lipofilicidade e apresentou bons resultados em outros modelos de câncer, escolhemos essa molécula para realizar nossa pesquisa.

Inicialmente realizamos uma curva de doses de GO de 5 a 100 µM com tempos de tratamento de 24 e 48 horas. Observamos redução significativa no número de células viáveis a partir da dose de 5 µM com 24 horas de tratamento. Então, realizamos a estimativa da concentração inibitória de 50% das células (CI50) por regressão linear que resultou em 40 µM com 24 horas de tratamento. Posteriormente,

confirmamos o valor da CI50 através do ensaio de contagem de células viáveis e escolhemos essa concentração para os experimentos subsequentes.

O próximo experimento que realizamos foi a quantificação da enzima lactato desidrogenase (LDH) no meio de cultura das células após o período de tratamento de 24 horas. Observamos que o GO não aumentou a LDH após o tratamento, excluindo a hipótese de o GO reduzir o número de células viáveis por indução de necrose. Posteriormente, realizamos experimentos para avaliação de estresse oxidativo através dos ensaios DCFH-DA, TBARS, GSH e Catalase. Apesar de estudos anteriores com outros modelos de câncer terem encontrado aumento do estresse oxidativo após o tratamento com GO (DE CORDOVA et al., 2011; LOCATELLI et al., 2008, 2009a), nossos resultados não revelaram o mesmo com as células HepG2. Interessantemente, observamos somente um aumento nos níveis de catalase após o tratamento com GO, sugerindo que essa enzima poderia estar controlando os níveis de H_2O_2 nas células tratadas.

A avaliação morfológica das células após tratamento usando microscópio invertido de contraste de fase revelou que as células apresentavam acúmulo de vesículas no citoplasma. Em razão de alguns estudos apontarem que o acúmulo de gotas lipídicas está associado com os mecanismos de autofagia (MARTINET et al., 2006) e apoptose (BOREN; BRINDLE, 2012), realizamos o experimento de coloração de gotas lipídicas com Oil Red. Através desse experimento conseguimos confirmar que as vesículas se tratavam de gotas lipídicas e que nosso tratamento com GO aumentava a quantidade de lipídeos nas células. Esse achado nos direcionou para a pesquisa do envolvimento de autofagia e apoptose.

Após a obtenção desses resultados, executamos o ensaio de quantificação de organelas vesiculares ácidas (AVOs) usando laranja de acridina e o ensaio de apoptose com Anexin V e Iodeto de propídeo, ambos por citometria de fluxo. Somente nosso controle positivo com cisplatina mostrou aumento na percentagem de células com AVOs e de células em apoptose, demonstrando o não envolvimento dos mecanismos de autofagia e apoptose no efeito do GO com 24 horas de tratamento. O resultado do ensaio de autofagia está de acordo com estudos prévios, os quais não encontraram indução de autofagia no mecanismo do GO (DE CORDOVA et al., 2011; LOCATELLI et al., 2009a). Contudo, o resultado do ensaio de apoptose não foi semelhante ao encontrado em outros estudos, pois esses reportaram a indução de apoptose como mecanismo do GO (DE CORDOVA et al., 2011; LOCATELLI et al.,

2009a; SERRANO et al., 1998). Dessa forma, hipotetizamos que a indução de apoptose poderia ocorrer após tempo maior que 24 horas de tratamento, sendo necessário novo experimento para avaliação da apoptose com maior tempo de exposição das células ao tratamento com GO.

Resolvemos primeiramente continuar com nossa investigação sobre o mecanismo envolvido no tratamento por 24 horas. Então, procedemos com a avaliação do ciclo celular através da marcação com 7-AAD e análise por citometria de fluxo. Detectamos parada do ciclo celular em fase S após o tratamento com GO por 24 horas. Isso sugere que o GO causou estresse genotóxico durante a replicação do DNA, que pode ocorrer por depleção de dNTP, inibição química de DNA polimerases, indução de síntese de estruturas de DNA aberrante, replicação incompleta ou quebra da dupla fita de DNA (BARTEK; LUKAS; LUKAS, 2004).

A seguir, realizamos a Análise Morfométrica Nuclear para verificar a possibilidade de aumento na percentagem de núcleos grandes e regulares, os quais estão associados com senescência (estado permanente de parada de ciclo celular). No entanto, não foi observada indução de senescência. Com o objetivo de confirmar o efeito antiproliferativo do GO com 24 horas de tratamento, realizamos a avaliação da expressão da proteína Ki 67. Essa proteína tem sido usada por muitos anos como um marcador de proliferação, visto que é geralmente altamente expressa em células que estão proliferando e pouco expressa em células quiescentes (GERDES et al., 1984). Nosso resultado mostrou que o GO foi capaz de reduzir significativamente a expressão da Ki 67 após 24 horas de tratamento, corroborando a parada de ciclo celular. Interessantemente, um estudo recente mostrou que a Ki 67 apresenta um papel importante na progressão da fase S do ciclo celular e na manutenção da heterocromatina Xi, visto que estimula à expressão de genes relacionados à replicação do DNA e progressão do ciclo celular (SUN et al., 2017). Isso sugere que a redução da expressão da Ki 67 esteja relacionada à parada de ciclo celular em S.

Continuamos nossa investigação sobre o mecanismo antiproliferativo do GO através da quantificação dos níveis de ATP celular. Um estudo anterior havia reportado que o GO foi capaz de reduzir abruptamente os níveis de ATP celular após dose de 1mM e induziu morte celular de hepatócitos de ratos com tratamento de 30 minutos (NAKAGAWA; TAYAMA, 1995). Esse estudo também mostrou que o GO causou desacoplamento parcial da fosforilação oxidativa mitocondrial em mitocôndrias isoladas de hepatócitos de ratos com doses a partir de 12,5 µM. Sendo

assim, realizamos quantificação dos níveis de ATP celular por HPLC. Nosso resultado mostrou redução significativa dos níveis de ATP após 24 horas de tratamento com GO, concordando com estudos anteriores (LOCATELLI et al., 2009a; NAKAGAWA; TAYAMA, 1995). Dado que a sinalização para a proliferação celular só ocorre quando há reserva energética suficiente (FOGARTY; HARDIE, 2010), acreditamos que a redução dos níveis de ATP celular sinalize para a célula a necessidade de parar a proliferação. Então, a expressão da proteína Ki 67, importante para progressão da fase S do ciclo celular, é reduzida levando à parada do ciclo celular.

Posteriormente, realizamos ensaio para avaliação da viabilidade celular após retratamento das células com GO com até 5 tratamentos em intervalos de 24 horas. Essa avaliação por período mais prolongado permitiu avaliar se as células poderiam apresentar resistência ao GO após retratamento, além de possibilitar maior semelhança aos regimes terapêuticos clínicos. Nossos resultados mostraram que os retratamentos com 40 µM e 20 µM de GO mantiveram o efeito antiproliferativo, no entanto as células que receberam somente um tratamento com GO voltaram a proliferar, assemelhando-se às células controle no 5º dia.

Em razão do GO ter reduzido os níveis de ATP celular em nosso estudo e existirem relatos na literatura de que o ácido gálico e seus derivados podem desacoplar a fosforilação oxidativa mitocondrial (NAKAGAWA; TAYAMA, 1995; SERRANO et al., 1998), decidimos avaliar a toxicidade mitocondrial através da Microscopia Eletrônica de Transmissão (MET). Realizamos análise das mitocôndrias de amostras: controle (veículo DMSO 0,2%), GO 40 µM por 24 horas (1 tratamento) e GO 40 µM a cada 24 horas (2 tratamentos). Nossos resultados mostraram que o uso de 2 tratamentos a cada 24 horas reduziu a densidade mitocondrial e alterou a morfologia das mitocôndrias, visto que promoveu aumento da área mitocondrial, rompimento das cristas mitocondriais e inchaço mitocondrial. Analisamos também a densidade de autofagossomos nas mesmas imagens e não observamos alteração após o tratamento, confirmando nosso resultado de citometria de fluxo, o qual não mostrou indução de autofagia após tratamento com GO.

Em seguida, realizamos experimentos para confirmar as alterações mitocondriais utilizando os marcadores MitoTracker™ Green e MitoTracker™ Red com análise por citometria de fluxo. O primeiro é usado para determinar a massa mitocondrial, uma vez que cora com fluorescência verde todas as mitocôndrias independentemente do seu potencial de membrana; já o segundo, cora com

fluorescência vermelha as mitocôndrias e sua acumulação depende do potencial de membrana. Nossos resultados confirmaram o envolvimento da toxicidade mitocondrial no efeito do GO, posto que observamos redução do número de mitocôndrias e de sua atividade após tratamento único por 24 horas. Além disso, o uso de 2 tratamentos a cada 24 horas mostrou maior toxicidade, visto que causou inchaço mitocondrial e consequente perda da funcionalidade da organela que está de acordo com nossos resultados de MET. Interessantemente, os resultados de citometria já mostraram redução no número de mitocôndrias a partir de 1 tratamento com GO, diferente do encontrado na análise ultraestrutural por MET que mostrou redução da densidade mitocondrial somente com 2 tratamentos com GO. Uma vez que no método por citometria de fluxo é analisada uma quantidade muito superior de células comparado à MET, acreditamos que isso proporcione maior poder de detecção de alterações nas mitocôndrias.

Em virtude do nosso achado de toxicidade mitocondrial e sua conhecida ligação com a indução de apoptose por via intrínseca (KROEMER; GALLUZZI; BRENNER, 2007), realizamos novo experimento para análise de apoptose após 2 tratamentos com GO a cada 24 h. Nossos resultados mostraram que o uso de 2 tratamentos com GO induziu as células à apoptose tardia e um leve aumento de necrose. Dessa forma, concluímos que o tratamento prolongado causou disfunção mitocondrial que culminou em apoptose. Esses resultados estão de acordo com outros estudos que também encontraram indução de apoptose após tratamento com GO em outros tipos de câncer (DE CORDOVA et al., 2011; LOCATELLI et al., 2008, 2009b).

Até esse momento do trabalho, nossos resultados juntos sugeriam que o GO quando em contato por 24 horas com as células HepG2 inibia seu crescimento por diminuir a atividade mitocondrial que resultava na redução dos níveis de ATP celular. Essa redução de aporte energético levava à redução da Ki 67, a qual produzia parada do ciclo celular em fase S. Com relação ao efeito de 2 tratamentos com GO a cada 24 horas, nossos resultados mostravam perda da funcionalidade mitocondrial, inchaço mitocondrial e apoptose. Além disso, não houve resistência ao tratamento após múltiplos tratamentos com GO. Entretanto, ainda não estava claro a relação entre o acúmulo de gotas lipídicas e o efeito antiproliferativo observados após tratamento de 24 horas. Resolvemos então, em um primeiro momento, escrever um artigo reportando apenas os resultados do efeito antiproliferativo. Com relação ao aparente efeito tóxico do GO, que nós evidenciamos pela detecção de gotas lipídicas,

decidimos aprofundar este aspecto, que para nós é muito importante já que traduz um tipo de toxicidade, e os resultados obtidos submetemos para outro periódico científico.

Submetemos o artigo “Octyl gallate reduces ATP levels and Ki67 expression leading HepG2 cells to cell cycle arrest and mitochondria-mediated apoptosis” a revista Toxicology in vitro e um dos revisores nos perguntou a relação do p53 com os efeitos do GO, visto que um outro estudo havia mostrado que o ácido gálico e o galato de dodecila aumentavam a expressão de p53 em ratos intoxicados com tetracloreto de carbono (PERAZZOLI et al., 2017). Com o objetivo de responder ao questionamento do revisor, realizamos experimentos para avaliar a expressão do p53 e p21 pela técnica de Western blot. Infelizmente, apesar de várias tentativas não conseguimos avaliar a expressão do p53, acreditamos que por algum problema com o anticorpo utilizado. Porém, conseguimos êxito na avaliação da expressão do p21. Dado que o p21 é um alvo direto da indução transcricional do supressor tumoral p53, respondemos ao questionamento com nosso resultado da expressão do p21, o qual não mostrou diferença após o tratamento de 24 horas com GO. O resultado do p21 foi então incluído no nosso artigo. Interessantemente, nosso resultado foi semelhante a outro estudo que não encontrou aumento do p21 em resposta a redução de Ki 67 em células de carcinoma colorretal HCT116 e de adenocarcinoma de mama MDA-MB-231 (SUN et al., 2017).

Após a finalização do nosso primeiro artigo sobre o efeito do GO nas células HepG2, prosseguimos com as análises das gotas lipídicas. O método convencional de coloração das gotas lipídicas com Oil Red e obtenção das imagens usando microscópio de campo claro apresenta algumas limitações como baixa resolução, informação fora de foco, dificuldade de análise de amostras espessas, assim como não permite a associação de marcações fluorescentes. Assim, desenvolvemos um método para avaliação quantitativa de gotas lipídicas coradas com Oil Red utilizando microscopia confocal de varredura a laser. Esse método permitiu a análise da projeção máxima de várias secções da amostra melhorando a qualidade das imagens e a associação com DAPI e posterior Análise Morfométrica Nuclear. Como ainda não há relato na literatura de que o GO induz o acúmulo de gotas lipídicas nas células HepG2, utilizamos o ácido oleico, o qual é muito utilizado para induzir acúmulo de lipídeos nessas células (CAO et al., 2016; CUI; CHEN; HU, 2010; ZENG et al., 2016). Escrevemos uma Short Communication intitulada “A simple, fast, precise and unbiased method of analyzing lipid droplets combining Oil Red staining, nuclear

morphometric analysis and confocal laser scanning microscopy” descrevendo o protocolo para marcação das células e análise das imagens pelo método da contagem de pontos e submetemos à revista “Histochemistry and Cell Biology”.

Subsequentemente, quantificamos os triglicerídeos no lisado celular para avaliar se o conteúdo das gotas lipídicas se tratava de triglicerídeos. Nossos resultados mostraram que o GO, assim como o controle positivo com AO induziu o aumento na concentração de triglicerídeos, confirmando nossa hipótese. Em seguida, repetimos o experimento convencional de marcação com Oil Red incluindo um controle positivo tratado com ácido oleico e obtivemos êxito. Além disso, analisamos a densidade de gotas lipídicas e a área das gotas lipídicas utilizando nossas imagens de MET. Nossos resultados mostraram que o GO não modificou a densidade de gotas lipídicas, contudo induziu ao aumento da área das gotas lipídicas, concordando com nosso experimento com Oil Red.

Ao mesmo tempo realizamos a análise da expressão do gene SREBP-1c, o qual é o principal fator de transcrição que controla a síntese de ácidos graxos no fígado (PETTINELLI; OBREGÓN; VIDELA, 2011). Nosso resultado não mostrou alteração na expressão do SREBP1-c após 24 horas de tratamento com GO. Analisamos também a expressão da proteína mTOR, visto que a atuação da via de sinalização Akt/mTOR/SREBP-1c no metabolismo lipídico é amplamente conhecida (LI et al., 2015; PORSTMANN et al., 2008). Interessantemente, o GO reduziu a expressão dessa proteína. Caso o acúmulo de lipídeos estivesse sendo regulado via mTOR e SREBP-1c, seria esperado um aumento na expressão de mTOR e SREBP-1c. Como a redução da expressão da proteína mTOR relaciona-se com redução de proliferação celular, esse resultado concordou com nosso estudo anterior que mostrou parada de ciclo celular e redução da proteína Ki 67 (LIMA et al., 2018).

Uma outra hipótese que avaliamos foi o envolvimento dos receptores PPARα e PPARγ no mecanismo do GO, visto que esses receptores atuam principalmente na regulação de vias metabólicas que controlam a oxidação de ácidos graxos e o metabolismo lipídico (AMENT; MASOODI; GRIFFIN, 2012). Atualmente, não há relatos na literatura sobre a relação desses receptores com os efeitos do GO. Dessa forma, analisamos a expressão dos genes PPARα e PPARγ. Entretanto, não foi observada modificação significativa na expressão desses genes após tratamento com GO. Como nosso estudo anterior mostrou que o GO foi capaz de diminuir a atividade mitocondrial e o número de mitocôndrias após tratamento de 24 horas (LIMA et al.,

2018), sugere-se que a redução da β-oxidação de ácidos graxos mitocondrial esteja relacionada ao acúmulo de gotas lipídicas. Esse achado já foi relatado em outro estudo que mostrou a relação entre o acúmulo de gotas lipídicas e a indução de apoptose em outras linhagens de câncer utilizando quimioterápicos (BOREN; BRINDLE, 2012).

Em razão de o GO ser utilizado em alguns países como aditivo em alimentos (EUROPEAN PARLIAMENT AND THE COUNCIL OF THE EUROPEAN UNION, 2008; U.S. FOOD AND DRUG ADMINISTRATION, 2018) e as células HepG2 serem utilizadas como modelo *in vitro* para estudos sobre esteatose (ALKHATATBEH; LINCZ; THORNE, 2016; CUI; CHEN; HU, 2010; ZENG et al., 2016), decidimos escrever uma Short Communication relatando o efeito do GO no acúmulo de lipídeos.

Nosso estudo intitulado “Octyl gallate induces hepatic steatosis in HepG2 cells through a mTOR/SREBP-1c-independent pathway” foi submetido para a revista “Food and Chemical Toxicology”. Nesse estudo mostramos pela primeira vez a capacidade do GO em induzir o acúmulo de lipídeos em modelo *in vitro* de esteatose hepática. Além disso, mostramos que a via de sinalização Akt/mTOR/SREBP-1c não está envolvida no mecanismo do GO e sugerimos o envolvimento da redução da β-oxidação de ácidos graxos mitocondrial como mecanismo principal. Também relatamos que a modificação da expressão dos genes PPAR-α e PPAR-γ não está envolvida no mecanismo do GO. O estudo indica que o GO pode causar Doença hepática gordurosa não alcóolica, sendo necessários mais estudos que avaliem o efeito do GO como aditivo alimentar em modelo *in vivo* e os mecanismos envolvidos.

Através dos dados obtidos nesse estudo, podemos concluir que (I) o tratamento a curto prazo das células HepG2 com galato de octila reduz a proliferação celular por atingir as mitocôndrias, reduzindo seu número e sua atividade; (II) A toxicidade mitocondrial induzida pelo GO leva à redução dos níveis de ATP; (III) A redução dos níveis de ATP sinaliza para parada de proliferação reduzindo os níveis da proteína Ki 67; (IV) A redução da proteína Ki 67 leva à parada do ciclo celular em fase S; (V) O tratamento prolongado com GO causa perda da funcionalidade mitocondrial, inchaço mitocondrial e apoptose; (VI) O GO induz acúmulo de gotas lipídicas sem envolver a regulação Akt/mTOR/SREBP-1c nem a modificação da expressão dos genes PPAR-α e PPAR-γ; (VII) A quantificação de gotas lipídicas usando microscopia confocal de varredura a laser permite grande ganho na qualidade das imagens possibilitando quantificação mais precisa.

2. REFERÊNCIAS

ADEN, David P. et al. Controlled synthesis of HBsAg in a differentiated human liver carcinoma-derived cell line. **Nature**, [s. l.], v. 282, n. 5739, p. 615–616, 1979. Disponível em: <http://www.nature.com/doifinder/10.1038/282615a0>. Acesso em: 29 dez. 2017.

ALKHATATBEH, MOHAMMAD J.; LINCZ, LISA F.; THORNE, RICK F. Low simvastatin concentrations reduce oleic acid-induced steatosis in HepG2 cells: An in vitro model of non-alcoholic fatty liver disease. **Experimental and Therapeutic Medicine**, [s. l.], v. 11, n. 4, p. 1487–1492, 2016. Disponível em: <http://www.ncbi.nlm.nih.gov/pubmed/27073470>. Acesso em: 14 jan. 2018.

AMENT, Zsuzsanna; MASOODI, Mojgan; GRIFFIN, Julian L. Applications of metabolomics for understanding the action of peroxisome proliferator-activated receptors (PPARs) in diabetes, obesity and cancer. **Genome medicine**, [s. l.], v. 4, n. 4, p. 32, 2012. Disponível em: <http://www.ncbi.nlm.nih.gov/pubmed/22546357>. Acesso em: 18 fev. 2018.

BARTEK, J.; LUKAS, C.; LUKAS, J. Checking on DNA damage in S phase. **Nat Rev Mol Cell Biol**, [s. l.], v. 5, n. 10, p. 792–804, 2004. Disponível em: <https://www.ncbi.nlm.nih.gov/pubmed/15459660>

BOLONDI, Luigi et al. Position paper of the Italian Association for the Study of the Liver (A.I.S.F.): the multidisciplinary clinical approach to hepatocellular carcinoma. **Digestive and Liver Disease**, [s. l.], v. 45, p. 712–723, 2013. Disponível em: <http://www.dldjournalonline.com/article/S1590-8658(13)00014-5/pdf>. Acesso em: 31 jan. 2018.

BOREN, J.; BRINDLE, K. M. Apoptosis-induced mitochondrial dysfunction causes cytoplasmic lipid droplet formation. **Cell Death & Differentiation**, [s. l.], v. 19, n. 9, p. 1561–1570, 2012. Disponível em: <http://www.ncbi.nlm.nih.gov/pubmed/22460322>. Acesso em: 16 fev. 2018.

BORGHT, Sara Vander et al. Breast Cancer Resistance Protein (BCRP/ABCG2) Is Expressed by Progenitor Cells/Reactive Ductules and Hepatocytes and Its Expression Pattern Is Influenced by Disease Etiology and Species Type: Possible Functional Consequences. **Journal of Histochemistry & Cytochemistry**, [s. l.], v. 54, n. 9, p. 1051–1059, 2006. Disponível em: <http://www.ncbi.nlm.nih.gov/pubmed/16709727>. Acesso em: 24 jan. 2018.

BOSCH, F. X. et al. Primary liver cancer: worldwide incidence and trends. **Gastroenterology**, [s. l.], v. 127, n. 5 Suppl 1, p. S5–S16, 2004. Disponível em: <http://www.ncbi.nlm.nih.gov/pubmed/15508102>

BRUIX, J.; LLOVET, J. M. Prognostic prediction and treatment strategy in hepatocellular carcinoma. **Hepatology**, [s. l.], v. 35, n. 3, p. 519–524, 2002. Disponível em: <http://www.ncbi.nlm.nih.gov/pubmed/11870363>

CANCER GENOME ATLAS RESEARCH NETWORK. ELECTRONIC ADDRESS: WHEELER@BCM.EDU, Adrian et al. Comprehensive and Integrative Genomic Characterization of Hepatocellular Carcinoma. **Cell**, [s. l.], v. 169, n. 7, p. 1327–1341.e23, 2017. Disponível em: <http://www.ncbi.nlm.nih.gov/pubmed/28622513>. Acesso em: 21 jan. 2018.

CAO, Peiqiu et al. The effect of chitooligosaccharides on oleic acid-induced lipid accumulation in HepG2 cells. **Saudi pharmaceutical journal : SPJ : the official publication of the Saudi Pharmaceutical Society**, [s. l.], v. 24, n. 3, p. 292–8, 2016. Disponível em: <http://www.ncbi.nlm.nih.gov/pubmed/27275117>. Acesso em: 14 jan. 2018.

CASTELLI, Germana; PELOSI, Elvira; TESTA, Ugo. Liver cancer: Molecular characterization, clonal evolution and cancer stem cells. **Cancers**, [s. l.], v. 9, n. 9, 2017. Disponível em: <https://www.ncbi.nlm.nih.gov/pmc/articles/PMC5615342/pdf/cancers-09-00127.pdf>. Acesso em: 21 jan. 2018.

CHEN, Bin et al. Relating hepatocellular carcinoma tumor samples and cell lines using gene expression data in translational research. **BMC medical genomics**, [s. l.], v. 8 Suppl 2, n. Suppl 2, p. S5, 2015. Disponível em: <http://www.ncbi.nlm.nih.gov/pubmed/26043652>. Acesso em: 24 jan. 2018.

CHEN, George G. et al. Mutation of p53 in recurrent hepatocellular carcinoma and its association with the expression of ZBP-89. **The American journal of pathology**, [s. l.], v. 162, n. 6, p. 1823–9, 2003. Disponível em: <http://www.ncbi.nlm.nih.gov/pubmed/12759240>. Acesso em: 21 jan. 2018.

CHEN, Qian et al. Effects of Natural Products on Fructose-Induced Nonalcoholic Fatty Liver Disease (NAFLD). **Nutrients**, [s. l.], v. 9, n. 12, p. 96, 2017. Disponível em: <http://www.ncbi.nlm.nih.gov/pubmed/28146130>. Acesso em: 15 fev. 2018.

COLLISON, Kate S. et al. Effect of dietary monosodium glutamate on *trans* fat-induced nonalcoholic fatty liver disease. **Journal of Lipid Research**, [s. l.], v. 50, n. 8, p. 1521–1537, 2009. Disponível em: <http://www.ncbi.nlm.nih.gov/pubmed/19001666>. Acesso em: 15 fev. 2018.

COLLISON, Kate S. et al. Prediabetic changes in gene expression induced by aspartame and monosodium glutamate in Trans fat-fed C57Bl/6 J mice. **Nutrition & Metabolism**, [s. l.], v. 10, n. 1, p. 44, 2013. Disponível em: <http://www.ncbi.nlm.nih.gov/pubmed/23783067>. Acesso em: 15 fev. 2018.

CORDOVA, Clarissa A. S. et al. Solid lipid nanoparticles improve octyl gallate antimetastatic activity and ameliorate its renal and hepatic toxic effects. **Anti-Cancer Drugs**, [s. l.], v. 28, n. 9, p. 977–988, 2017. Disponível em: <http://www.ncbi.nlm.nih.gov/pubmed/28746057>. Acesso em: 24 jan. 2018.

COTRIM, Helma Pinchemel. **Esteatose Hepática | Sociedade Brasileira de Hepatologia**. 2018. Disponível em: <http://sbhepatologia.org.br/imprensa/esteatose-hepatica/>. Acesso em: 1 mar. 2018.

CUI, Wei; CHEN, Stephen L.; HU, Ke-Qin. Quantification and mechanisms of oleic acid-induced steatosis in HepG2 cells. **American journal of translational research**, [s. l.], v. 2, n. 1, p. 95–104, 2010. Disponível em: <http://www.ncbi.nlm.nih.gov/pubmed/20182586>. Acesso em: 14 jan. 2018.

DE CORDOVA, Clarissa A. S. et al. Octyl and dodecyl gallates induce oxidative stress and apoptosis in a melanoma cell line. **Toxicology in vitro : an international journal published in association with BIBRA**, [s. l.], v. 25, n. 8, p. 2025–34, 2011. Disponível em: <http://linkinghub.elsevier.com/retrieve/pii/S0887233311002165>. Acesso em: 9 ago. 2017.

ELER, Gabrielle Jacklin et al. Kinetics of the transformation of n-propyl gallate and structural analogs in the perfused rat liver. **Toxicology and Applied Pharmacology**, [s. l.], v. 273, n. 1, p. 35–46, 2013. Disponível em: <https://www.sciencedirect.com/science/article/pii/S0041008X13003827?via%3Dihub>. Acesso em: 30 mar. 2018.

ELER, Gabrielle Jacklin et al. *n* -Octyl Gallate as Inhibitor of Pyruvate Carboxylation and Lactate Gluconeogenesis. **Journal of Biochemical and Molecular Toxicology**, [s. l.], v. 29, n. 4, p. 157–164, 2015. Disponível em: <http://www.ncbi.nlm.nih.gov/pubmed/25487712>. Acesso em: 14 fev. 2018.

EUROPEAN PARLIAMENT AND THE COUNCIL OF THE EUROPEAN UNION. **REGULATION (EC) No 1333/2008 OF THE EUROPEAN PARLIAMENT AND OF THE COUNCIL of 16 December 2008 on food additives**. 2008. Disponível em: <http://eur-lex.europa.eu/legal-content/EN/TXT/?uri=CELEX:32008R1333>. Acesso em: 19 fev. 2018.

FITZMORRIS, P. et al. Management of hepatocellular carcinoma. **J Cancer Res Clin Oncol**, [s. l.], 2014. Disponível em: <http://www.ncbi.nlm.nih.gov/pubmed/25158999>

FOGARTY, S.; HARDIE, D. G. Development of protein kinase activators: AMPK as a target in metabolic disorders and cancer. **Biochim Biophys Acta**, [s. l.], v. 1804, n. 3, p. 581–591, 2010. Disponível em: <https://www.ncbi.nlm.nih.gov/pubmed/19778642>

FOOD AND AGRICULTURE ORGANIZATION OF UNITED NATIONS; WORLD HEALTH ORGANIZATION. GENERAL STANDARD FOR FOOD ADDITIVES. [s. l.], 1995. Disponível em: <http://www.fao.org/fao-who-codexalimentarius/sh-proxy/en/?lnk=1&url=https%253A%252F%252Fworkspace.fao.org%252Fsites%252Fcodex%252FStandards%252FCODEX%2BSTAN%2B192-1995%252FCXS_192e.pdf>. Acesso em: 14 fev. 2018.

FORNER, A.; LLOVET, J. M.; BRUIX, J. Hepatocellular carcinoma. **Lancet**, [s. l.], v. 379, n. 9822, p. 1245–1255, 2012. Disponível em: <https://www.ncbi.nlm.nih.gov/pubmed/22353262>

GENTILUCCI, Umberto Vespasiani et al. Chemotherapy-induced steatohepatitis in colorectal cancer patients. **Journal of clinical oncology : official journal of the American Society of Clinical Oncology**, [s. l.], v. 24, n. 34, p. 5467; author reply 5467-8, 2006. Disponível em: <http://ascopubs.org/doi/10.1200/JCO.2006.08.1828>. Acesso em: 15 fev. 2018.

GERDES, J. et al. Cell cycle analysis of a cell proliferation-associated human nuclear antigen defined by the monoclonal antibody Ki-67. **J Immunol**, [s. l.], v. 133, n. 4, p. 1710–1715, 1984. Disponível em: <https://www.ncbi.nlm.nih.gov/pubmed/6206131>

GERETS, H. H. J. et al. Characterization of primary human hepatocytes, HepG2 cells, and HepaRG cells at the mRNA level and CYP activity in response to inducers and their predictivity for the detection of human hepatotoxins. **Cell biology and toxicology**, [s. l.], v. 28, n. 2, p. 69–87, 2012. Disponível em: <http://www.ncbi.nlm.nih.gov/pubmed/22258563>. Acesso em: 24 jan. 2018.

GONÇALVES WOLF, Vanessa et al. Octyl gallate, a food additive with potential beneficial properties to treat Helicobacter pylori infection. **Food & Function**, [s. l.], v. 8, 2017. Disponível em: <http://pubs.rsc.org/en/content/articlepdf/2017/fo/c7fo00707h>. Acesso em: 14 fev. 2018.

GUO, Qie et al. Ubenimex suppresses Pim-3 kinase expression by targeting CD13 to reverse MDR in HCC cells. **Oncotarget**, [s. l.], v. 8, n. 42, p. 72652–72665, 2017. Disponível em: <http://www.ncbi.nlm.nih.gov/pubmed/29069816>. Acesso em: 24 jan. 2018.

HSU, F.; CHANG, H.; CHANG, S. Evaluation of antifungal properties of octyl gallate and its synergy with cinnamaldehyde. **Bioresource Technology**, [s. l.], v. 98, n. 4, p. 734–738, 2007. Disponível em: <http://www.ncbi.nlm.nih.gov/pubmed/16750625>. Acesso em: 19 jan. 2018.

HUYNH, Hung et al. Over-expression of the mitogen-activated protein kinase (MAPK) kinase (MEK)-MAPK in hepatocellular carcinoma: Its role in tumor progression and apoptosis. **BMC Gastroenterology**, [s. l.], v. 3, n. 1, p. 19, 2003. Disponível em: <http://www.ncbi.nlm.nih.gov/pubmed/12906713>. Acesso em: 21 jan. 2018.

INCA. **Câncer de Fígado**. 2017. Disponível em: <http://www.inca.gov.br/conteudo_view.asp?id=330>. Acesso em: 27 ago. 2017.

INOUE, M. et al. Selective induction of cell death in cancer cells by gallic acid. **Biol Pharm Bull**, [s. l.], v. 18, n. 11, p. 1526–1530, 1995. Disponível em: <https://www.ncbi.nlm.nih.gov/pubmed/8593472>

JAVITT, N. B. Hep G2 cells as a resource for metabolic studies: lipoprotein, cholesterol, and bile acids. **FASEB journal : official publication of the Federation of American Societies for Experimental Biology**, [s. l.], v. 4, n. 2, p. 161–8, 1990. Disponível em: <http://www.ncbi.nlm.nih.gov/pubmed/2153592>. Acesso em: 29 dez. 2017.

JENSEN, Thomas et al. Fructose and Sugar: A Major Mediator of Nonalcoholic Fatty Liver Disease. **Journal of Hepatology**, [s. l.], 2018. Disponível em: <http://www.ncbi.nlm.nih.gov/pubmed/29408694>. Acesso em: 15 fev. 2018.

JOINT FAO/WHO EXPERT COMMITTEE. **SPECIFICATIONS FOR IDENTITY AND PURITY AND TOXICOLOGICAL EVALUATION OF SOME ANTIMICROBIALS AND ANTIOXIDANTS**. 1964. Disponível em: <http://www.inchem.org/documents/jecfa/jecmono/v38aje04.htm>. Acesso em: 16 fev. 2018.

JOINT FAO/WHO EXPERT COMMITTEE. **EVALUATION OF MERCURY, LEAD, CADMIUM AND THE FOOD ADDITIVES AMARANTH, DIETHYLPYROCARBONATE, AND OCTYL GALLATE**. 1972. Disponível em: <http://www.inchem.org/documents/jecfa/jecmono/v004je07.htm>. Acesso em: 16 fev. 2018.

KROEMER, G.; GALLUZZI, L.; BRENNER, C. Mitochondrial membrane permeabilization in cell death. **Physiol Rev**, [s. l.], v. 87, n. 1, p. 99–163, 2007. Disponível em: <https://www.ncbi.nlm.nih.gov/pubmed/17237344>

LATHA, R. C.; DAISY, P. Therapeutic potential of octyl gallate isolated from fruits of Terminalia bellerica in streptozotocin-induced diabetic rats. **Pharm Biol**, [s. l.], v. 51, n. 6, p. 798–805, 2013. Disponível em: <https://www.ncbi.nlm.nih.gov/pubmed/23675839>

LI, Jibin et al. CD147 reprograms fatty acid metabolism in hepatocellular carcinoma cells through Akt/mTOR/SREBP1c and P38/PPARα pathways. **Journal of Hepatology**, [s. l.], v. 63, n. 6, p. 1378–1389, 2015. Disponível em: <https://www.sciencedirect.com/science/article/pii/S0168827815005462?_rdoc=1&_fmt=high&_origin=gateway&_docanchor=&md5=b8429449ccfc9c30159a5f9aeaa92ffb>. Acesso em: 16 fev. 2018.

LIMA, K. G. et al. Gallic acid reduces cell growth by induction of apoptosis and reduction of IL-8 in HepG2 cells. **Biomed Pharmacother**, [s. l.], v. 84, p. 1282–1290, 2016. Disponível em: <https://www.ncbi.nlm.nih.gov/pubmed/27810785>

LIMA, Kelly Goulart et al. Octyl gallate reduces ATP levels and Ki67 expression leading HepG2 cells to cell cycle arrest and mitochondria-mediated apoptosis. **Toxicology in Vitro**, [s. l.], v. 48, p. 11–25, 2018. Disponível em: <http://linkinghub.elsevier.com/retrieve/pii/S0887233317303831>. Acesso em: 4 jan. 2018.

LIU, Tiantian; YUAN, Xiaotian; XU, Dawei. Cancer-Specific Telomerase Reverse Transcriptase (TERT) Promoter Mutations: Biological and Clinical Implications. **Genes**, [s. l.], v. 7, n. 7, 2016. Disponível em: <http://www.ncbi.nlm.nih.gov/pubmed/27438857>. Acesso em: 21 jan. 2018.

LLOVET, J. M. et al. Design and endpoints of clinical trials in hepatocellular carcinoma. **J Natl Cancer Inst**, [s. l.], v. 100, n. 10, p. 698–711, 2008. a. Disponível em: <http://www.ncbi.nlm.nih.gov/pubmed/18477802>

LLOVET, Josep M. et al. Sorafenib in Advanced Hepatocellular Carcinoma. **New England Journal of Medicine**, [s. l.], v. 359, n. 4, p. 378–390, 2008. b. Disponível em: <http://www.ncbi.nlm.nih.gov/pubmed/18650514>. Acesso em: 29 dez. 2017.

LOCATELLI, C. et al. Ester derivatives of gallic acid with potential toxicity toward L1210 leukemia cells. **Bioorg Med Chem**, [s. l.], v. 16, n. 7, p. 3791–3799, 2008. Disponível em: <http://www.ncbi.nlm.nih.gov/pubmed/18295493>

LOCATELLI, C.; FILIPPIN-MONTEIRO, F. B.; CRECZYNSKI-PASA, T. B. Alkyl esters of gallic acid as anticancer agents: a review. **Eur J Med Chem**, [s. l.], v. 60, p. 233–239, 2013. Disponível em: <http://www.ncbi.nlm.nih.gov/pubmed/23291333>

LOCATELLI, Claudriana et al. Gallic acid ester derivatives induce apoptosis and cell adhesion inhibition in melanoma cells: The relationship between free radical generation, glutathione depletion and cell death. **Chemico-Biological Interactions**, [s. l.], v. 181, n. 2, p. 175–184, 2009. a. Disponível em: <http://www.ncbi.nlm.nih.gov/pubmed/19577552>. Acesso em: 29 dez. 2017.

LOCATELLI, Claudriana et al. Gallic acid ester derivatives induce apoptosis and cell adhesion inhibition in melanoma cells: The relationship between free radical generation, glutathione depletion and cell death. **Chemico-Biological Interactions**, [s. l.], v. 181, n. 2, p. 175–184, 2009. b. Disponível em: <http://www.ncbi.nlm.nih.gov/pubmed/19577552>. Acesso em: 9 ago. 2017.

LU, Y. et al. Gallic acid suppresses cell viability, proliferation, invasion and angiogenesis in human glioma cells. **Eur J Pharmacol**, [s. l.], v. 641, n. 2–3, p. 102–107, 2010. Disponível em: <http://www.ncbi.nlm.nih.gov/pubmed/20553913>

MACDONALD, Bryan T.; TAMAI, Keiko; HE, Xi. Wnt/beta-catenin signaling: components, mechanisms, and diseases. **Developmental cell**, [s. l.], v. 17, n. 1, p. 9–26, 2009. Disponível em: <http://www.ncbi.nlm.nih.gov/pubmed/19619488>. Acesso em: 21 jan. 2018.

MAIOLI, Margherita et al. Synthesis of magnolol and honokiol derivatives and their effect against hepatocarcinoma cells. **PLOS ONE**, [s. l.], v. 13, n. 2, p. e0192178, 2018. Disponível em: <http://www.ncbi.nlm.nih.gov/pubmed/29415009>. Acesso em: 23 fev. 2018.

MARQUARDT, Jens U.; ANDERSEN, Jesper B.; THORGEIRSSON, Snorri S. Functional and genetic deconstruction of the cellular origin in liver cancer. **Nature Reviews Cancer**, [s. l.], v. 15, n. 11, p. 653–667, 2015. Disponível em: <http://www.ncbi.nlm.nih.gov/pubmed/26493646>. Acesso em: 21 jan. 2018.

MARTINET, Wim et al. In Situ Detection of Starvation-induced Autophagy. **Journal of Histochemistry & Cytochemistry**, [s. l.], v. 54, n. 1, p. 85–96, 2006. Disponível em: <http://journals.sagepub.com/doi/10.1369/jhc.5A6743.2005>. Acesso em: 23 fev. 2018.

MAURYA, Brajesh Kumar; TRIGUN, Surendra Kumar. Fisetin Attenuates AKT Associated Growth Promoting Events in AflatoxinB1 Induced Hepatocellular Carcinoma. **Anti-Cancer Agents in Medicinal Chemistry**, [s. l.], v. 18, 2017. Disponível em: <http://www.ncbi.nlm.nih.gov/pubmed/29298655>. Acesso em: 23 fev. 2018.

MAZZAFERRO, Vincenzo et al. Liver Transplantation for the Treatment of Small Hepatocellular Carcinomas in Patients with Cirrhosis. **New England Journal of Medicine**, [s. l.], v. 334, n. 11, p. 693–700, 1996. Disponível em: <http://www.ncbi.nlm.nih.gov/pubmed/8594428>. Acesso em: 31 jan. 2018.

MCGLYNN, K. A.; PETRICK, J. L.; LONDON, W. T. Global epidemiology of hepatocellular carcinoma: an emphasis on demographic and regional variability. **Clin Liver Dis**, [s. l.], v. 19, n. 2, p. 223–238, 2015. Disponível em: <https://www.ncbi.nlm.nih.gov/pubmed/25921660>

MENTER, Alan et al. Guidelines of care for the management of psoriasis and psoriatic arthritis. **Journal of the American Academy of Dermatology**, [s. l.], v. 61, n. 3, p. 451–485, 2009. Disponível em: <http://www.ncbi.nlm.nih.gov/pubmed/19493586>. Acesso em: 15 fev. 2018.

MITCHELL, Richard. et al. **Robbins & Contran - Fundamentos de Patologia**. 7. ed. Rio de Janeiro.

NAKAGAWA, Y.; TAYAMA, S. Cytotoxicity of propyl gallate and related compounds in rat hepatocytes. **Arch Toxicol**, [s. l.], v. 69, n. 3, p. 204–208, 1995. Disponível em: <https://www.ncbi.nlm.nih.gov/pubmed/7717878>

NATIONAL CANCER INSTITUTE. **Liver (Hepatocellular) Cancer Screening (PDQ®)–Health Professional Version**. 2017. Disponível em: <https://www.cancer.gov/types/liver/hp/liver-screening-pdq#section/all>. Acesso em: 27 ago. 2017.

OKEN, M. M. et al. Toxicity and response criteria of the Eastern Cooperative Oncology Group. **American journal of clinical oncology**, [s. l.], v. 5, n. 6, p. 649–55, 1982. Disponível em: <http://www.ncbi.nlm.nih.gov/pubmed/7165009>. Acesso em: 29 dez. 2017.

PAN, Qiu-Zhong et al. Annexin A3 as a Potential Target for Immunotherapy of Liver Cancer Stem-Like Cells. **STEM CELLS**, [s. l.], v. 33, n. 2, p. 354–366, 2015. Disponível em: <http://www.ncbi.nlm.nih.gov/pubmed/25267273>. Acesso em: 24 jan. 2018.

PANG, Roberta W. C.; POON, Ronnie T. P. Cancer stem cell as a potential therapeutic target in hepatocellular carcinoma. **Current cancer drug targets**, [s. l.], v. 12, n. 9, p. 1081–94, 2012. Disponível em: <http://www.ncbi.nlm.nih.gov/pubmed/22873219>. Acesso em: 24 jan. 2018.

PERAZZOLI, Marlene Raimunda Andreola et al. Gallic Acid and Dodecyl Gallate Prevents Carbon Tetrachloride-Induced Acute and Chronic Hepatotoxicity by Enhancing Hepatic Antioxidant Status and Increasing p53 Expression. **Biological & pharmaceutical bulletin**, [s. l.], v. 40, n. 4, p. 425–434, 2017. Disponível em: <https://www.jstage.jst.go.jp/article/bpb/40/4/40_b16-00782/_article>. Acesso em: 15 nov. 2017.

PETTINELLI, P.; OBREGÓN, A. M.; VIDELA, L. A. Molecular mechanisms of steatosis in nonalcoholic fatty liver disease. **Nutricion hospitalaria**, [s. l.], v. 26, n. 3, p. 441–50, 2011. Disponível em: <http://www.ncbi.nlm.nih.gov/pubmed/21892559>. Acesso em: 16 fev. 2018.

PORSTMANN, Thomas et al. SREBP Activity Is Regulated by mTORC1 and Contributes to Akt-Dependent Cell Growth. **Cell Metabolism**, [s. l.], v. 8, n. 3, p. 224–236, 2008. Disponível em: <http://www.ncbi.nlm.nih.gov/pubmed/18762023>. Acesso em: 16 fev. 2018.

PORTA, Camillo; PAGLINO, Chiara; MOSCA, Alessandra. Targeting PI3K/Akt/mTOR Signaling in Cancer. **Frontiers in oncology**, [s. l.], v. 4, p. 64, 2014. Disponível em: <http://www.ncbi.nlm.nih.gov/pubmed/24782981>. Acesso em: 21 jan. 2018.

PUGH, R. N. et al. Transection of the oesophagus for bleeding oesophageal varices. **Br J Surg**, [s. l.], v. 60, n. 8, p. 646–649, 1973. Disponível em: <https://www.ncbi.nlm.nih.gov/pubmed/4541913>

QIU, Guo-Hua et al. Distinctive pharmacological differences between liver cancer cell lines HepG2 and Hep3B. **Cytotechnology**, [s. l.], v. 67, n. 1, p. 1–12, 2015. Disponível em: <http://www.ncbi.nlm.nih.gov/pubmed/25002206>. Acesso em: 29 dez. 2017.

ROS, Jenny E. et al. High expression of MDR1, MRP1, and MRP3 in the hepatic progenitor cell compartment and hepatocytes in severe human liver disease. **The Journal of Pathology**, [s. l.], v. 200, n. 5, p. 553–560, 2003. Disponível em: <http://www.ncbi.nlm.nih.gov/pubmed/12898590>. Acesso em: 24 jan. 2018.

SAEKI, K. et al. Apoptosis-inducing activity of lipid derivatives of gallic acid. **Biological & pharmaceutical bulletin**, [s. l.], v. 23, n. 11, p. 1391–4, 2000. Disponível em: <http://www.ncbi.nlm.nih.gov/pubmed/11085375>. Acesso em: 19 jan. 2018.

SCHMIDT-ARRAS, Dirk; ROSE-JOHN, Stefan. IL-6 pathway in the liver: From physiopathology to therapy. **Journal of Hepatology**, [s. l.], v. 64, n. 6, p. 1403–1415, 2016. Disponível em: <https://www.sciencedirect.com/science/article/pii/S0168827816000830>. Acesso em: 21 jan. 2018.

SCHULZE, Kornelius et al. Exome sequencing of hepatocellular carcinomas identifies new mutational signatures and potential therapeutic targets. **Nature genetics**, [s. l.], v. 47, n. 5, p. 505–511, 2015. Disponível em: <http://www.ncbi.nlm.nih.gov/pubmed/25822088>. Acesso em: 21 jan. 2018.

SERRANO, A. et al. Derivatives of gallic acid induce apoptosis in tumoral cell lines and inhibit lymphocyte proliferation. **Arch Biochem Biophys**, [s. l.], v. 350, n. 1, p. 49–54, 1998. Disponível em: <http://www.ncbi.nlm.nih.gov/pubmed/9466819>

SHIBATA, Tatsuhiro; ABURATANI, Hiroyuki. Exploration of liver cancer genomes. **Nature Reviews Gastroenterology & Hepatology**, [s. l.], v. 11, n. 6, p. 340–349, 2014. Disponível em: <http://www.ncbi.nlm.nih.gov/pubmed/24473361>. Acesso em: 21 jan. 2018.

SUN, X. et al. Ki-67 contributes to normal cell cycle progression and inactive X heterochromatin in p21 checkpoint-proficient human cells. **Mol Cell Biol**, [s. l.], 2017. Disponível em: <https://www.ncbi.nlm.nih.gov/pubmed/28630280>

TORRE, L. A. et al. Global Cancer Incidence and Mortality Rates and Trends--An Update. **Cancer Epidemiol Biomarkers Prev**, [s. l.], v. 25, n. 1, p. 16–27, 2016. Disponível em: <https://www.ncbi.nlm.nih.gov/pubmed/26667886>

TUMMALA, Krishna S. et al. Hepatocellular Carcinomas Originate Predominantly from Hepatocytes and Benign Lesions from Hepatic Progenitor Cells. **Cell Reports**, [s. l.], v. 19, n. 3, p. 584–600, 2017. Disponível em: <http://www.ncbi.nlm.nih.gov/pubmed/28423321>. Acesso em: 24 jan. 2018.

U.S. FOOD AND DRUG ADMINISTRATION. Food Additives & Ingredients - Food Additive Status List. [s. l.], 2018. Disponível em: <https://www.fda.gov/Food/IngredientsPackagingLabeling/FoodAdditivesIngredients/ucm091048.htm#ftnO>. Acesso em: 19 fev. 2018.

UOZAKI, Misao et al. Antiviral effect of octyl gallate against DNA and RNA viruses. **Antiviral Research**, [s. l.], v. 73, n. 2, p. 85–91, 2007. Disponível em: <http://www.ncbi.nlm.nih.gov/pubmed/16950523>. Acesso em: 19 jan. 2018.

WANG, Xin et al. Epirubicin-Adsorbed Nanodiamonds Kill Chemoresistant Hepatic Cancer Stem Cells. **ACS Nano**, [s. l.], v. 8, n. 12, p. 12151–12166, 2014. Disponível em: <http://pubs.acs.org/doi/10.1021/nn503491e>. Acesso em: 24 jan. 2018.

WORLD HEALTH ORGANIZATION. **Evaluation of Certain Food Additives and Contaminants**, 1997. Disponível em: <http://apps.who.int/iris/bitstream/10665/41962/1/WHO_TRS_868.pdf>. Acesso em: 14 fev. 2018.

WORLD HEALTH ORGANIZATION. **Hepatitis B**. 2017a. Disponível em: <http://www.who.int/mediacentre/factsheets/fs204/en/>. Acesso em: 29 dez. 2017.

WORLD HEALTH ORGANIZATION. **Hepatitis C**. 2017b. Disponível em: <http://www.who.int/mediacentre/factsheets/fs164/en/>. Acesso em: 29 dez. 2017.

YOSHIOKA, K. et al. Induction of apoptosis by gallic acid in human stomach cancer KATO III and colon adenocarcinoma COLO 205 cell lines. **Oncol Rep**, [s. l.], v. 7, n. 6, p. 1221–1223, 2000. Disponível em: <http://www.ncbi.nlm.nih.gov/pubmed/11032918>

ZENG, Lu et al. Alisol A 24-Acetate Prevents Hepatic Steatosis and Metabolic Disorders in

HepG2 Cells. **Cellular physiology and biochemistry : international journal of experimental cellular physiology, biochemistry, and pharmacology**, [s. l.], v. 40, n. 3–4, p. 453–464, 2016. Disponível em: <http://www.ncbi.nlm.nih.gov/pubmed/27889747>. Acesso em: 14 jan. 2018.

ZHAI, B.; SUN, X. Y. Mechanisms of resistance to sorafenib and the corresponding strategies in hepatocellular carcinoma. **World J Hepatol**, [s. l.], v. 5, n. 7, p. 345–352, 2013. Disponível em: <http://www.ncbi.nlm.nih.gov/pubmed/23898367>

ZHANG, S. Q. et al. Octyl gallate markedly promotes anti-amyloidogenic processing of APP through estrogen receptor-mediated ADAM10 activation. **PLoS One**, [s. l.], v. 8, n. 8, p. e71913, 2013. Disponível em: <http://www.ncbi.nlm.nih.gov/pubmed/23977176>

ZHAO, Fei et al. The Effect and Mechanism of Tamoxifen-Induced Hepatocyte Steatosis in Vitro. **International Journal of Molecular Sciences**, [s. l.], v. 15, n. 3, p. 4019–4030, 2014. Disponível em: <http://www.ncbi.nlm.nih.gov/pubmed/24603540>. Acesso em: 14 jan. 2018.

ZHU, Zhijun. Milan criteria and its expansions in liver transplantation for hepatocellular carcinoma. **Hepatobiliary surgery and nutrition**, [s. l.], v. 5, n. 6, p. 498–502, 2016. Disponível em: <http://www.ncbi.nlm.nih.gov/pubmed/28124007>. Acesso em: 31 jan. 2018.

Pontifícia Universidade Católica do Rio Grande do Sul
Pró-Reitoria de Graduação
Av. Ipiranga, 6681 - Prédio 1 - 3º. andar
Porto Alegre - RS - Brasil
Fone: (51) 3320-3500 - Fax: (51) 3339-1564
E-mail: prograd@pucrs.br
Site: www.pucrs.br